Université du Québec
Institut National de la Recherche Scientifique
Centre Eau Eńergie Matériaux Télécommunications

Design and Analysis of Spectral- and Energy-Efficient Spatial Modulation

by

Mohammad Irfan

A dissertation submitted in partial fulfillment of the requirements for the degree of
Doctor of Philosophy in Telecommunications

Evaluation Jury

External examiner	Walaa Hamouda Concordia University
External examiner	Salama Ikki Lakehead University
Internal examiner	Leszek Szczecinski INRS, Université du Québec
Research supervisor	Sonia Aïssa INRS, Université du Québec

Abstract

3rd generation partnership project (3GPP) has started work on specifications for 5G-Advanced in the form of Release-18. Multi-antenna systems are envisioned as key for enabling various features and use-cases in 5G-Advanced and beyond. However, the existing multiple-input multiple-output (MIMO) systems have significant implementation limitations, including high energy consumption, inter-carrier interference (ICI), and inter-antenna synchronization (IAS) which causes large implementation, operational, and detection complexities. These issues arise due to the simultaneous activation of all transmit antennas for transmission. The aforementioned limitations are even more significant in massive MIMO implementations, which is a key towards realizing the service requirements of 5G-Advanced and beyond. The shortcomings of MIMO systems can be addressed to a good extent by adopting the recently developed concept, widely known as spatial modulation (SM). In contrast to the existing MIMO techniques, SM offers a good trade-off in terms of data-rate, energy efficiency, and complexity, which makes it attractive for many use-cases.

This thesis aims at the design and modeling of data-rate and energy efficient SM techniques. This thesis can be broadly divided into two parts based on two major problems of SM. The low data-rate of SM as compared to the conventional spatial multiplexing (SMx) is one major issue. Secondly, reliability or bit error rate (BER) performance of SM is another major issue. The limited data-rate of SM arise due to the result of in-efficient modeling, whereas the reliability issues arise due to the antenna activation mechanism of SM. Specifically, Part 1 of this thesis includes two Chapter 2 and Chapter 3, which focus on data-rate enhancements. Part 2 of this thesis includes Chapter 4 and Chapter 5, which focus on enhancing the reliability performance of SM technique(s).

The SM technique is a member of the broader index-modulation (IM) family. IM has found immense applications in various domain, including at the subcarrier level of orthogonal frequency division multiplexing (OFDM), at the symbol-level of a single carrier system, at the antenna level of a MIMO system and at the code level of direct sequence spread spectrum. The data-rate and reliability issues exist in all IM techniques. While the main focus of this thesis is SM, the solutions proposed here for data-rate enhancement in Part 1 and reliability enhancements in Part 2 are equally applicable to all IM techniques and is thoroughly highlighted throughout this thesis.

Particularly, in Part I, Chapter 2 first systematically study the reasons behind low data-rate of IM techniques. Then, explicit design guidelines are proposed in order to enhance the data-rate and energy efficiency of IM techniques. Using both simulation results and theoretical analysis, it is shown that the proposed guidelines helps in enhancing the data-rate, energy efficiency and reliability performances of IM techniques. The guidelines proposed in Chapter 2 are extended for SM technique in Chapter 3 to show the superiority of SM technique over the existing MIMO techniques in terms of data-rate, energy efficiency, reliability, and complexity. Then in Part II, Chapter 4 study the problem of optimal antenna activation in SM techniques when channel state

information (CSI) is not available at the transmitter of SM. It is shown that equiprobable antenna activation is an optimal strategy when CSI is not available at transmitter of SM. Moreover, a space-time mapping method for enabling equiprobable antenna activation in SM techniques is developed in Chapter 4. Using simulations and theoretical analysis, it is shown that the proposed method can achieve reliability enhancements in SM techniques. Finally, Chapter 5 studies the antenna activation problem in SM techniques when CSI is available at transmitter of SM. In Chapter 5, it is shown that maximally irregular antenna activation is desirable. A simple method based on similarities among information bits is proposed in Chapter 5 to enable maximally irregular antenna activation. Using both simulation results and theoretical analysis, it is shown that use of the proposed irregular antenna activation in SM techniques can achieve higher reliability enhancements. In a nutshell, the solutions detailed in this thesis addresses two major limitations of SM technique, i.e., data-rate and reliability.

Acknowledgment

I would like to thank my research adviser Professor Sonia Aïssa and my family for their support during this project. I am also thankful to Fonds de Recherche du Québec Nature et technologies and Natural Sciences and Engineering Research Council of Canada for their financial support.

Contents

List of Figures

List of Tables

Chapter 1

Introduction

Recently released reports point to the rapidly increasing rate of the global data traffic [1]. The global Internet traffic, which was 1.5 ZB per year in 2017, is expected to reach 4.8 ZB by 2022, with the data traffic from wireless and mobile devices accounting for more than 71% of it [1]. Besides high data-rate, high energy efficiency is another fundamental requirement of future wireless communication systems. Indeed, the share of the total global power usage pertaining to information and communication technologies including wireless, which was 4.7% in 2012 is expected to reach 14% in 2020 and contribute up to 23% of the globally released greenhouse gas emissions by 2030 [2]. Joint optimization of the SE and EE of wireless communication systems is, however, a challenging task; and significant research advances would be needed before the high-efficiency requirements can be met in B5G (beyond 5G) systems.

The concept of index modulation (IM) promise high energy savings [3, 4]. In comparison to classical communication systems, IM-based systems utilize fewer resource elements for information transmission. In particular, a subgroup of subcarriers in OFDM, subgroup of antennas in multiple-input multiple-output (MIMO), a subgroup of codes in direct sequence spread spectrum and a subgroup of time slots in single carrier systems can be used to transmit useful information [5]. The partial utilization of the resource elements leads to energy savings due to the use of fewer communication blocks including converters, amplifiers, phase shifters, and filters. However, the maximum SE of IM-based systems is generally lower than the limit of a classical communication system with the same settings [3, 4]. A classical communication system with N subcarriers in case of OFDM, N transmit antennas in case of MIMO spatial multiplexing, N codes in direct sequence

spread spectrum, and N time-slots in a single-carrier system, operating with a modulation scheme of level M, can achieve a maximum of $N \log_2 M$ bits per transmission [3, 4]. Though IM-based communications promise improvements in EE, the low data-rate and reliability of these techniques remains a challenging problem.

The 3rd generation partnership project (3GPP) rolled specifications for new radio (NR) in its fifteenth release. Enhanced mobile broad band (eMBB) and ultra-reliable low latency communication (URLLC) are two major service requirements of NR. The later releases of NR also introduced a new service requirement called reduced capability (RedCap). A RedCap user equipment (UE) is expected to have limited processing capabilities with fewer transmitter and receiving antennas operating in smaller bandwidths with smaller data-rate requirements and smaller power consumption. The target vertical of RedCap UE's is industrial wireless sensors, video surveillance, wearables and will operate in frequency range 1 and frequency range 2 defined by 3GPP. IM-based systems with a good trade-off between data-rate and energy efficiency and its superior reliability performance over conventional communication systems makes it a suitable candidate for RedCap UEs in NR. However, the use of IM-based systems in NR is far from reality due to a number of unsolved problems. Two major problems of IM-based communication systems are its low data-rate as compared to the existing communication systems and its smaller reliability performance. The reliability performance of IM-based systems is shown to be higher than the existing communication systems in the available literatures [3, 4]. However, due to the lack of proper design guidelines, the reliability of IM-based systems can be further improved. Poor reliability of IM techniques is caused by the random activation of subcarriers, antennas, time-slots or codes. In IM techniques, a subset of the aforementioned resources are activated regardless of the channel knowledge. In fact, these resources are activated based on information bits, which results in near-uniform activation of subcarriers, antennas, time-slots, or codes hence causing performance degradation. The main motivation of this thesis is to propose solutions for enhancing data-rate and reliability of IM techniques, which are the two limiting factors of IM techniques in practice. Addressing these issues can bring IM techniques a step closer to its application in NR.

1.1 Research Problems

The concept of IM has found immense application in several communication domains, including the time-slot domain of single carrier communication systems [6], space domain of MIMO [7], subcarrier level of OFDM and at the code domain of direct-sequence spread spectrum [8]. The working principles of IM in all these mentioned domains in terms of mapping information bits to the time, antenna, subcarrier and code resources at the transmitter and retrieving the information bits at the receiver is identical. The amount of information bits which can be mapped to a time, antenna, subcarrier and code resource and how effective it can be retrieved at the receiver defines the data-rate and reliability performance of an IM technique. This problem of mapping information bits to the resources is the root cause of several issues in the design and operation of IM-based systems. Mapping of the information bits to the resources and its effect on several performance metrics is an open issue and is not well addressed in the available literature's.

The advantages of IM techniques over conventional communication techniques in terms of energy efficiency, reliability, and complexity has been widely studied in the available literature's over the last decade. Thanks to the aforementioned gains of IM techniques and its superior trade-off among different performance measures, several application areas for these techniques have been identified and studied over the last decade. Instead of finding application areas for IM techniques, majority of the solutions presented in this thesis mainly circle around the problem of mapping information bits to the resources and then studying its affect on several key performance metrics. More specifically, this thesis aims at enhancing the data-rate and reliability performances of the IM techniques. The research problems addressed in this thesis are categorized as follows.

1.1.1 Data Rate of Index Modulation Techniques

The existing literatures has well studied the data-rate of IM techniques. The IM techniques makes a partial use of the available time-slots, subcarriers, antennas and code resources. This argument is largely used in the available literatures to justify the statement that the data-rate of IM techniques is smaller than that of conventional communication techniques. The marginal data-rate performance of IM techniques, which arise due to the inefficient information bit mapping at the transmitter has vilified IM techniques in terms of data-rate. The so-called partial utilization of IM techniques can

be explored to enhance the data-rate of IM techniques beyond the conventional communication techniques, which is the main motivation of Chapter 2 and Chapter 3. Particularly, the low data-rate of OFDM with IM is addressed in Chapter 2 and the low data-rate when implementing IM technique in the space domain of MIMO, known as spatial modulation is addressed in Chapter 3. The methodologies behind addressing the low data-rate problem of IM techniques in Chapter 2 and Chapter 3 is drawn in Section. 1.3.1.

1.1.2 Reliability of Index Modulation Techniques

The use of partial resource utilization when using IM techniques allows us to boost the power level at the corresponding time-slot, subcarrier, antenna and code resources used for transmission, which leads to a better signal quality at the receiver. This helps in enhancing the error rate performance, which is another attraction behind the use of IM techniques. While the reliability of IM techniques is shown to be superior as compared to conventional communication systems, the working principles behind the resources activation in IM techniques leads to a loss in reliability performance. Different resources activation strategies in IM techniques are effective in terms of reliability performance. The choice of an optimal strategy depends on the availability of channel state information (CSI) at the transmitter. An optimal antenna activation method for SM technique is devised in Chaper 4 when CSI is not available at the transmitter. Moreover, a near-optimal antenna activation method is proposed in Chapter 5 for the case when CSI is available at transmitter. Detailed methodologies behind Chaper 4 and Chaper 5 are respectively presented in Section. 6.3.2.

1.2 Research Objectives

The main research problems of IM techniques, i.e., the low data-rate and reliability of IM techniques were mentioned in the previous section. A detailed overview of the research objectives and each of the research objective are explained in this section. A high-level overview of the research objectives is provided in Fig. 1.1. Based on the major issues of IM, the research objectives can be divided into two categories, i.e., data-rate and reliability.

As mentioned earlier, the available literature's claims that the the data-rate of an IM technique is smaller as compared to conventional communication techniques [9]. In fact, it is widely believed

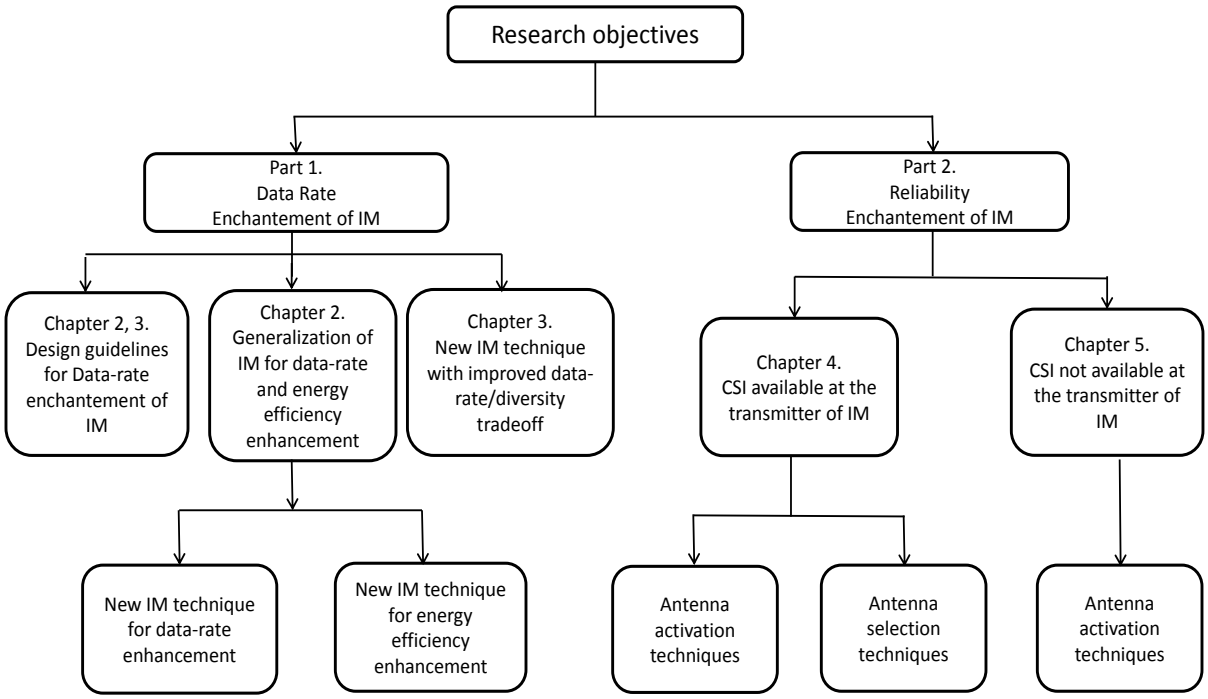

Figure 1.1: A high-level overview of the research objectives

that the application of IM technique in different domains, i.e., SM, SC-IM, CIM, and OFDM-IM enhances can enhance energy efficiency and error performance at the expense of a loss in data-rate. Therefore, the better trade-off between data-rate and energy efficiency offered by IM techniques as compared to conventional communication techniques is seen as the most attractive advantage of IM techniques [9]. However, when observing the working principles of IM techniques at the baseband modulation level, it can be concluded that the idea of IM techniques is in fact an extension of the existing baseband modulation concept. In fact, the concept of IM techniques can be seen as a very high-level generalization of the existing baseband modulations. However, this so-called high-level generalization of the baseband modulations is in its infancy stage due to the lack of comprehensive design guidelines. Therefore, towards enhancing the data-rate, energy efficiency, and error performances of IM techniques, our research objective is to devise a set of comprehensive design guidelines by solving complex optimization problems and probabilistic analysis. Moreover, new IM techniques are also proposed to enhance the data-rate, energy efficiency and reliability performances.

In IM techniques, the data-rate, energy efficiency and error performance (reliability) mainly depends on the bit to resource (subcarrier in case of OFDM, antenna in case of MIMO, time-slot in case of single carrier system, and code in case of spread spectrum) indices of IM techniques. In the context of SM techniques, we study the effect of bit to antenna indices mapping on the data-rate, energy efficiency and error performance analysis. In fact, the error performance and data-rate of SM techniques depends on several factors including the available number of transmit antennas at transmitter and the availability of CSI at transmitter. The availability of CSI at transmitter is a crucial factor in choosing a method for mapping bits to antenna indices, also known as antenna activation through out this thesis. Therefore, based on the availability of CSI at transmitter, antenna activation methods are proposed to address the existing inefficient mapping and to overcome the related performance losses. The problem of antenna activation in SM is addressed in Chapter 4 and Chapter 5.

Based on the above high-level discussion of the research objectives, the contribution of this thesis is categorized into four chapters and the detailed research objectives of each chapter is presented as follows.

1.2.1 Orthogonal Frequency Division Multiplexing with Index Modulation

The objective of Chapter 2, in the context of OFDM-IM is to address the well the well-known low data-rate problem of IM techniques in general and OFDM-IM in particular. The low data-rate problem of OFDM-IM technique was addressed by deriving the minimum required number of subcarriers per group, and the minimum number of active subcarriers in each group, of the conventional OFDM-IM technique. It is proven that when number of subcarriers per grop and the number of active subcarriers per group satisfy the derived limits, then OFDM-IM can deliver higher data-rate and energy efficiencies than classical OFDM. The data-rate gains of OFDM-IM comes at the expense of increased detection complexity. Therefore, a OFDM with generalized IM (OFDM-GIM) technique is presented, where a variable number of subcarriers per group are allowed to be activated. Then, two variants of OFDM-GIM are designed based on the activation pattern of the subcarriers: the first achieves superior data-rate with reduced detection complexity as compared to OFDM-IM, and the second is tailored for low data rate communications with higher energy efficiency requirements. Besides optimal maximum likelihood detection, a less-complex sub-optimal

detector was proposed. A closed-form expression for the bit error rate (BER) of OFDM-IIM and the two variants of OFDM-GIM is derived, considering transmissions over Nakagami fading channels and multiple-antenna reception. Finally, OFDM-IM and OFDM-GIM are compared with state-of-the-art techniques to validate their superiority in terms of BER, achievable rate, and energy efficiency.

1.2.2 Multiple Active Spatial Modulation

The low data-rate problem of SM technique is tackled in Chapter 3. It is widely believed that the data-rate performance of SM technique is smaller than that of SMx. Chapter 3 challenges this myth and proves that a variant of SM technique can surpass the data-rate performance of SMx. Particularly, we aim to justify the following two statements using mathematical derivations. First, in comparison to SMx and loosely based on the finding of Chapter 2, it is proven that the MASM technique can achieve similar data-rate to SMx but with smaller number of transmit antennas, smaller number of active antennas, and less number of receive antennas. Secondly, it is proven that when the MASM and SMx are operated with the same number of transmit antennas, the MASM technique can achieve higher data-rate while using fewer active transmit antennas and fewer receive antennas. Furthermore, the low data-rate and diversity trade-off problem of MASM is highlighted, and a proposal of an enhanced MASM (E-MASM) technique is shown to achieve a better trade-off between data-rate and diversity as compared to SMx. Finally, in comparison to SMx, E-MASM is shown to achieve higher a better trade-off between data-rate and diversity.

Data-rate enhancement of OFDM with IM and MASM are detailed in Chapter 2 and Chapter 3, respectively. Particularly, in Chapter 2 it is proven that OFDM-IM can surpass classical OFDM in terms of data-rate. Moreover, in Chapter 3, it is proven that the MASM technique can surpass the data-rate performance of SMx. The remaining two chapter of this thesis address the reliability issues of SM techniques. The research objectives of each of the remaining chapters is detailed as follows.

1.2.3 Equiprobable Antenna Activation in Spatial Modulation

In SM technique, when the number of antennas is not an integer power of two, the antenna activation becomes challenging. In such a case, only a subset of the available transmit antennas whose cardinality is an integer power of two is used. This leads to antenna activation with unequal probability, which causes high error rates and losses in the data-rate. The same limitations and performance losses equally exist in quadrature spatial modulation (QSM) and generalized spatial modulation (GSM), the two prominent variants of SM. In Chapter 4, in contrast to the conventional approach of antenna activation within each symbol period, a space-time bit-mapping method in which the antenna selection procedure is extended to multiple symbol periods is proposed. Use of the proposed method in SM, QSM, and GSM techniques, is shown to achieve performances close to their full potential for any given number of transmit antennas, with only a marginal increment in detection complexity.

1.2.4 Irregular Antenna Activation and Antenna Selection in Spatial Modulation

Each transmit antenna in SM-based communication is uniformly activated, which can lead to poor channels for transmission, causing performance degradation. Though antenna selection can be used to tackle this problem of uniform antenna activation (U-AA), it requires additional antenna elements, high computational complexity, and signalling overhead. In Chapter 5, we propose an irregular antenna activation (I-AA) technique. First, during each symbol period, an integer number r, which can take value between zero and the total number of transmit antennas, is assigned to consecutive equal bits. Then the sequence of r consecutive equal bits is used to choose the antenna(s) for transmission, resulting in I-AA. A rate-optimized I-AA is developed to utilize better channels for transmission. In prominent variants of SM, the use of I-AA is shown to yield higher data rates and smaller error rates as compared to operations with the conventional U-AA. Moreover, a joint rate- and Euclidean-distance optimized antenna selection (REAS) and a rate-optimized low-complexity AS (RLAS) for SM with I-AA are proposed. The use of the proposed I-AA without AS in prominent variants of the SM technique is shown to achieve better error rate performance as compared to U-AA with AS. Also, the use of I-AA in the proposed REAS and RLAS yields improvements in the data

rates and error rates as compared to U-AA with AS, at a negligible extra complexity and signalling overhead.

1.3 Methodology

In this section, we describe how the objectives set in the previous section are met.

1.3.1 Data-rate Enhancements

Data-rate enhancement of IM-based OFDM, known as OFDM with index modulation and IM-based MIMO known as spatial modulation was performed. The methodologies behind each of the above mentioned IM-based systems are presented as follows.

Data-rate Enhancement of OFDM with Index Modulation

The working principles behind IM techniques is studied to better understand its working principles, which makes it easier to address the low data-rate problem of IM techniques as compared to the conventional communication systems. Particularly, the working principle of IM techniques is broken down in the context of baseband modulation. It was concluded that the IM concept is an extension of the existing modulation schemes. Explicitly, the IM concept is a generalization of the existing baseband modulation techniques. This allowed us to mathematically proved that the IM concept can achieve higher data-rate than the conventional communication systems. The proof was largely facilitated by optimization theory. We used the findings of the proof to propose comprehensive design guidelines. The guidelines helps in better understanding the potential of IM in terms of data-rate, energy efficiency and complexity. Such guidelines were missing in the existing literature. Moreover, a generalized concept of IM was proposed with comprehensive design guidelines for choosing various parameters of the system. Trade-off between data-rate, energy efficiency and detection complexity were thoroughly analysed.

After proving the high potential of IM in terms of data-rate and energy efficiency, probability theory was used to study reliability performance of OFDM with index modulation. A closed form bit error rate (BER) expression was derived. Then, an expression for throughput performance was

derived. Using Matlab, Monte Carlo simulations were performed to study the reliability performance of OFDM-IM. The derived BER expression were verified using the simulation results. Particularly, higher gains were shown when the resource parameters of OFDM-IM were chosen as per the proposed design guidelines. Based on the comparative study, several application areas of OFDM-IM in practical communication systems were identified. Our detailed contribution are summarized as follows.

- The minimum number of resources, in terms of the number of subcarriers per group, and the number of active subcarriers within a group, are derived under a constrained modulation level, with the purpose to maximize the data-rate and energy efficiency of OFDM-IM beyond the conventional limits of classical OFDM.
- The pursuit of higher SE and EE with OFDM-IIM increases the search space of a maximum likelihood (ML) detector and, hence, the detection complexity. A novel OFDM-GIM technique (OFDM with generalized IM) was proposed. Two variants were developed based on the activation pattern of the subcarriers, where the first variant was shown to achieve higher data-rate and the second variant was shown to achieve smaller data-rate with superior energy efficiency performance.
- A closed-form BER expression was derived considering transmissions subject to Nakagami fading and multiple antenna reception. Analytical and simulation results of BER were shown to closely match in the SNR range of interest. Importantly, compared to classical OFDM and other OFDM-IM techniques, the proposed two variants of OFDM-GIM were shown to achieve superior data-rate and energy efficiency with superior BER performance.

Data-rate Enhancement of Multiple Active Spatial Modulation

The concept of IM in MIMO is known as spatial modulation. The potential of SM in terms of performance gains is no secret. In fact, a good amount of literature is available on the potential of spatial modulation, especially in terms of energy efficiency, complexity and reliability. What is also not a secret is the myth about the low data-rate of SM. Particularly, in the available literature, it is widely believed that SM can not surpass the data-rate performance of the well-known spatial multiplexing (SMx). The second part of this thesis counters this myth. Using optimization theory,

it was proved that a variant of SM can surpass the data-rate performance of SMx. The proof was used to develop design guidelines for SM technique. Then, using probability theory, an expression for the reliability performance of SM technique was derived. The derived expression was used to analyse the rate performance as well. Using Matlab, Monte Carlo simulation were performed to show the effectiveness of SM technique, both in terms of reliability and rate performance. It was verified that a variant of SM technique has the potential to surpass the rate performance of SMx.

The trade-off between data-rate and diversity of SM technique was also analysed and it was observed that the data-rate versus diversity performance of SM techniques are poor as compared to SMx. An enhanced SM technique was proposed to achieve a better trade-off between data-rate and diversity. It was shown that the enhanced SM techniques can achieve superior data-rate and diversity trade-off as compared to SMx. Using probability theory, rate and reliability performances of the proposed enhanced SM technique was analysed. Then, using Monte Carlo simulations, the higher rate and reliability performance of the proposed enhanced SM technique was verified.

The contributions of this part is summarized as follows

- It was proved that the SM technique requires fewer active radio frequency (RF) chains and receive antennas to surpass the data-rate performance of SMx.
- It was proved that the SM technique requires fewer transmit antennas and receive antennas to match the data-rate performance of SMx.
- It was shown that the data-rate and diversity trade-off of SMx can be overcome by the proposed enhanced SM technique.

1.3.2 Reliability Enhancements

Reliability enhancement of IM-based systems was studied in MIMO domain, i.e., reliability enhancement of SM technique and its variant was studied. Particularly, an in-depth study of the antenna activation mechanism in SM technique and its variants was performed. It was concluded that the antenna activation mechanism of SM technique and its variants causes severe performance degradation. As a quick thought, it was concluded that uniform antenna activation is optimal when the channel state information (CSI) is not available at the transmitter and that irregular antenna acti-

vation is optimal when the CSI is known at the transmitter. Each of these two cases are presented in the following subsections.

Reliability Enhancements of Spatial Modulation without CSI at Transmitter

As mentioned above, it is optimal to activate each transmit antenna of SM technique and its variants with equal probability when CSI is not available at the transmitter. The existing SM techniques uses a combinatorial method based on a block of information bits at the transmitter for antenna activation. This enables equiprobable antenna activation only when the number of transmit antennas is a power of two, which is a rare case, especially in practical systems. When the number of antennas is not a power of two, the available antennas are activated with unequal probabilities. Such unequal antenna activation results in a largely unequal protection of the transmitted bits, thus affecting the reliability performance. Moreover, the non-uniform antenna activation in SM techniques is also responsible for a loss in data-rate. Both the losses in reliability data-rate increases when the number of transmit antennas increases, which makes it a more severe problem for the application of SM technique in NR.

To enable equiprobable antenna activation in SM techniques, we extend the antenna activation process of SM technique and its variants over the spatial and temporal domains. This enables nearly equiprobable antenna activation. The optimal number of time slots for the extension of antenna activation was derived. Using probability theory, an expression for BER was derived. An expression for coding gain advantages of using equiprobable antenna activation over the conventional antenna activation in SM technique was also derived. Using Matlab, Monte Carlo simulations were performed and the performance gains in data-rate enhancement and reliability when using equaiprobable antenna activation was verified.

The contribution of this part is summarized as follows

- The problem of antenna activation causing performance degradation in data-rate and reliability in SM techniques was thoroughly studied.
- A space-time mapping design in which the encoding procedure is extended to multiple symbol periods was proposed and it was shown that the proposed mapping can enhance rate and reliability performance.

Reliability Enhancements of Spatial Modulation with CSI at Transmitter

Antenna selection and power allocation has been widely studied when CSI is available at the transmitter of a SM-based system. After a thorough analysis of the antenna activation mechanism, we showed that equiprobable antenna activation is not an optimal strategy when the CSI is available at the transmitter of a SM-based system. Instead, maximum irregular antenna activation is optimal when the CSI is available at the transmitter. This motivated us to develop a new antenna activation method for SM techniques, the so-called irregular antenna activation.

Similarities among short information bits at the transmitter were exploited. It was shown that different sequences of information bits based on consecutive similarities with the sequence at the transmitter naturally occurs with different probabilities. An expression for such probabilities was derived, which was then used to derive an expression for the rate performance of SM technique implementing the proposed irregular antenna activation. Using the rate expression and the event probabilities, a mapping between the events and antenna indices was developed so that the overall rate can be enhanced. Next, using probability theory and order statistics, an expression for the BER of SM technique implementing the proposed irregular antenna activation was developed. Using Matlab, Monte Carlo simulations were performed to verify the reliability gains of using irregular antenna activation over equiprobable antenna activation.

Antenna selection was also studied when using irregular antenna activation. An antenna selection method was developed. Using probability theory and order statistics, a closed form expression for BER of SM technique implementing irregular antenna activation and the proposed antenna selection was derived. Using Matlab, Monte Carlo simulations were performed to verify the reliability gains of using irregular antenna activation with antenna selection over equiprobable antenna activation with antenna selection.

The main contributions of this part are summarized as follows

- A novel method for antenna activation in SM techniques is proposed. The concept consists in assigning an integer value to consecutive equal information bits, and using the obtained values for antenna activation.
- Two rate optimized antenna selection methods, namely joint rate and Euclidean-distance optimized antenna selection and rate-optimized low-complexity antenna selection were proposed.

- Using order statistics, closed form expression for BER of SM implementing irregular antenna activation was derived with/without the antenna selection methods was derived for transmission subject to Rayleigh fading channels and single- or multiple-antenna reception.

- The main performance gains related to the use of irregular antenna activation in SM technique was shown to be two-fold. Firstly, it was shown that higher rates can be achieved as compared to SM with equiprobable antenna activation. Secondly, better error rates can be obtained as compared to SM with equiprobable antenna activation. SM implementing irregular antenna activation without antenna selection was shown to achieve even better error rate performance as compared to SM with uniform antenna activation with antenna selection. Lastly, SM techniques implementing the proposed irregular antenna activation and antenna selection methods are shown to outclass SM implementing equiprobable antenna activation and antenna selection with a negligible overhead in complexity and signalling.

Part I

Chapter 2

Generalization of Index-Modulation: Breaking the Conventional Limits on Data Rate and Energy Efficiency

2.1 Introduction

Application of IM at the subcarrier level of OFDM first appeared in [11], and its error propagation problem was addressed in [12]. The low data-rate of the OFDM based IM techniques in [11] and [12] were addressed by the well-known OFDM-IM technique [5]. The concept of OFDM-IM consists in activating a subset of K subcarriers, from a group of N subcarriers, and loading them with M-ary amplitude/phase modulation (APM) symbols such that the indices of the K active subcarriers and the APM symbols mutually carry useful information. The $N - K$ silent subcarriers of OFDM-IM contribute to energy savings at the cost of data-rate [4].

The achievable data-rate of OFDM-IM is well studied in [13], and it was concluded that OFDM-IM can surpass conventional OFDM only for smaller values of M at a certain range of the signal-to-noise ratio (SNR). The low data-rate can be improved by merging OFDM-IM with other data-rate improving techniques. Dual-mode (DM) OFDM-IM [14] and multi-mode (MM) OFDM-IM [15] are two prominent methods for improving the data-rate performance of OFDM-IM. In particular,

[0]The contents of this chapter are extracted from [10].

MM-OFDM-IM and DM-OFDM-IM activate all the subcarriers, and use dual and multiple distinguishable modes of the M-ary APM constellation points along with M-ary APM symbols to enhance data-rate. The high data-rate of the techniques in [14] and [15] is only achieved when sacrificing the energy savings and smaller detection and implementation complexity of conventional OFDM-IM. In practice, OFDM-IM is vulnerable to carrier frequency offset and Doppler shifts. The impact of inter-carrier interference (ICI), on the other hand, is less severe compared to classical OFDM and the methods of [14] and [15], thanks to the $N-K$ silent subcarriers in OFDM-IM [16]. The silent subcarriers were used for clipping signals [17], and multi-level dither signals [18], to reduce the peak-to-average power ratio of OFDM-IM.

The inherent properties and implementation advantages of OFDM-IM over the methods of [14] and [15] motivated several efforts towards data-rate enhancement by studying the selection of the OFDM-IM resources parameters N, K, and M, [19–21].[1] In [19], the impact of the subcarriers' activation ratio, i.e., $\frac{K}{N}$, on the data-rate performance of OFDM-IM has concluded that $K = N-1$ is the optimal number of active subcarriers. According to [16] and [5], the choice of $K = N-1$ reduces energy savings and increases ICI as well as the detection and implementation complexity, especially at high values of N. In [20], an expression for optimal K as a function of N and M is derived. In [21], investigation of the effect of the subcarriers' group size N on the data-rate performance of OFDM-IM concluded a minimum condition of $N \geq 2M$ for enabling higher data-rate.

Apart from the methods of [14, 15, 19–21] , enhanced OFDM-IM [22] and layered OFDM-IM [23] also improve the data-rate performance. Particularly, in [22], the in-phase and quadrature components of the M-APM symbol are used to chose indexes of the active subcarriers. Interleaved subcarrier mapping in OFDM-IM for achieving frequency diversity is investigated in [24]. In [23], the N subcarriers are divided into multiple layers, and the OFDM-IM concept is applied in each layer. Similar to [19–21], selection of the resources (N, K, M), their interrelations and impacts on the key performances of high data-rate achieving methods [14, 15, 22–25], can further enhance the data-rate and energy efficiency with simplified detection and implementation.

[1] As the parameters (N, K, M) indicate the resources used, e.g., the subcarriers group size N and the number of active subcarriers K, for simplicity (N, K, M) will also be referred to as resource elements.

2.1.1 Motivation and Contributions

In [19–21], the selection procedures of the design elements (N, K, M) only consider one of the elements and its effect on the data-rate performance of OFDM-IM. Specifically, only the number of active subcarriers K and its effect on the data-rate are presented in [19] and [20]. In [21], only the subcarriers' group size N and its effect of the data-rate performance are considered. The interrelations of the design parameters (N, K, M) and their effect on the data-rate, energy efficiency, and detection complexity of OFDM-IM, remain unknown. Also, the choice of smaller values for (N, K, M) in OFDM-IM, to enable higher data-rate and energy efficiency with reduced detection complexity compared to classical OFDM, is still unresolved.[2] Furthermore, new OFDM-IM techniques, which make use of a smaller set of the resource elements (N, K, M) as compared to OFDM-IM, to surpass the data-rate and energy efficiency of classical OFDM, are desirable in terms of reduced detection and implementation complexity with relaxed constraints on the resource element N.

Taking conventional OFDM-IM as a starting point, and motivated by the above, the main contributions of this paper can be summarized as follows:

(i) The minimum number of resources, in terms of the number of subcarriers per group, and the number of active subcarriers within a group, are derived under a constrained modulation level, with the purpose to maximize the data-rate and energy efficiency of OFDM-IM beyond the η_{c} bits/s/Hz and EE_{c} bits/J limits of classical OFDM. The technique fulfilling the minimum conditions on the resources elements (N, K, M) presented here for performance enhancement is termed OFDM with improved IM (OFDM-IIM).

(ii) The pursuit of higher data-rate and energy efficiency with OFDM-IIM increases the search space of a maximum likelihood (ML) detector and, hence, the detection complexity. Here, a novel OFDM-GIM technique (OFDM with generalized IM) is proposed. Two variants are developed based on the activation pattern of the subcarriers: OFDM-GIM_1 achieves higher data-rate with reduced detection complexity as compared to OFDM-IIM, whereas OFDM-GIM_2 is tailored for low-data-rate communications, and shown to achieve superior energy efficiency performance as compared to classical OFDM, OFDM-IM, OFDM-IIM, and OFDM-GIM_1.

[2] OFDM under the use of M-APM with P_{t} watt [W] transmit power allocated to a subcarrier of unit duration, can achieve a maximum data-rate of $\eta_{\mathrm{c}} = \log_2 M$ bits/s/Hz with a maximum energy efficiency of $\mathrm{EE}_{\mathrm{c}} = \frac{\log_2 M}{P_{\mathrm{t}}}$ bits/J.

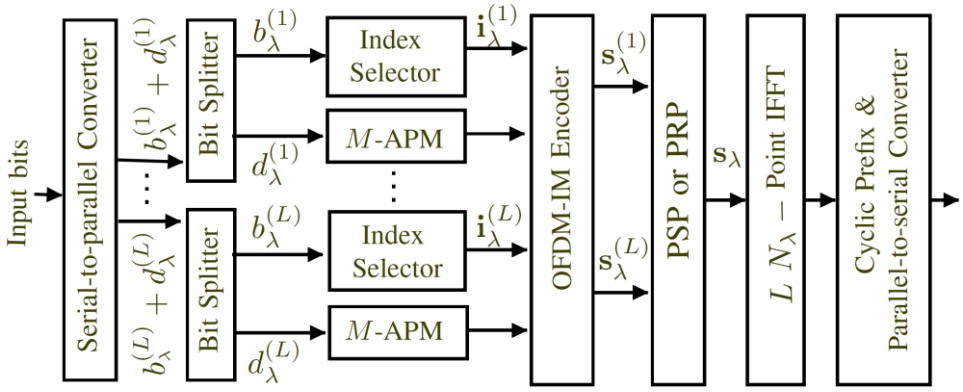

Figure 2.1: Transmitter block diagram of OFDM-IM, OFDM-IIM, and OFDM-GIM (ignoring subscript λ in the variables involved corresponds to OFDM-IM and OFDM-IIM, whereas variables with $\lambda = 1, 2$ correspond to the two variants of OFDM-GIM).

(iii) A closed-form BER expression, valid for OFDM-IM, OFDM-IIM, and OFDM-GIM, is derived considering transmissions subject to Nakagami fading and multiple-antenna reception. Analytical and simulation results of BER are shown to closely match in the SNR range of interest. Importantly, compared to classical OFDM and other OFDM-IM techniques, the proposed OFDM-IIM and the two variants of OFDM-GIM are shown to achieve superior data-rate and energy efficiency with better BER performance, for all values of the modulation level M.

In detailing the above-highlighted contributions, the remainder of the paper is organized as follows. Next, Section 2 summarizes OFDM-IM. Section 2.2 details OFDM-IIM, and also lays down an important motivation for OFDM-GIM, which is proposed in Section 2.3. The detection and complexity analysis is presented in Appendix A.4, and the performance analysis is carried out in Appendix A.5. Numerical results are discussed in Section 2.6, and Section 2.7 concludes the chapter.

2.1.2 Transmitter Architecture and Working Principle

Figure 2.1 depicts the block diagram of OFDM-IM with LN subcarriers, divided into L groups each having N subcarriers. First, a block of $b^{(l)} + d^{(l)}$ bits enters the l^{th} group, $l = 1, \cdots, L$, where only K out of N subcarriers are allowed for M-ary APM symbol transmission, while the remaining $N - K$ subcarriers are kept silent [5]. K out of N subcarriers can form $\binom{N}{K}$ patterns of active subcarriers. The block of $b^{(l)} = \lfloor \log_2 \binom{N}{K} \rfloor$ input bits is used to select a unique pattern $\mathbf{i}^{(l)}$. Then,

the K active subcarriers of the chosen pattern $\mathbf{i}^{(l)}$ are loaded with the K complex symbols, formed by $d^{(l)} = K \log_2 M$ input bits after being mapped through M-ary APM.[3]

After the OFDM-IM encoding, the resultant symbols $\mathbf{s}^{(l)}$ should have K non-zero complex entries and $(N - K) \geq 1$ zero entries. Therefore, the complex entries on the K active subcarriers of each group can be scaled by $\sqrt{\frac{N}{K}}$ to satisfy $E\{\mathbf{s}\ \mathbf{s}^H\} = LN$, where $\mathbf{s} = [\mathbf{s}^{(1)}, \cdots, \mathbf{s}^{(L)}]$. The latter is known as *power reallocation policy* (PRP). In the *power saving policy* (PSP), on the other hand, the K active subcarriers are left unchanged and, hence, $E\{\mathbf{s}\ \mathbf{s}^H\} = LK < LN$. After PSP or PRP, which will be thoroughly discussed in later sections, LN-point inverse fast Fourier transform (IFFT) is performed on $\mathbf{s}$, followed by the cyclic prefix addition and parallel-to-serial (P/S) operation. The resulting signal is then transmitted through a wireless channel categorized by the gain vector $\mathbf{h} \in \mathbb{C}^{LN}$.

2.1.3 Detection of OFDM-IM Signal

The received signal after the removal of cyclic prefix and LN-point FFT is given by $\mathbf{y}^{(l)} = \mathbf{h}^{(l)}\mathbf{s}^{(l)} + \mathbf{u}^{(l)}$, where the elements of the additive white Gaussian noise (AWGN) vector $\mathbf{u}^{(l)}$ are independent and identically distributed (i.i.d.) according to $\mathcal{CN}(0, N_0/2)$.

To recover the $b^{(l)} + d^{(l)}$ bits at the receiver, knowledge of the pattern used, i.e., $\mathbf{i}^{(l)}$, and the transmit symbols $\mathbf{s}^{(l)}$, is required, which can be jointly estimated by using a group-wise decision on each group of N subcarriers, according to the ML principle as follows:

$$[\widehat{\mathbf{i}}^{(l)}, \widehat{\mathbf{s}}^{(l)}] = \arg \min_{\mathbf{i}^{(l)}, \mathbf{s}^{(l)}} \sum_{q=1}^{R} |\mathbf{y}^{(l)} - \mathbf{h}^{(l)}\ \mathbf{s}^{(l)}(q)|^2, \tag{2.1}$$

where $\widehat{\mathbf{i}}^{(l)}$ and $\widehat{\mathbf{s}}^{(l)}$ are the estimated pattern and symbol vector of the l^{th} group, $\mathbf{s}^{(l)} \in \mathbf{S}$, and the code-book $\mathbf{S} \in \mathbb{C}^{R \times N}$, where $R = \binom{N}{K} M^K$. From (4.4), note that the subcarrier indices and the modulated symbol on the subcarrier are jointly detected. Therefore, an event where the subcarrier index is successfully estimated and the symbol on the subcarrier is estimated in error or an event where the subcarrier index is estimated in error and the symbol on the subcarrier is successfully detected may occur.

[3]The b_λ and d_λ input bits will also be referred to as "*index bits*" and the "*mod bits*", respectively.

2.1.4 Performance Metrics

Energy efficiency, data-rate and detection complexity are the metrics used to evaluate the performance of OFDM-IM.

Data Rate

Ignoring the effect of CP, the maximum data-rate of OFDM-IM is given by

$$\eta = b + d = \frac{1}{N}\left(K \log_2 M + \left\lfloor \log_2 \binom{N}{K} \right\rfloor\right) \text{ bits/s/Hz.} \tag{2.2}$$

Energy Efficiency

In OFDM-IM, the number of active subcarriers is such that $1 \leq K < N$. Therefore, two transmit-power management policies (PSP and PRP) can be used, resulting in different energy efficiency as detailed below.

- *Power Saving Policy*: In PSP, the complex entries on the active subcarriers are kept unchanged and, therefore, $E\{\mathbf{s}\ \mathbf{s}^H\} = LK$. When used in conjunction with PSP, the maximum energy efficiency of OFDM-IM, in terms of transmitted bits per joule, is given by

$$\text{EE}^{\text{PSP}} = \frac{N\ \eta}{K\ P_{\text{t}}} \text{ bits/J.} \tag{2.3}$$

- *Power Reallocation Policy*: Adopted in the literature on IM (cf. [5–7]), the K complex entries formed by $d = K \log_2 M$ *mod bits* in PRP is scaled by a factor of $\sqrt{\frac{N}{K}}$ to ensure $E\{\mathbf{s}\ \mathbf{s}^H\} = LN$. The ensuing energy efficiency of this policy is given by

$$\text{EE}^{\text{PRP}} = \frac{\eta}{P_{\text{t}}} \text{ bits/J.} \tag{2.4}$$

Detection Complexity

According to (4.4), the overall detection complexity of OFDM-IM is given by $\delta^{\text{ML}} = f(\text{ML}) + f(M)$, where $f(\text{ML})$ is the total number of complex operations (additions and multiplications) per sub-

carrier for estimating $[\widehat{\mathbf{i}}^{(l)}, \widehat{\mathbf{s}}^{(l)}]$ in (4.4), and $f(M)$ is the demodulation complexity per subcarrier, given by $f(M) = M$ [7]. The point-wise complex multiplication $\mathbf{h}^{(l)}\mathbf{s}^{(l)}$ in (4.4) requires $4N$ multiplications and $2N$ additions, while the complex subtraction $\mathbf{y}^{(l)} - \mathbf{h}^{(l)}\mathbf{s}^{(l)}$ requires $2N$ operations. Thus, a total of $8N$ operations per row of the code-book, $8NR = 8N\binom{N}{K}M^K$ operations per group, and $8\binom{N}{K}M^K$ operations per subcarrier, are required to estimate $\widehat{\mathbf{i}}^{(l)}$ and $\widehat{\mathbf{s}}^{(l)}$. Therefore, the overall complexity per subcarrier is given by

$$\delta^{\mathrm{ML}} = 8\binom{N}{K}M^K + \frac{KM}{N}. \tag{2.5}$$

2.1.5 Myths and Realities of OFDM-IM

In the literature [3–8, 14, 15, 26, 27], it is widely believed that the data-rate of OFDM-IM is less than that of OFDM, $\eta < \eta_{\mathrm{c}}$, due to the partial utilization of the N available subcarriers for symbol transmission, i.e., $K < N$. Also, it is believed that the $\eta_{\mathrm{c}} - \eta$ gap increases further as M increases [4]. Therefore, according to (2.4), the energy efficiency of OFDM-IM under PRP is always less than the energy efficiency of classical OFDM, i.e., $\mathrm{EE}^{\mathrm{PRP}} < \mathrm{EE}_{\mathrm{c}}$. Also, the energy efficiency under PSP is only higher than that of OFDM when $\frac{N}{K} \geq \frac{\log_2 M}{\eta}$.

According to (2.2)-(2.5), the data-rate, energy efficiency under PSP, energy efficiency under PRP, and the detection complexity, depend on the choice of the resources parameters, i.e., N, K and M. Hence, inefficient selection of (N, K, M) in OFDM-IM leads to poor data-rate and energy efficiencies with high detection and implementation complexity. In [28], the authors resolved the minimum complexity condition of IM in a MIMO setting using $K = M = 1$.[4]

In reality, the working principle of OFDM-IM is such that each subcarrier can take one out of $M+1$ complex realizations, where the additional realization/constellation point is $0+0j$. Hence, the concept of OFDM-IM technique is similar to the use of $(M+1)$-ary APM. Therefore, the data-rate in (2.2) can be upper bounded by $\eta \leq \log_2(M+1)$. The concept of classical OFDM fails to map $\log_2(M+1)$ bits into a complex symbol at a given subcarrier, considering $(M+1) \neq 2^r; r \in \mathbb{Z}^+$. This enforces the significance of OFDM-IM, which has the ability of mapping $0 \leq (b+d) \neq \mathbb{Z}^+ \leq \log_2(M+1)$ bits to any given subcarrier. However, inefficient selection of the resource elements

[4] In SSK [28], the $d = \log_2 N$ *index bits* are solely transmitted through the index of a single active antenna, i.e., $K = 1$, without any symbol transmission, i.e., $M = 1$, which is equivalent to having the choice of resources $(N, 1, 1)$.

(N, K, M), which is vastly the case in the available literature, has vilified IM-based techniques in terms of data-rate, i.e., $\eta < \log_2 M$.

In the next section, minimum conditions on the resources parameters (N, K, M) and expressions for the required N and K are derived to enhance the data-rate and, hence, the energy efficiency of OFDM-IM beyond classical OFDM. The scheme implementing the obtained conditions on (N, K, M) for a target data-rate is the so-called OFDM-IIM.

2.1.6 Index Modulation Techniques in Other Domains

The concept of IM has also found application in other communication domains, including the time-slot domain as detailed in the single-carrier IM system (SC-IM) presented in [6], the space domain of MIMO (cf. generalized spatial modulation (GSM) [7]), the beamspace level of MIMO [25], and the code domain of direct-sequence spread spectrum (DSSS) (cf. code-index modulation (CIM) [8]). At the transmitter, the working principle of OFDM-IM, GSM, CIM, and SC-IM are identical in terms of mapping $b+d$ (*index bits + mod bits*) to K active resource elements out of the N available elements. The resource elements are antennas in GSM, codes in CIM, and time-slots in SCIM. At the receiving end, detection and de-mapping of the $b + d$ bits in GSM, CIM and SC-IM, is also identical to the OFDM-IM detection in (4.4).

The data-rate, energy efficiency, and detection complexity, per resource element of GSM, CIM, and SC-IM, is equal to (2.2), (2.3), (2.4), (2.5). This paper's techniques and guidelines in the form of OFDM-IIM and OFDM-GIM are equally applicable to SC-IM, GSM, and CIM, to overcome the data-rate limitations of spatial multiplexing (SMx), DSSS, and SC system, respectively, with improved energy efficiency performance.

2.2 OFDM with Improved Index Modulation

2.2.1 data Rate

The transmitter architecture illustrated in Fig. 2.1, its working principle, corresponding detection (4.4), and the performance metrics defined in (2.2)-(2.5) for conventional OFDM-IM, are equally

applicable to OFDM-IIM. The difference between both schemes lies in the use of the resources elements (N, K, M).

We formulate the following problem to realize the gains of OFDM-IIM.

$$\text{Maximize} \quad \eta \tag{2.6a}$$

$$\text{s.t.} \quad \log_2 M \leq \eta \leq \log_2(M+1) \tag{2.6b}$$

$$N, K \in \mathbb{Z}^+. \tag{2.6c}$$

According to Appendix A.1, the following conclusions can be drawn.

- When $N < M$, the maximum data-rate of OFDM-IM is less than that of classical OFDM.
- When $M \leq N < 2M$, the maximum data-rate of OFDM-IM equals that of classical OFDM.
- When $N \geq 2M$, the maximum data-rate of OFDM-IM is greater than that of classical OFDM.

In conclusion, Appendix A.1 proves that OFDM-IM has the ability to outclass the data-rate of classical OFDM, when following proper design guidelines.

2.2.2 Energy Efficiency

The energy efficiency expressions of OFDM-IIM under PSP and PRP are similar to OFDM-IM, respectively given by (2.3) and (2.4). As OFDM-IIM enables $\eta \geq \log_2 M$ (cf. Proposition 3), it can be concluded that its energy efficiency under both power management policies (PSP and PRP) is higher than that of classical OFDM. Also, according to (2.4) and (A.3b), the upper limit on the energy efficiency of OFDM-IIM under PRP, i.e., $\text{EE}^{\text{PRP}} = \frac{1}{P_\text{t}} \log_2(M+1)$ bits/J, can be achieved by further increasing N beyond $2M$.

2.2.3 Detection Complexity

According to Proposition 3 and Eq. (2.5), the data-rate and energy efficiency enhancement with OFDM-IIM, especially at higher values of M, will significantly increase the overall detection complexity due to the use of $N \geq 2M$.

Finally, it is concluded that OFDM-IIM achieves the gains in data-rate and energy efficiency at the cost of higher detection complexity. Further reducing of the subcarrier's group size N such that the data-rate and energy efficiency limit of classical OFDM, i.e., $\log_2 M$ bits/s/Hz and $\mathrm{EE_c}$ bits/J, is surpassed, can reduce the overall detection complexity. Next, a high data-rate and energy efficiency achieving technique with considerably lower detection complexity as compared to OFDM-IIM is proposed.

2.3 OFDM with Generalized Index Modulation

In OFDM-GIM, each of the L groups is allowed to activate a variable number of subcarriers, i.e., $0 \leq i \leq N_\lambda$. The possible active subcarriers in a pattern are sorted out as $[N_\lambda, N_\lambda - 1, \cdots, 0]$, for which $[1, \binom{N_\lambda}{N_\lambda - 1}, \cdots, 1]$ number of such patterns exists, resulting in $m_\lambda = \sum_{i=0}^{N_\lambda} \binom{N_\lambda}{i} = 2^{N_\lambda}$ distinct patterns/realizations. Hence, $b_\lambda = N_\lambda$ *index bits* can be used to select a pattern, while $d_\lambda = K_\lambda \log_2 M = \frac{N_\lambda}{2} \log_2 M$ *mod bits* are loaded on the active subcarriers after being mapped through M-ary APM, where K_λ denotes the average number of active subcarriers per group out of N_λ subcarriers, given by $K_\lambda = \frac{N_\lambda}{2}$ for $m_\lambda = 2^{N_\lambda}$. This setup results in an average data-rate of $\eta_\lambda = 1 + 0.5 \log_2 M$ bits/s/Hz, which is higher, equal, or less than classical OFDM system when $M = 2$, $M = 4$ or $M \geq 8$, respectively. A similar structure to OFDM-GIM is reported in [29]. The main difference between [29] and OFDM-GIM lies in the activation pattern of the subcarriers. Next, based on the activation pattern of the subcarriers, two variants of OFDM-GIM are designed for achieving high data-rate and energy efficiency.

2.3.1 OFDM-GIM$_1$; Design Tailored for High Data Rate

The main purpose of OFDM-GIM$_1$ ($\lambda = 1$ in Fig. 2.1) is to achieve higher data-rate and energy efficiency than OFDM with reduced detection complexity as compared to OFDM-IIM. This also means that this scheme is used to overcome the limitation of $\eta_1 < \log_2 M$ for $M \geq 8$ in the main concept of OFDM-GIM.

To proceed further, we introduce a design parameter B_1, such that $1 < B_1 \in \mathbb{Z}^+ \leq N_1 + 1$, and only use the patterns having active subcarriers $[N_1, N_1 - 1, \cdots, N_1 - B_1 + 1]$ for any given B_1. [5]

[5]The design parameter B_1 also has an effect on the detection complexity as will be discussed later in Section A.4.

For instance, when $B_1 = 3$, then all the patterns having N_1, $N_1 - 1$, and $N_1 - 2$ active subcarriers are used, while the remaining patterns are discarded. The total number of patterns formed by a chosen N_1 and B_1 is given by

$$m_1 = \sum_{i=N_1-B_1+1}^{N_1} \binom{N_1}{i}. \tag{2.7}$$

In particular, when $B_1 = 1$, only one pattern, i.e., $m_1 = \binom{N_1}{N_1} = 1$ exists, having $i = N_1$ active subcarriers, with $b_1 = \lfloor \log_2 m_1 \rfloor = 0$ *index bits* and $d_1 = N_1 \log_2 M$ *mod bits*, which results in a data-rate of $\eta_1 = \eta_{\mathrm{c}} = \log_2 M$ bits/s/Hz with energy efficiency $\frac{\log_2 M}{P_{\mathrm{t}}}$ bits/J. Thus, the operation of OFDM-GIM$_1$ with $B_1 = 1$ becomes similar to classical OFDM, making the latter a special case of the former.

The expression in (2.7) for a given (N_1,B_1) pair does not always result in a total of 2^r patterns, $r \in \mathbb{Z}^+$. For instance, $(N_1, B_1) = (4, 3)$ results in a total of $m_1 = 11$ patterns. We discard three patterns of length $i = N_1 - B_1 + 1 = 2$ to satisfy the $m_1 = 2^r$ condition, and also maximize the average active subcarriers, i.e., K_1. As such, out of the total $\binom{N_1}{N_1-B_1+1} = \binom{4}{2} = 6$ patterns, only $11 - \sum_{i=N_1-B_1+2=3}^{N_1=4} \binom{N_1}{i} = 3$ patterns are required. For a given B_1, the required number of patterns having $i = N_1 - B_1 + 1$ active subcarriers is

$$\kappa_1 = 2^{b_1} - \sum_{i=N_1-B_1+2}^{N_1} \binom{N_1}{i}. \tag{2.8}$$

Using (2.8), the average number of active subcarriers K_1 for a given (N_1, B_1) pair is

$$K_1 = \frac{1}{2^{b_1}} \left[\sum_{i=N_1-B_1+2}^{N_1} i \binom{N_1}{i} + \kappa_1 (N_1 - B_1 + 1) \right], \tag{2.9}$$

where $\frac{1}{2^{b_1}} \binom{N_1}{i}$ is the occurrence probability of a pattern with $N_1 - B_1 + 1 < i \leq N_1$ active subcarriers, and $\frac{1}{2^{b_1}} \kappa_1$ is the occurrence probability of a pattern with $i = N_1 - B_1 + 1$ active subcarriers. The data-rate expression after formulation of K_1 and b_1 is straightforward, given by

$$\eta_1 = \frac{1}{N_1} \left(K_1 \log_2 M + b_1 \right) \quad \text{bits/s/Hz}, \tag{2.10}$$

where, as aforementioned, $b_1 = \lfloor \log_2 m_1 \rfloor$. The upper bound on (2.10), η_1^{up}, is obtained by setting $b_1 = \log_2 m_1$. Similar to (2.2), (2.3), (2.4), and (2.5), the choice of N_1 and B_1 affects the overall data-rate, energy efficiency under PSP, energy efficiency under PRP, and detection complexity performance of OFDM-GIM$_1$.

In the Appendix A.2, we determine optimal (N_1, B_1) in terms of low complexity, high data-rate, and high energy efficiency, under the constraint $\eta_1 \geq \log_2 M$. Based on Appendix A.2, the following can be concluded.

Low Complexity Conditions

According to (A.15a) and (A.15b), the low complexity conditions are $N_1 = 1$ when $M \leq 4$, and $N_1 = M - 1$ when $M > 4$. It is worth recalling that OFDM-IIM (cf. Proposition 3) requires a minimum of $N = 2M$ subcarriers per group to overcome the $\log_2 M$ bits/s/Hz limit, whereas OFDM-GIM$_1$ requires a group of $N_1 = M - 1$ subcarriers to achieve similar data-rate. Therefore, under similar data-rate requirements, it can be concluded that $N > N_1$, $K > K_1$, $\binom{N}{K} > N_1 + 1$, and $M^K > M^{K_1}$, which concludes that OFDM-GIM$_1$ is expected to achieve lower detection complexity compared to OFDM-IIM for a given data-rate requirement.[6]

Data Rate

In Appendix A.2.2, it was observed that the data-rate of OFDM-GIM$_1$ increases with increasing B_1 and/or B_1 and reaches the limit $\log_2(M + 1)$ bits/s/Hz, which is higher than the data-rate performance of classical OFDM.

Energy Efficiency

In Appendix A.2.3, the minimum conditions for $\max(\mathrm{EE}_1^{\mathrm{PSP}})$ and $\min(\delta_1^{\mathrm{ML}})$ are derived as (A.17)

$$\begin{cases} N_1 = 1, & \text{if } M < 8, \\ N_1 = M - 1, & \text{if } M \geq 8. \end{cases} \tag{2.11}$$

The high energy efficiency and low detection complexity conditions presented in (A.17) for the case of PSP are equally applicable to PRP. In particular, when ignoring the minimum complexity condition, the maximization of $\mathrm{EE}_1^{\mathrm{PRP}}$ becomes similar to the analysis presented in Section A.2.2.

[6]The complexity of OFDM-GIM$_1$ will be extensively discussed in Section A.4.

2.3.2 OFDM-GIM$_2$; Design Tailored for High Energy Efficiency

The main purpose of this scheme ($\lambda = 2$ in Fig.2.1) is to achieve higher energy efficiency by maximizing $\frac{N_2}{K_2}$ for a target data-rate η_{target}, where N_2 is the subcarriers group size and K_2 is the average number of active subcarriers per group. This is expected to yield more transmit power savings per group under PSP, hence making OFDM-GIM$_2$ more suitable for battery-constrained low data rate communications.

First, an integer design parameter B_2, with $1 < B_2 < N_2$, is selected, and patterns of $[1, \cdots, B_2]$ active subcarriers are preferred to use. Accordingly, the total number of patterns formed by OFDM-GIM$_2$ for any given N_2 and B_2 is $m_2 = \sum_{j=1}^{B_2} \binom{N_2}{j}$, where the maximum length of a pattern is B_2. Similar to OFDM-GIM$_1$ (cf. Eq. (2.8)), we make use of only κ_2 out of the total m_2 patterns to minimize K_2 and, hence, maximize $\frac{N_2}{K_2}$. Here, $\kappa_2 = 2^{b_2} - \sum_{j=1}^{B_2-1} \binom{N_2}{j}$. An approach similar to the one employed in obtaining (2.9) is used to calculate the average number of active subcarriers in a group, yielding

$$K_2 = \frac{1}{2^{b_2}} \left[\sum_{j=1}^{B_2-1} j \binom{N_2}{j} + B_2 \kappa_2 \right]. \tag{2.12}$$

The data-rate expression is similar to (2.10), and is given by (2.13) where $b_2 = \lfloor \log_2 m_2 \rfloor$.

$$\eta_2 = \frac{1}{N_2} \left(K_2 \log_2 M + b_2 \right) \quad \text{bits/s/Hz}. \tag{2.13}$$

2.4 Detection and Complexity Analysis

The detection and complexity analysis of OFDM-IM, OFDM-IIM, OFDM-GIM$_1$ and OFDM-GIM$_2$ is presented in Appendix A.4. Particularly, a maximum likelihood detector in Appendix A.4.1 and a low-complexity detector in Appendix A.4.2 are proposed. It was concluded that the proposed low-complexity detector in Appendix A.4.2 achieves significantly smaller detection complexity as compared to optimal maximum likelihood detection in Appendix A.4.1.

2.5 Performance Analysis

BER performance analysis of OFDM-IM, OFDM-IIM, OFDM-GIM$_1$ and OFDM-GIM$_2$ in a Nakagami fading channel under the assumption of multiple antenna reception is drawn in Appendix A.5

2.6 Comparative Results and Practical Applications

Now, we present numerical results for the BER, achievable rate, and energy efficiency performance. For simplicity, we assume $P_{\mathrm{t}} = \log_2 M$ W, so that the energy per bit $E_{\mathrm{b}} = \frac{E_{\mathrm{s}}}{\log_2 M} = 1$J, where E_{s} is the symbol energy. As per the assumptions, a classical OFDM system can achieve a maximum rate of $\eta_{\mathrm{c}} = \log_2 M$ bits/s/Hz, with a maximum energy efficiency $\mathrm{EE}_{\mathrm{c}} = 1$ bit/J. Throughout the rest of the paper, the triplets pertaining to the plots of OFDM-IM and OFDM-IIM denote (N, K, M), whereas in OFDM-GIM$_1$ they represent (N_1, B_1, M). First, a comparison of the BER performance of OFDM-IIM and OFDM-GIM against classical OFDM is presented.

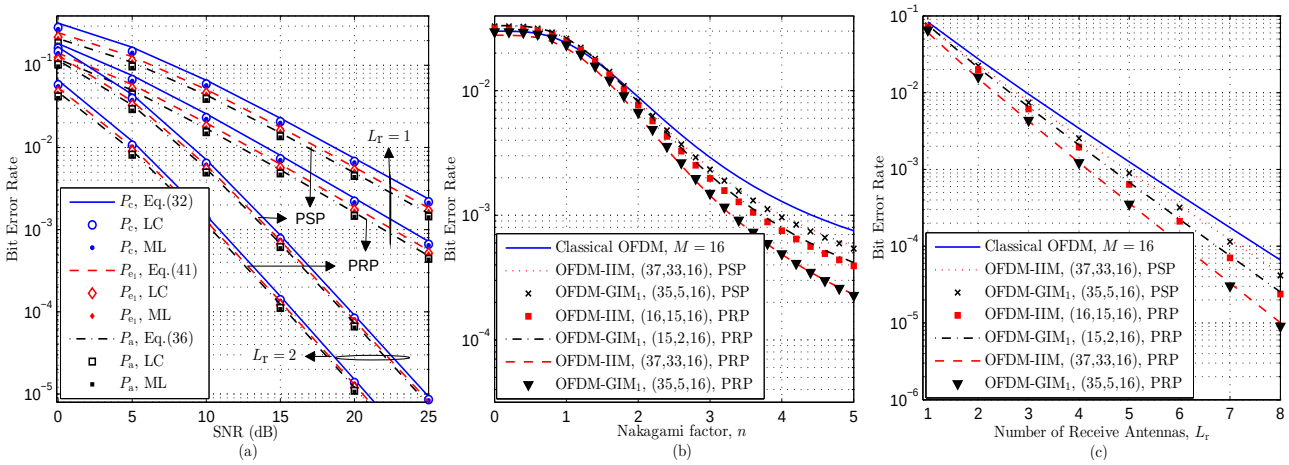

Figure 2.2: BER performance comparison: (a) OFDM-GIM$_1$ with $(N_1, B_1, M) = (2, 3, 2)$ under ML and LC detectors; (b) BER versus Nakagami factor n at 18 dB SNR using $L_{\mathrm{r}} = 1$ receive antenna; (c) BER versus L_{r} at 10 dB SNR and $n = 3$.

2.6.1 Bit Error Rate

Figure. 2.2(a) depicts a comparison of P_{a} (A.27), P_{c} (A.23), and $P_{\mathrm{e_1}}$ (A.32), against Monte-Carlo simulation results to show the effectiveness of the derived expressions. BER performance results in a Rayleigh flat-fading environment ($n = 0$) are compared for $(N_1, B_1, M) = (2, 3, 2)$. The theoretical and simulation results for the error rates P_{a}, P_{c}, and $P_{\mathrm{e_1}}$ closely match under ML and LC detectors for different values of the number of receive antennas L_{r}, confirming the derived expressions. The BER results were also verified for OFDM-IIM and OFDM-GIM$_2$. Next, the BER performance of OFDM-IIM and OFDM-GIM$_1$ under PSP and PRP policies is compared to classical OFDM.

BER under Power Saving Policy

According to (A.27), under PSP policy, the error probability of classical OFDM P_{b} and the error probability of subcarrier activity P_{a} are such that $P_{\mathrm{b}} < P_{\mathrm{a}}$ for $M = 2$ and $P_{\mathrm{a}} < P_{\mathrm{b}}$ for $M > 4$. Therefore, as per (A.24), $P_{\mathrm{b}} < P_{\mathrm{e}_\lambda}$ for smaller values of the modulation level M. Using OFDM-IIM with $n = 0$ and $L = 1$ in (A.24), we found SNR losses of 3dB, 1.5dB, 0.5dB, and 0.2dB with OFDM-IIM against classical OFDM for $M = 2$, $M = 4$, $M = 16$, and $M = 64$, respectively. However, when increasing the Nakagami factor n and/or the number of receive antennas L_{r}, the difference $P_{\mathrm{b}} - P_{\mathrm{e}_\lambda}$ decreases and can even satisfy $P_{\mathrm{b}} - P_{\mathrm{e}_\lambda} < 0$ under PSP for higher values of M, as shown in Fig. 2.2(b-c), and thoroughly discussed as follows.

BER under Power Reallocation Policy

Figure 2.2(b) depicts the BER performance versus the Nakagami factor when $L_{\mathrm{r}} = 1$ receive antenna is used. Under better channels (higher values of n), the OFDM-IIM and OFDM-GIM$_1$ techniques can both surpass classical OFDM under PSP and PRP. Figure 2.2(c) depicts the BER for varying number of receive antennas L_{r}. The OFDM-IIM and OFDM-GIM$_1$ techniques can surpass classical OFDM, and their BER performance gain increase with an increasing number of receive antennas L_{r} and/or the Nakagami factor n. Smaller BER at higher values of n and/or L_{r} under PSP is due to the $\frac{b_\lambda}{N_\lambda \eta_\lambda} P_{\mathrm{a}}$ term in (A.24). Under PRP, the gains are partly due to the mentioned term in (A.24) and to the high transmit power related to the $\frac{N_\lambda}{K_\lambda}$ ratio. Next, the achievable rate and energy efficiency of OFDM-IIM and OFDM-GIM$_1$ in comparison to classical OFDM are discussed.

2.6.2 Achievable Rate and Energy Efficiency

The number of correctly estimated bits that can be recovered at a given subcarrier is considered as a measure of rate, given by $\xi_\lambda = \eta_\lambda \ (1 + P_{\mathrm{e}_\lambda} \log_2 P_{\mathrm{e}_\lambda} + (1 - P_{\mathrm{e}_\lambda}) \log_2 (1 - P_{\mathrm{e}_\lambda}))$ bits/s/Hz [30], and the energy efficiency is given by $E_\lambda = \frac{\xi_\lambda}{P_{\mathrm{t}}}$ bits/J. Both expressions are valid for OFDM-IIM and OFDM-GIM.

Remark 2

It is widely believed that IM techniques can surpass classical OFDM in terms of BER and achievable rate only when $M \leq 4$ [5, 13]. The OFDM-IIM and OFDM-GIM$_1$ techniques can also surpass classical OFDM for $M \leq 4$. For instance, at a target rate of 1 bit/s/Hz, we found that OFDM-GIM$_2$ with $(N_2, B_2, M) = (9, 3, 2)$ can achieve 2dB SNR gain, 50% higher rate, and 270% higher energy efficiency than classical OFDM. As per Proposition 3 and Eq. (A.15b), OFDM-IIM and OFDM-GIM$_1$ can surpass classical OFDM for all values of M. However, at higher values of M, gain in the rate performance of OFDM-IIM and OFDM-GIM$_1$ over classical OFDM is such that $\lim_{M\to\infty} \dfrac{\log_2(M+1) - \log_2 M}{\log_2 M} = 0$. Therefore, for smaller values of M, typically for $M \leq 16$, the rate and energy efficiency improvements in OFDM-IIM and OFDM-GIM$_1$ are dominated by η_λ, whereas for $M \geq 16$ the gains are dominated by P_{e_λ}. Next, the BER, achievable rate, and the energy efficiency performance of OFDM-IIM and OFDM-GIM$_1$ are evaluated for $M = 16$ and $M = 64$ to demonstrate their superiority over a classical OFDM system at higher values of M.

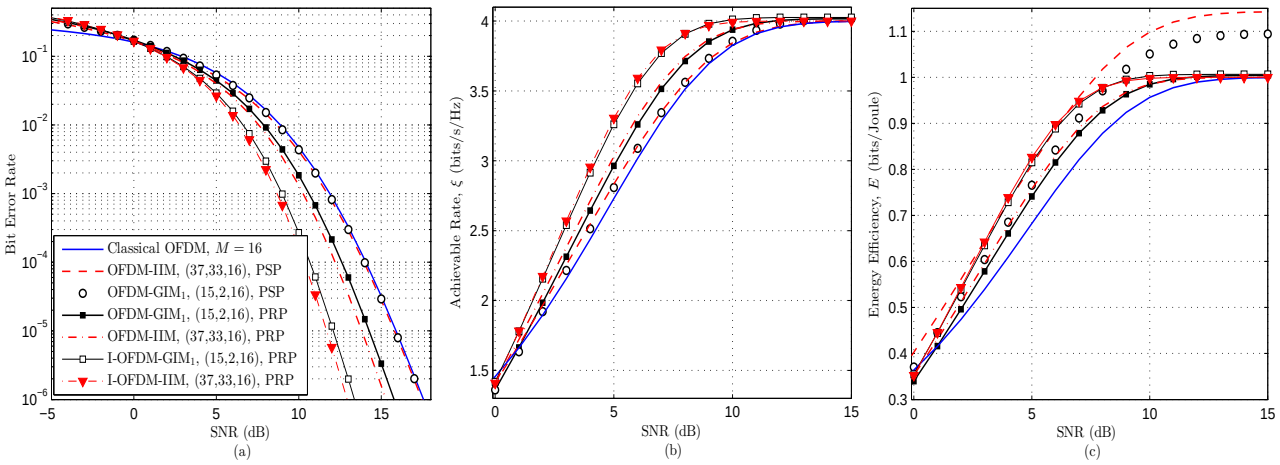

Figure 2.3: Performance comparison for $M = 16$ using $L_r = 4$ receive antennas and Nakagami factor $n = 2$: (a) BER, (b) Achievable rate, and (c) Energy efficiency (the legends of (b) and (c) are as in (a)).

2.6.3 Performance Comparison for Higher Modulation Levels

Figure 2.3(a) presents BER comparison of the considered IM techniques when $M = 16$. OFDM-IIM and OFDM-GIM$_1$ achieve slightly better BER compared to classical OFDM even under PSP. Under PRP, OFDM-GIM$_1$ and OFDM-IIM respectively achieve 2dB and 2.5dB SNR gains over

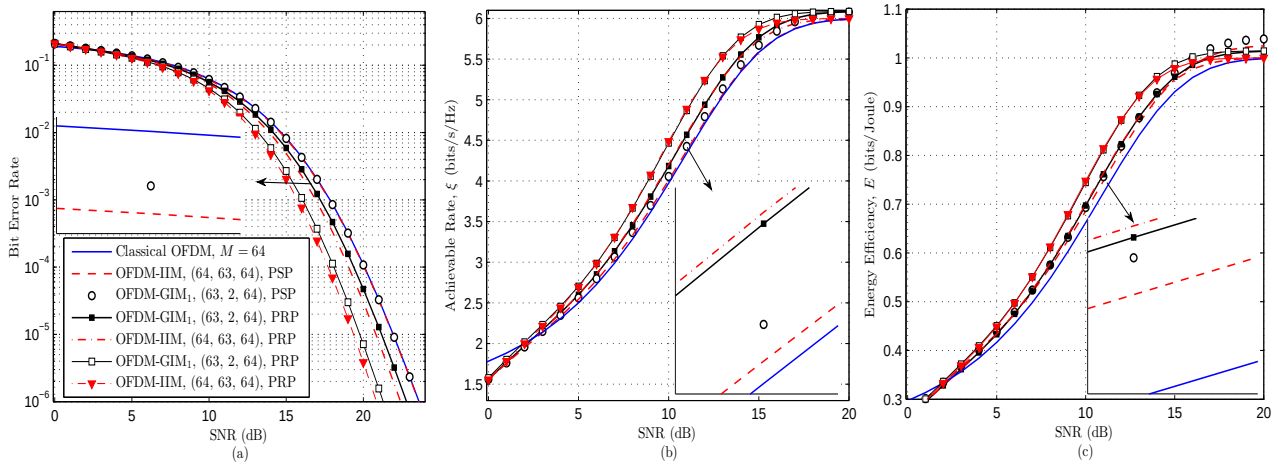

Figure 2.4: Performance comparison for $M = 64$ using $L_r = 4$ receive antennas and Nakagami factor $n = 2$: (a) BER, (b) Achievable rate, and (c) Energy efficiency (the legends of (b) and (c) are as in (a)).

classical OFDM at a BER of 10^{-5}. To exploit frequency diversity, we used interleaved subcarrier mapping originally proposed in the context of OFDM-IM in [24]. The OFDM-IIM and OFDM-GIM$_1$ techniques implementing interleaved subcarrier mapping are denoted by I-OFDM-IIM and I-OFDM-GIM$_1$, respectively. The I-OFDM-IIM and I-OFDM-GIM$_1$ techniques respectively achieve 4dB and 4.3dB SNR gain over classical OFDM at a BER of 10^{-5}. Fig. 2.3(b) shows the achievable rate results of the IM techniques considered in Fig. 2.3(a). First, OFDM-IIM and OFDM-GIM$_1$ can outperform classical OFDM even under PSP for SNR$\geq$ 1dB, thanks to their low BER and higher data-rate. Under PRP, OFDM-GIM$_1$ and OFDM-IIM achieve further improvements due to their 2dB and 2.5dB SNR gains over classical OFDM. The high rate performance of I-OFDM-IIM and I-OFDM-GIM$_1$ is the result of their smaller BER compared to the remaining techniques under study. Fig. 2.3(c) depicts the energy efficiency results of the IM techniques considered in Fig. 2.3(a) and Fig. 2.3(b). OFDM-IIM and OFDM-GIM$_1$ outperform classical OFDM due to their higher data-rate and smaller BER. Further gain in energy efficiency performance of OFDM-IIM and OFDM-GIM$_1$ can be achieved using PSP and/or I-OFDM-IIM and I-OFDM-GIM$_1$.

Figure 2.4(a) presents BER comparison of OFDM-IIM, I-OFDM-IIM, OFDM-GIM$_1$, and I-OFDM-GIM$_1$ against classical OFDM when $M = 64$. The OFDM-IIM and OFDM-GIM$_1$ techniques under PSP achieve slightly better BER as compared to OFDM. Under PRP, OFDM-GIM$_1$ and OFDM-IIM respectively achieve 1dB and 1.2dB SNR gain over OFDM. I-OFDM-GIM$_1$ and I-OFDM-IIM achieve 3dB and 3.1dB SNR gain over classical OFDM, respectively. Fig. 2.4(b) shows the rate performance of the techniques considered in Fig. 2.4(a). Thanks to the high data-

rate and low BER of OFDM-IIM, I-OFDM-IIM, OFDM-GIM$_1$, and I-OFDM-GIM$_1$, the considered techniques outperform classical OFDM for SNR>2dB. The energy efficiency performance is illustrate in Fig. 2.4(c). It can be observed that OFDM-IIM, I-OFDM-IIM, OFDM-GIM$_1$, and I-OFDM-GIM$_1$ achieve higher energy efficiency compared to classical OFDM.

The reported gains are obtained at the expense of detection complexity when using the ML detector. Detection complexities of OFDM-IIM and OFDM-GIM$_1$ under ML and LC detectors, with the resource parameters considered in Figs. 2.3 and 2.4 are provided in Table 2.1. The complexity of I-OFDM-IIM is equal to OFDM-IIM and that of I-OFDM-GIM$_1$ is equal to OFDM-GIM$_1$. Although the detection complexity of OFDM-GIM$_1$ under ML detector is significantly smaller compared to OFDM-IIM, it is still not computationally feasible in practical systems. Therefore, the LC detector and the methods of [31] can be employed for low complexity detections.

Tableau 2.1: Detection complexity of OFDM-IIM and OFDM-GIM$_1$ under ML and LC detectors in comparison with classical OFDM.

Technique	Design Vector	$\delta_\lambda^{\mathrm{ML}}$	$\delta_\lambda^{\mathrm{LC}}$
OFDM	1, 1, 16	144	144
$(N,\ K,\ M)$	1, 1, 64	576	576
OFDM-IIM	37, 33, 16	1.05×10^{47}	150.27
$(N,\ K,\ M)$	64, 63, 64	2.01×10^{118}	583
OFDM-GIM	15, 2, 16	1.78×10^{19}	151
$(N_1,\ K_1,\ M)$	63, 2, 64	9.77×10^{114}	583

2.6.4 Application of OFDM-IIM and OFDM-GIM in IEEE 802.11

IEEE 802.11ax can support 2048 subcarriers with $M = 1024$ and is focused on performance improvement in dense environments [32]. IEEE 802.11be is a new amendment that builds on IEEE 802.11ax targeting extremely high rates, with applications including remote office, cloud computing, augmented reality (AR), virtual reality (VR), and video calling [32]. Thanks to the less severe ICI [16], reduced PAPR [17, 18], higher rate and better reliability of the OFDM-IIM and OFDM-GIM$_1$ techniques, they can offer further performance enhancements in IEEE 802.11ax/be. The support for 2048 subcarriers and $M = 1024$ in IEEE 802.11ax/be aligns well with the minimum requirements of OFDM-IIM and OFDM-GIM$_1$ for achieving higher performance. Particularly, the B_1 design parameter of OFDM-GIM$_1$ can be used to adjust the desired number of active subcarriers for reducing ICI and PAPR in dense environments while still maintain the desired rate performance. The IEEE 802.11ay standard with advanced power savings as its key feature and a peak rate of 20 Gbps operating in 60 GHz is under development for ultra-short range communications [33]. The

use cases of IEEE 802.11ay include mobile offloading, office docking, fixed wireless, wearable devices, AR, and VR. Superior rate and reliability performances of OFDM-IIM and OFDM-GIM$_1$, especially in better quality channels, can further improve the rate and reliability performances of IEEE 802.11ay. Particularly, the two techniques can offer enhanced performances with improved power savings, especially under the PSP policy. Finally, the IEEE 802.11ba wake-up radio will serve as a switch for main radio in a smart home, warehouse, or wearable device, to improve the energy efficiency of stations. The wake-up radio part of IEEE 802.11ba is expected to consume less than one milliwatt power in an active state, and will make use of simple On-Off-Keying (OOK) modulation in a narrow bandwidth with short-range transmissions [34]. The low-rate and energy-efficient OFDM-GIM$_2$ also uses OOK modulation and is, therefore, an attractive candidate for the transmission of wake-up packets for turning on the main radio in IEEE 802.11ba.

2.7 Concluding Remarks

This chapter systematically studied the low data-rate problem of IM techniques. The proposed OFDM-IIM was shown to surpass classical OFDM under the constraint $N \geq 2M$ when properly selecting the design parameters (N, K, M). The OFDM-GIM$_1$ technique was shown to relax the $N \geq 2M$ condition of OFDM-IIM by half, as it only requires $N \geq M - 1$ subcarriers in a group to outperform classical OFDM. Unlike previous works, it was shown that OFDM-IIM and OFDM-GIM$_1$ can surpass classical OFDM even at a high-rate transmission. OFDM-GIM$_2$ was designed for low data-rate communications demanding superior energy efficiency performance. The concept of IIM, GIM and the proposed design guidelines, were shown to equally hold valid for IM techniques in other domains. The use of IIM and GIM in the space, code, and time domains can outclass the BER, achievable rate, and energy efficiency performance of conventional MIMO (SMx), DSSS, and SC systems. Furthermore, under equal rate requirement, the use of IIM can achieve savings of bandwidth in OFDM, antenna elements in MIMO, codes/bandwidth in DSSS, and time slots in a SC system. The use of GIM$_1$ allows to further relax the required conditions to achieve the mentioned gains in OFDM, MIMO, DSSS, and SC systems (cf. savings in the number of transmit and receive antennas in GSM over SMx [35]).

Chapter 3

Multiple Active Spatial Modulation: A Possibility of more than Spatial Multiplexing

3.1 Introduction

SM is a promising MIMO transmission technique, wherein a single RF chain is activated at the transmitter to radiate an M-APM symbol within a time slot [37]. By setting the number of active RF chains to unity ($N_{\mathrm{a}} = 1$), the well-known ICI and IAS problems of MIMO can be avoided [35,37], while the index of the active RF chain and the M-ary APM symbol are used to convey useful information to the receiver. Accordingly, SM can achieve higher data-rate than single-antenna systems but less than SMx, due to the $N_{\mathrm{a}} = 1$ operation principle [35,37]. Increasing the modulation level, M, and/or the number of transmit antennas, N_{t}, is one way of enhancing data-rate. This, however, comes at the expense of poor reliability, i.e. high BER, and extra cost and complexity, which limits the potential of SM to fully exploit the merits of MIMO in 5G and beyond.

Notable among the techniques proposed to improve performance in terms of data-rate are quadrature SM (QSM) [38] and GSM [7]. Their data-rate enhancement is the result of enlarging the spatial dimension using multiple RF chains, i.e. $1 < N_{\mathrm{a}} < N_{\mathrm{t}}$. However, the gains over

[0]The contents of this chapter are extracted from [36].

SM are still marginal compared to the performance of SMx. To achieve further gains in data-rate, GSM in [35], a.k.a. multiple active SM (MASM), is enabled to transmit N_{a} independent symbols with M-ary APM in a given time slot, using the available $1 < N_{\mathrm{a}} < N_{\mathrm{t}}$ RF chains. The flexible choice of N_{a} in MASM generalizes the concept of SM, and provides greater freedom to effectively trade between data-rate, energy efficiency, ICI, IAS, and detection complexity.

In MASM, the zero ICI and IAS condition is known, i.e. $N_{\mathrm{a}} = 1$ [37], but the choice of N_{t} and N_{a} to achieve higher data-rate is not yet resolved [35]. In [39], a suboptimal N_{a} for a fixed N_{t} and M is acquired using computer simulations to achieve performance gain in terms of data-rate. However, their use of a fixed N_{t} results in large N_{a} and large codebook size and, hence, higher detection complexity. Unlike [39], this paper formulates $\min(N_{\mathrm{t}},\, N_{\mathrm{a}},\, N_{\mathrm{r}})$ for a generalized M to prove that MASM can outperform the data-rate performance of SMx, also achieving further gains in energy efficiency, detection complexity, and the required $(N_{\mathrm{a}},\, N_{\mathrm{r}})$. This also enables MASM to reduce the extra cost of antenna elements, the ICI and IAS, the implementation complexity, and the space and power requirements, as compared to SMx. Furthermore, the paper highlights the low diversity problem of MASM, and proposes an enhanced MASM technique (E-MASM) capable of achieving superior data-rate and diversity tradeoff compared to SMx.

3.2 Multiple Active Spatial Modulation

Figure 3.1 illustrates the system model of MASM ($\nu = N_{\mathrm{a}}$) with N_{t} transmit and N_{r} receive antennas. At each time slot, a block of $b_1 + b_2$ bits enter the transmitter. The $b_1 = \lfloor \log_2 \binom{N_{\mathrm{t}}}{N_{\mathrm{a}}} \rfloor$ bits activate a set of $1 < N_{\mathrm{a}} < N_{\mathrm{t}}$ RF chains using a pre-defined mapping table. The b_2 bits are split into N_{a} streams, each of length $b_2^{(\nu)} = \log_2 M$ bits, then mapped through M-APM, and radiated using the N_{a} RF chains over a wireless channel characterized by the gain matrix $\mathbf{H} \in \mathbb{C}^{N_{\mathrm{r}} \times N_{\mathrm{t}}}$. The received signal of MASM is given by $\mathbf{y} = \sqrt{\frac{\rho}{N_{\mathrm{a}}}}\mathbf{H}\mathbf{x} + \mathbf{w}$, where ρ is the SNR at each receive antenna. The additive white Gaussian noise $\mathbf{w} \in \mathbb{C}^{N_{\mathrm{r}} \times 1}$ and the entries of $\mathbf{H}$ follow $\mathcal{CN}(0, 1)$. The transmit vector $\mathbf{x} \in \mathbb{C}^{N_{\mathrm{t}} \times 1}$ $(E(|\mathbf{x}|)^2 = 1)$ with N_{a} non-zero entries is drawn from a code-book $\mathbf{S}$ of size $2^{b_1} M^{N_{\mathrm{a}}/\alpha}$ ($\alpha = 1$ for MASM). At the receiver, the information encoded in $\mathbf{x}$ can be retrieved with the help of ML detection: $\widehat{\mathbf{x}} = \arg\min ||\mathbf{y} - \mathbf{H}\mathbf{x}||_{\mathrm{F}}^2$.

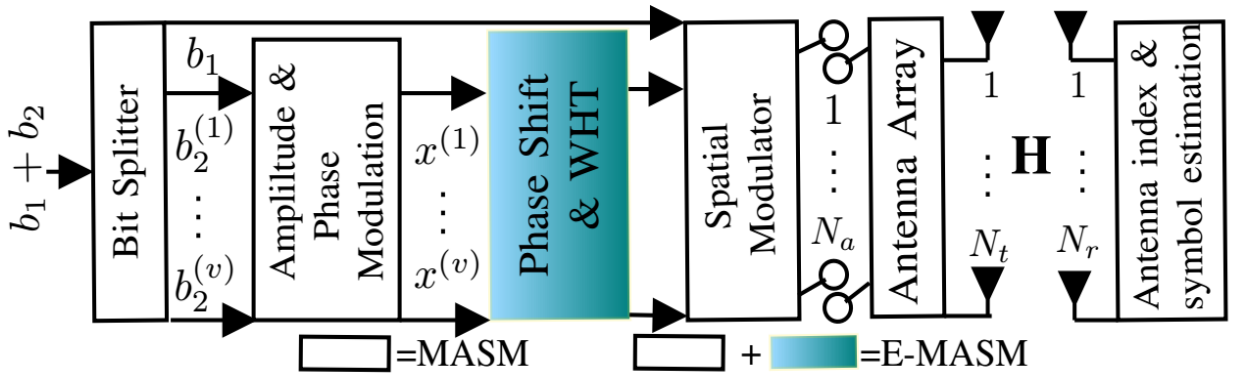

Figure 3.1: Block diagram of MASM and E-MASM techniques.

For $\rho = \infty$, $\mathbf{x} = \widehat{\mathbf{x}}$ and the MASM setup achieves a data-rate, energy efficiency, and ML detection complexity (in terms of complex operations), as shown in (3.1a), (3.1b) and (3.1c), respectively,

$$\eta = \left\lfloor \log_2 \binom{N_\mathrm{t}}{N_\mathrm{a}} \right\rfloor + N_\mathrm{a} \log_2 M \quad \text{bits/s/Hz}, \tag{3.1a}$$

$$\mathrm{EE} = \frac{\eta}{P_\mathrm{t}} \quad \text{bits/Joule}, \tag{3.1b}$$

$$\delta(\mathrm{ML}) = 2^{b_1} M^{N_\mathrm{a}/\alpha} N_\mathrm{r}(N_\mathrm{a} + 2), \tag{3.1c}$$

where P_t is the transmit power. As seen, the design parameters N_t and N_a dictate the achievable data-rate, energy efficiency, and detector's complex operations. Next, $\min(N_\mathrm{t}, N_\mathrm{a}, N_\mathrm{r})$ is formulated for constrained M in order to overcome the low data-rate and hence the low energy efficiency problem of MASM as compared to SMx.

3.3 Data Rate

Detailed design guidelines for data-rate enhancement of MASM techniques is presented in Appendix B.0.1, where the following was concluded.

- The maximum data-rate of MASM is less than spatial multiplexing when $N_\mathrm{t} < M$.
- The maximum data-rate of MASM equals the data-rate of sptial multiplexing when $M \leq N_\mathrm{t} < 2M$.

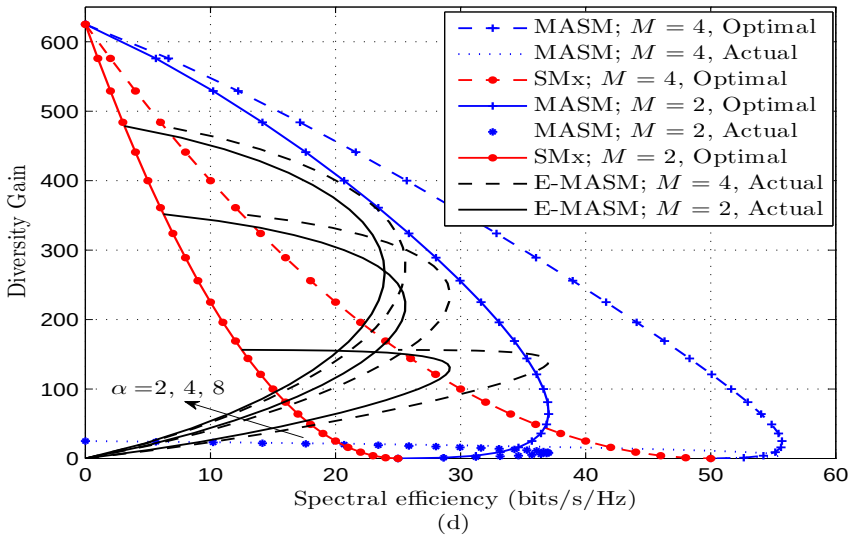

Figure 3.2: Data-rate/diversity tradeoff of SMx, MASM, and E-MASM.

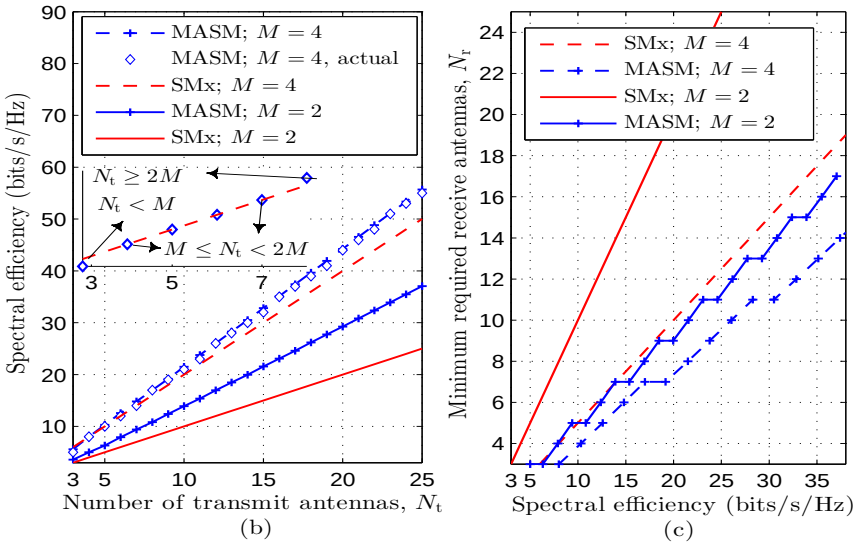

Figure 3.3: (b) SMx and MASM data-rate comparison for varying N_t, (c) Minimum required N_r vs. data-rate of SMx and MASM.

- The maximum data-rate of MASM is greater than the data-rate of spatial multiplexing when $N_t \geq 2M$.

Figure 3.3(b) compares the maximum achievable data-rate for $M = 2, 4$ and varying N_t. MASM is shown to achieve higher data-rate than SMx, with a gain that increases at higher values of N_t. The results under $N_t < M$, $M \leq N_t < 2M$ and $N_t \geq 2M$ confirm the theorems: MASM can achieve higher data-rate than SMx, or the same data-rate but with smaller N_t.

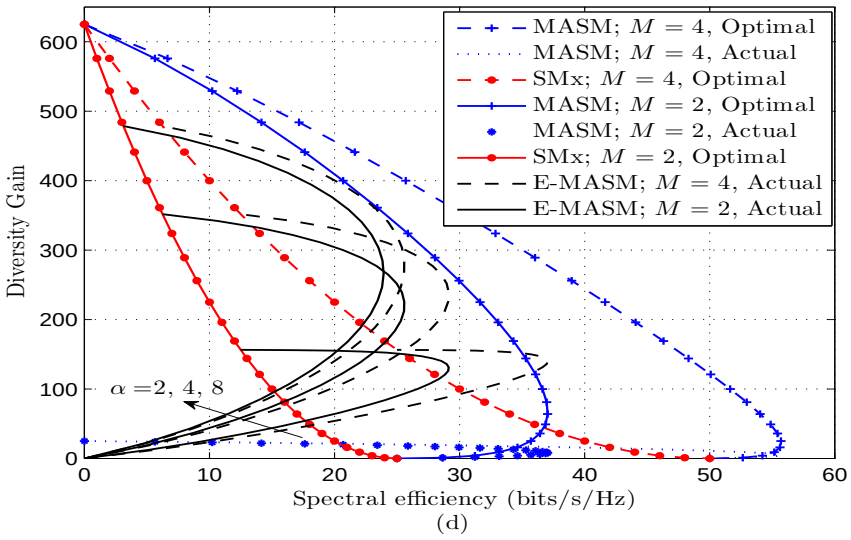

Figure 3.4: Data-rate/diversity trade-off of SMx, MASM, and E-MASM.

Figure 3.3(c) shows the minimum number of N_{r} or N_{a} for given data-rate requirement. MASM activates $N_{\mathrm{a}} < N_{\mathrm{t}}$ antennas and, hence, a minimum of N_{a} receive antennas is required, while SMx requires a minimum of N_{t} receive antennas. Thus, MASM can achieve similar data-rate performance to SMx but with smaller numbers of RF chains N_{a} and receive antennas N_{r}.

The use of $\min(N_{\mathrm{t}}, N_{\mathrm{a}}, N_{\mathrm{r}})$ also ensures the minimum size of code-book $\mathbf{S}$ for a target data-rate and/or energy efficiency. This enables the operation of MASM with minimal detection complexity under a given detection method (cf. (3.1c) for ML, and low-complexity MASM detection methods discussed in the reference list of [39]). The proposed design guidelines also provide a cost-effective, reduced ICI and IAS operation with fewer hardware units, aligning MASM with the requirements of 5G in general and uplink MIMO communications in particular.

3.3.1 Data Rate and Diversity Tradeoff

The optimal tradeoff between data-rate and diversity of a MIMO system is given by [40]:

$$d_{\mathrm{opt}}(r) = (N_{\mathrm{t}} - r)(N_{\mathrm{r}} - r), \quad 0 \leq r \leq \min(N_{\mathrm{t}}, N_{\mathrm{r}}). \tag{3.2}$$

MASM can achieve the same optimal tradeoff as (3.2) only if the silent antennas are rather used for transmission purpose, which is not realizable according to the operation principles of SMTs.

Therefore, the actual data-rate and diversity tradeoff of MASM is $N_{\mathrm{r}} - N_{\mathrm{a}}$, which is considerably smaller than (3.2).

Figure 3.4 plots such tradeoff performance for square SMx and MASM, with $N_{\mathrm{t}} = N_{\mathrm{r}} = 25$. As η for $N_{\mathrm{t}} \geq 2M$ is a first increasing and then decreasing function of N_{a}, multiple values of N_{a} can achieve similar data-rate and, hence, different diversity gains. Improving the low diversity of MASM motivates the proposal of the enhanced MSAM technique.

3.4 Enhanced Multiple Active Spatial Modulation (E-MASM)

In E-MSAM (cf. Fig. 3.1), the $b_1 = \lfloor \log_2 \binom{N_{\mathrm{t}}}{N_{\mathrm{a}}} \rfloor$ bits are used to activate N_{a} antennas and are divided into $\nu = \frac{N_{\mathrm{a}}}{\alpha}$ groups each having $1 \leq \alpha \leq N_{\mathrm{a}}$ active antennas, with α being a power of two. Active antennas in a group transmit the same data symbol, while the $\frac{N_{\mathrm{a}}}{\alpha}$ groups transmit independent symbols and, as such, $\hat{b_2} = \frac{N_{\mathrm{a}}}{\alpha} \log_2 M$. Walsh-Hadamard transform (WHT) is used to rearrange the constellation points for robustness against fading [41]. Without loss of generality, operation of the k^{th} group, $1 \leq k \leq \frac{N_{\mathrm{a}}}{\alpha}$, is discussed. Let $\mathbf{x}_k \in \mathbb{C}^{\alpha \times 1}$ be an α-length vector of similar entries. The phases of these entries are shifted according to $\overline{\mathbf{x}}_k = \mathbf{G}\mathbf{x}_k^{\mathrm{T}}$, where $\mathbf{G}$ is a diagonal matrix of order α with elements given by $\exp\left(\frac{j(i-1)2\pi}{M\alpha}\right)$, $i = 1, \cdots, \alpha$, when using M-ary PSK modulation. These elements for APM with $M \geq 8$ can be obtained via extensive search as shown in Table 1 of [35]. The significance of such phase shift is revealed later in this section. The WHT on $\overline{\mathbf{x}}_k$ is performed according to $\underline{\mathbf{x}}_k = \frac{1}{\sqrt{\alpha}} \Omega_\alpha \overline{\mathbf{x}}_k$, where $\frac{1}{\sqrt{\alpha}}$ is the normalization factor, and $\Omega_\alpha = \begin{bmatrix} \Omega_{\frac{\alpha}{2}} & \Omega_{\frac{\alpha}{2}} \\ \Omega_{\frac{\alpha}{2}} & -\Omega_{\frac{\alpha}{2}} \end{bmatrix}$, with $\Omega_1 = [1]$. After the WHT operation, the original symbols $\mathbf{x}_k$ are represented by their sum and differences, i.e. $\underline{\mathbf{x}}_k$. Hence, each symbol mutually carries the information of other $\alpha - 1$ symbols, and the equivalent channel after inverse-WHT at the receiver has a variance of α [41]. Without the phase shift operation, re-arrangement of the constellation points by the WHT operation could make $\alpha - 1$ symbols in $\underline{\mathbf{x}}_k$ equal to $0 + 0j$. Transmission of such symbols makes it impossible for the receiver to recognize the N_{a} active antennas, which can result in very high BER.

At the receiver, first an inverse WHT operation, i.e. $\overline{\mathbf{x}}_k = \frac{1}{\sqrt{\alpha}} \Omega_\alpha \underline{\mathbf{x}}_k$, followed by an inverse phase shift and ML detection take place. Overall, E-MASM can achieve a data-rate of $\hat{\eta} = b_1 + \hat{b_2}$ bits/s/Hz, an energy efficiency of $\frac{\hat{\eta}}{P_{\mathrm{t}}}$ bits/J, and a tradeoff between data-rate and diversity of $d^{\mathrm{E}}_{\mathrm{opt}}(N_{\mathrm{a}}, \alpha) = \left(N_{\mathrm{a}} - \frac{N_{\mathrm{a}}}{\alpha}\right)\left(N_{\mathrm{r}} - \frac{N_{\mathrm{a}}}{\alpha}\right)$.

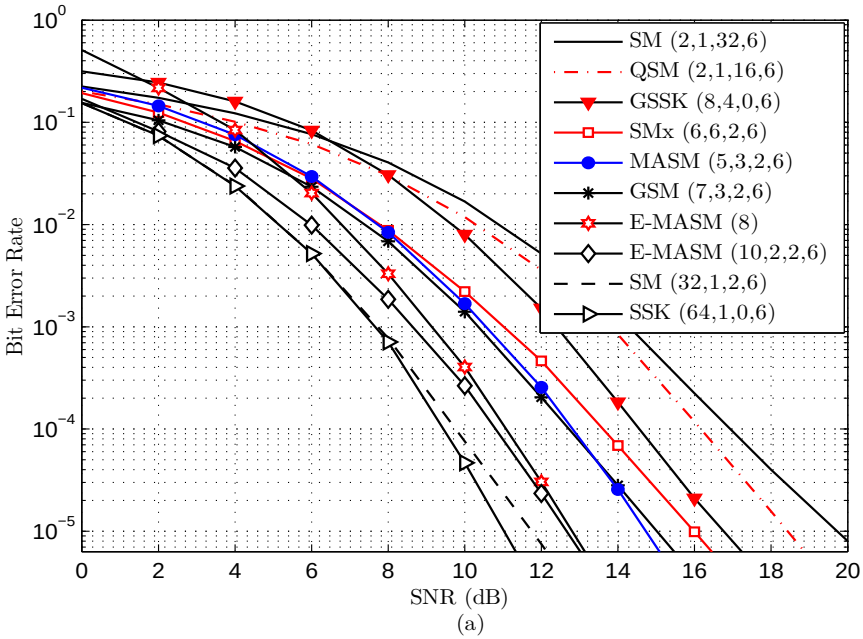

Figure 3.5: BER vs. SNR for 6 bits/s/Hz rate: Quadruplets pertain to $(N_{\mathrm{t}}, N_{\mathrm{a}}, M, N_{\mathrm{r}})$**.**

Figure 3.4 illustrates the data-rate and diversity tradeoff. E-MASM can also achieve the same data-rate for multiple values of N_{a} and, therefore, can achieve different diversity gains for a given data-rate. The figure shows that E-MASM offers better diversity gain than conventional SMx at some values of the data-rate.

3.5 Comparative Results and Discussions

As of now, the data-rate of MASM and E-MASM has been analyzed under the assumption of very high SNR, i.e. $\rho = \infty$, which may question the promising high diversity of E-MASM and the achievable data-rate of MASM. Next, we make use of an upper bound on the BER to show the merits of the proposed E-MASM in comparison to SM [37], MASM [35], SMx, QSM [38], GSM [7], space shift keying (SSK) [9, p. 36], generalized SSK (GSSK) [9, p. 39], for fixed transmission rate. Then, similar BER measurements are used to compare the achievable data-rate of these techniques for constrained numbers of transmit antennas N_{t} and modulation order M.

Bit Error rate

The BER performance of SMTs with $N_{\mathrm{a}} > 1$, i.e. MASM, E-MASM, GSM and SMx, is evaluated in Appendix. B.0.2. The results are presented as follows. Figure 3.5 shows the BER of the systems under comparison for 6 bits/s/Hz rate. Firstly, a 7dB SNR difference is observed between the two SM configurations, sub-optimal SM(2,1,32,6) and optimal SM(32,1,2,6), at a BER of 10^{-4}. The minimum BER with SMTs is only realizable at $\max(N_{\mathrm{t}})$, $\min(N_{\mathrm{a}})$, and $\min(M)$ (cf. SSK(64,1,0,6) in Fig. 3(a)). Secondly, the proposed E-MASM with $\alpha = 2$ achieves closer BER performance to the optimal case SM(32,1,2,6) and SSK(64,1,0,6), with smaller number of transmit antennas N_{t}. At a BER of 10^{-5}, the SNR gain with E-MASM is 2dB over MASM and GSM, 2.5dB over SMx, 3.5dB over GSSK, 5.5dB over QSM, and 6dB over the sub-optimal SM(2,1,32,6).

Data Rate

The achievable data-rate of SMTs as a function of SNR (ρ) under constrained M is $R \leq \lambda(1 + P_{\mathrm{e}} \log_2 P_{\mathrm{e}} + (1 - P_{\mathrm{e}}) \log_2(1 - P_{\mathrm{e}}))$ bits/s/Hz [30], which under $P_{\mathrm{t}} = 1$ also represents the achievable energy efficiency given by R bits/J.

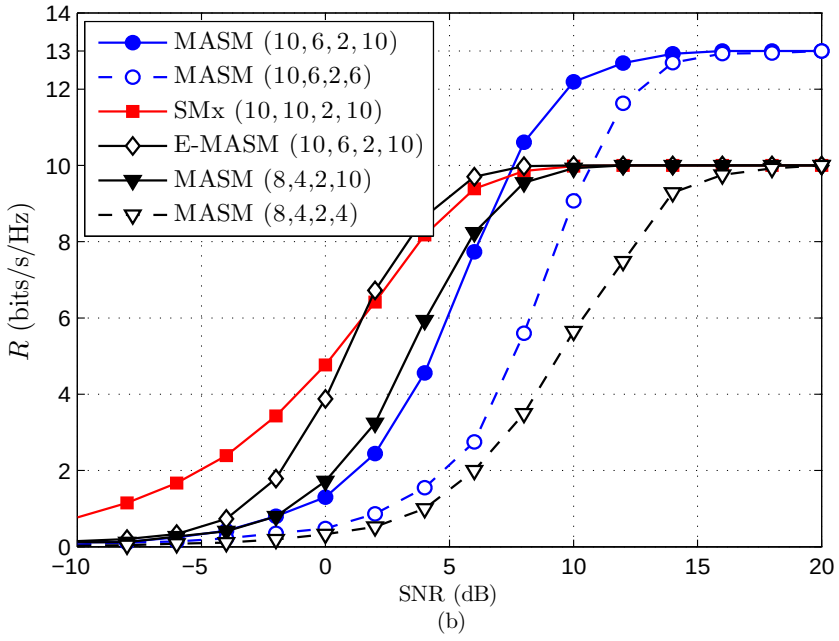

Figure 3.6: Achievable data-rate (R) vs. SNR. Quadruplets pertain to $(N_{\mathrm{t}}, N_{\mathrm{a}}, M, N_{\mathrm{r}})$.

Figure 3.6(b) presents the data-rate/energy efficiency versus SNR performance comparison. First, for $N_{\mathrm{t}} = 10$, the SM, GSM, SSK, GSSK and QSM techniques fail to achieve the 10 bits/s/Hz and 10 bits/J targets set by SMx and, as such, are excluded in the comparison. Second, MASM with (10,6,2,10) activates 4 less RF chains N_{a} than SMx, while still achieving 3 bits/s/Hz and 3 bits/J gains at higher SNRs. Similarly, MASM with (10,6,2,6) uses 4 less RF chains and 4 less receive antennas N_{r} than SMx, while still achieving 3 bits/s/Hz and 3 bits/J gains at higher SNRs. Third, the (8,4,2,10) and (8,4,2,4) configurations of MASM match the data-rate and energy efficiency performance of SMx at higher values of SNR but with fewer transmit antennas and RF chains. The latter configuration even requires 4 less receive antennas N_{r} compared to SMx. Finally, even if MASM cannot achieve similar data-rate to SMx at low SNR, the proposed E-MASM with $\alpha = 2$ is able to achieve higher data-rate than SMx for SNR greater than 2dB, thanks to its notable data-rate/diversity tradeoff.

In summary, this chapter first presented design guidelines to address the low data-rate problem of MASM. It proved that MASM requires fewer N_{a} and N_{r} to surpass the data-rate of SMx, or fewer N_{t}, N_{a} and N_{r} to match the said data-rate. MASM can deliver high data rates with fewer hardware units, low power and reduced ICI, IAS, cost, complexity, and device size, compared to SMx. Also, the data-rate and diversity tradeoff of conventional MIMO can be overcome by the proposed E-MASM technique.

Part II

Chapter 4

Space-time Mapping for Equiprobable Antenna Activation in Spatial Modulation

4.1 Introduction

The transmitter of a SM based communication system splits the information bits into two blocks, *index bits* and *modulated bits*, of length b and d, respectively. The $b = \log_2 N_\mathrm{t}$ number of *index bits* are used to activate one of the N_t available transmit antennas to radiate $d = \log_2 M$ number of *modulated bits* after mapping them through M-APM. Hence, an upper-bound on the achievable data-rate is given by

$$\overline{\eta}_{\mathrm{SM}} = b + d = \log_2 N_\mathrm{t} + \log_2 M \quad [\text{bits/s/Hz}]. \tag{4.1}$$

While the activation of a single transmit antenna in SM avoids the well-known inter-channel interference and inter-antenna synchronization problems associated with MIMO antenna configurations, the additional b *index bits* encoded in the spatial domain (index of an active transmit antenna) lead to enhancements in the data-rate [9, pp. 41].

[0]The contents of this chapter are extracted from [42].

Statement of the Problem: Firstly, consider the b bits gain in data-rate (cf. Eq. (4.1)). In practice, this gain is severely constrained by the number of transmit antennas, N_t. Two cases can be distinguished: $N_\mathrm{t} = 2^g$ and $N_\mathrm{t} \neq 2^g$, where $g \in \mathbb{Z}^+$. The two cases naturally occur with probability $P(N_\mathrm{t} = 2^g) = \frac{g}{2^g}$ and $P(N_\mathrm{t} \neq 2^g) = 1 - \frac{g}{2^g}$, respectively. When $N_\mathrm{t} = 2^g$, the upper-bound data-rate is shown in (4.1). When $N_\mathrm{t} \neq 2^g$, mapping a fractional number of $b = \log_2 N_\mathrm{t} \notin \mathbb{Z}^+$ *index bits* to the spatial domain in a given symbol period becomes challenging. Conventionally, $b = \lfloor \log_2 N_\mathrm{t} \rfloor$ *index bits* are used to ensure that $b \in \mathbb{Z}^+$ for choosing an active antenna in a given symbol period, where $\lfloor . \rfloor$ is the floor function. data-rate of SM when $N_\mathrm{t} \neq 2^g$ is given by

$$\eta_{\mathrm{SM}} = \lfloor \log_2 N_\mathrm{t} \rfloor + \log_2 M \quad [\text{bits/s/Hz}]. \tag{4.2}$$

From (4.1) and (4.2), it is clear that $\eta_{\mathrm{SM}} = \overline{\eta}_{\mathrm{SM}}$ when $N_\mathrm{t} = 2^g$, and $\eta_{\mathrm{SM}} < \overline{\eta}_{\mathrm{SM}}$ for all $N_\mathrm{t} \neq 2^g$.

Secondly, contrary to the case of $N_\mathrm{t} = 2^g$, in the more realistic case of $N_\mathrm{t} \neq 2^g$, SM activates the N_t available antennas with unequal probabilities. Such non-uniform activation increases with N_t, reaching almost 50% when $N_\mathrm{t} = 2^g - 1$, which results in a largely unequal protection of the transmitted bits, thus affecting the error rate performance. In general, the losses in data-rate and error rate performance, due to the unequal activation, increase with N_t. This limits the potential of SM in B5G, especially in massive-MIMO configurations, which motivated researchers to develop methods to overcome the said data-rate loss [43–45] and enable equiprobable activation [46].

Related Work: In [43], the M-APM constellation points in SM are first expanded in-phase, and then jointly employed with the unused transmit antennas. Such constellation expansion leads to increments in detection error. In [44], the *index bits* are converted to their equivalent base-N_t representation, and then mapped to the N_t antennas. This comes at the cost of error propagation, which increases with N_t. The bit-padding method proposed in [45] enables higher data-rate without any constraint on N_t, but at the expense of signaling overhead. In [46], the coding gain related to equiprobable activation in index-modulation assisted OFDM is quantified. Performance losses in SM when $N_\mathrm{t} \neq 2^g$ are well studied [43–45]. Besides, the non-uniform antenna activation and the resulting loss in data-rate equally exist in QSM [9, pp. 48] and GSM [9, pp. 44], as well as in more recent SM techniques including generalized precoding spatial modulation (GPSM) [47], signed quadrature spatial modulation (SQSM) [48], and joint transmitter-receiver spatial modulation (JSM) [49], though these issues have not been addressed yet to the best of the authors' knowledge.

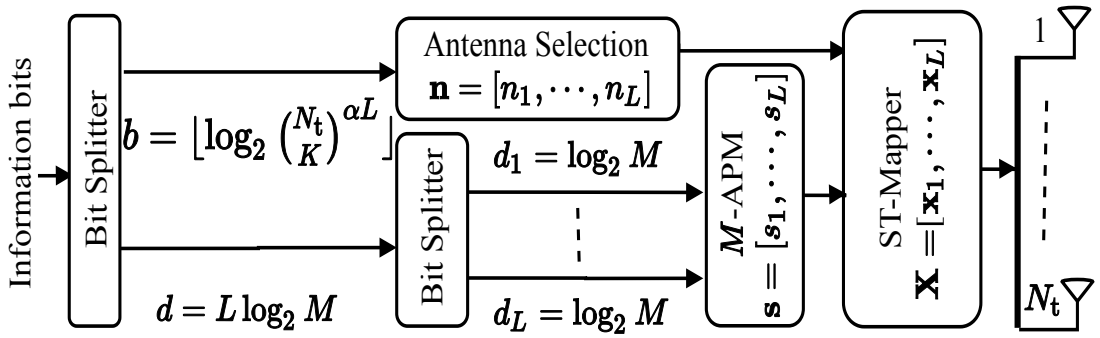

Figure 4.1: Transmitter of SM $(K = 1, \alpha = 1)$**, GSM (**$1 < K < N_t, \alpha = 1$**), and QSM (**$K = 1, \alpha = 2$**), under conventional mapping** $(L = 1)$ **and** *space-time* **mapping** $(L > 1)$**.**

Contribution: Addressing the problem highlighted above, this paper's key concept and the ensuing performance gain is itemized as follows: *(i)* In SM techniques, unlike the conventional approach for choosing the index of an active transmit antenna within each symbol period, we propose a *space-time* mapping approach in which the selection is extended to multiple symbol periods. The applicability and the gains of the proposed mapping are shown in the well-known SM, GSM, and QSM techniques. *(ii)* With *space-time* mapping assisted SM techniques, near-optimal data-rate and a coding gain over the conventional mapping can be achieved without any constraint on the number of transmit antennas, N_t. The distribution of the codeword over multiple symbol periods can result in an increment in detection complexity.

4.2 Space-Time Mapping in Spatial Modulation

Figure 4.1 illustrates the transmitter of a MIMO SM-based system with N_t antennas and M-ary APM, and design parameters, L, K and α, where L is the number of symbol periods over which the codeword of *space-time* mapping is spanned, K is the number of active antennas during each symbol period, and α is a constant. Variations of these parameters specify the techniques under study, i.e., SM, GSM and QSM, with conventional or *space-time* mapping. We start by describing the working principle of the proposed mapping in SM.

4.2.1 The Space-Time SM Transmitter

First, L number of symbol periods, such that $L > 1$, is chosen. The N_{t} available antennas over L symbol periods can form N_{t}^L distinct *space-time* realizations. Therefore, $b = \lfloor \log_2 N_{\mathrm{t}}^L \rfloor$ *index bits* can be encoded in the joint *space-time* domain. The *index bits* are fed to an antenna selection block which, according to a pre-defined mapping rule, generates a vector $\mathbf{n} = [n_1, \cdots, n_L]$ containing the indexes of the transmit antennas to be active in the L symbol periods. The mapping process will be detailed in Section 4.2.3 with an example.

Next, the $d = L \log_2 M$ *modulated bits* are split into L streams, each having $\log_2 M$ bits, and are then mapped through M-ary APM, resulting in the symbol vector $\mathbf{s} = [s_1, \cdots, s_L]$. For $l = 1, \cdots, L$, the complex symbol s_l is to be transmitted at the l^{th} symbol period using a transmit antenna identified by $n_l \in \mathbf{n}$.

The symbol vector $\mathbf{s}$ and the vector $\mathbf{n}$ containing the indexes of the active antennas are fed to the space-time mapper, which maps each symbol of $\mathbf{s}$ onto an active antenna according to $\mathbf{n}$. The mapper outputs codeword $\mathbf{X} = [\mathbf{x}_1, \cdots, \mathbf{x}_L] \in \mathbb{C}^{N_{\mathrm{t}} \times L}$ satisfying $E[\|\mathbf{X}\|_F^2] = KL$, the case of $K = 1$ being the single active antenna property of SM, and the transmit power per symbol period is $P_{\mathrm{t}} = \frac{1}{L} E[\|\mathbf{X}\|_F^2] = 1$. The resultant signal is transmitted over a Rayleigh fading channel characterized by the random matrix $\mathbf{H} \in \mathbb{C}^{N_{\mathrm{r}} \times N_{\mathrm{t}}}$, where N_{r} denotes the number of receive antennas.

4.2.2 The Space-Time SM Receiver

The received signal $\mathbf{y} \in \mathbb{C}^{N_{\mathrm{r}} L \times 1}$ is given by

$$\mathbf{y} = \tilde{\mathbf{H}} \tilde{\mathbf{x}} + \mathbf{v}, \tag{4.3}$$

where $\tilde{\mathbf{x}} = [\mathbf{x}_1^{\mathrm{T}}, \cdots, \mathbf{x}_L^{\mathrm{T}}] \in \mathbb{C}^{N_{\mathrm{t}} L \times 1}$, $\tilde{\mathbf{H}} = \mathbf{I} \otimes \mathbf{H} \in \mathbb{C}^{N_{\mathrm{r}} L \times N_{\mathrm{t}} L}$ in which $\mathbf{I}$ is the identity matrix of order L, and $\otimes$ is the Kronecker product, and where $\mathbf{v} \in \mathbb{C}^{N_{\mathrm{r}} L \times 1}$ denotes the noise vector with each of its entry following $\mathcal{CN}(0, N_{\mathrm{o}})$ distribution.

The ML detector makes a group-wise decision over L symbol periods to jointly estimate the indexes of the activated antennas, $\widehat{\mathbf{n}} = [\widehat{n}_1, \cdots, \widehat{n}_L]$, and the M-APM symbols, $\widehat{\mathbf{s}} = [\widehat{s}_1, \cdots, \widehat{s}_L]$.

Index bits b	Antenna Indexes $\mathbf{n}$	
	n_1	n_2
000	1	1
001	1	2
010	1	3
011	2	1
100	2	2
101	2	3
110	3	1
111	3	2

(a)

modulated bits d	Transmit symbol $\mathbf{s}$	
	s_1	s_2
00	-1	-1
01	-1	1
10	1	-1
11	1	1

(b)

Tableau 4.1: (a) Antenna activation $\mathbf{n} = [n_1, n_2]$ based on *index bits*; (b) Symbol vector $\mathbf{s} = [s_1, s_2]$ based on *modulated bits*

Modulated bits $d \rightarrow$		00		01		10		11	
Code word $\mathbf{X}$		$\mathbf{x}_1^{\mathrm{T}}$	$\mathbf{x}_2^{\mathrm{T}}$	$\mathbf{x}_1^{\mathrm{T}}$	$\mathbf{x}_2^{\mathrm{T}}$	$\mathbf{x}_1^{\mathrm{T}}$	$\mathbf{x}_2^{\mathrm{T}}$	$\mathbf{x}_1^{\mathrm{T}}$	$\mathbf{x}_2^{\mathrm{T}}$
Index bits	000	[-1 0 0]	[-1 0 0]	[-1 0 0]	[1 0 0]	[1 0 0]	[-1 0 0]	[1 0 0]	[1 0 0]
	001	[-1 0 0]	[0 -1 0]	[-1 0 0]	[0 1 0]	[1 0 0]	[0 -1 0]	[1 0 0]	[0 1 0]
	010	[-1 0 0]	[0 0 -1]	[-1 0 0]	[0 0 1]	[1 0 0]	[0 0 -1]	[1 0 0]	[0 0 1]
	011	[0 -1 0]	[-1 0 0]	[0 -1 0]	[1 0 0]	[0 1 0]	[-1 0 0]	[0 1 0]	[1 0 0]
	100	[0 -1 0]	[0 -1 0]	[0 -1 0]	[0 1 0]	[0 1 0]	[0 -1 0]	[0 1 0]	[0 1 0]
	101	[0 -1 0]	[0 0 -1]	[0 -1 0]	[0 1 0]	[0 1 0]	[0 0 -1]	[0 1 0]	[0 0 1]
	110	[0 0 -1]	[-1 0 0]	[0 0 -1]	[0 0 1]	[0 0 1]	[-1 0 0]	[0 0 1]	[1 0 0]
	111	[0 0 -1]	[0 -1 0]	[0 0 -1]	[0 0 1]	[0 0 1]	[0 -1 0]	[0 0 1]	[0 1 0]

Tableau 4.2: Space-time SM mapping, meaning all possible codewords $\mathbf{X} = [x_1, x_2]$ for the given *index bits* and *modulated bits* in Table 4.1.

That is,

$$[\widehat{\mathbf{n}}, \widehat{\mathbf{s}}] = \arg \min_{r} |\mathbf{y} - \tilde{\mathbf{H}}\tilde{\mathbf{x}}_r|^2, \tag{4.4}$$

where $\tilde{\mathbf{x}}_r = \mathrm{vec}(\mathbf{X}_r)$, in which vec(.) denotes vectorization and $\mathbf{X}_r$ is the r^{th} codeword for $r = 1, \cdots, R$. The total number of codewords is $R = (N_{\mathrm{t}}M)^L$ when using the proposed *space-time* mapping in SM technique, and $R = N_{\mathrm{t}}M$ for SM with conventional mapping. Under perfect detection, the data-rate of *space-time* SM is

$$\eta_{\mathrm{SM}}^{\mathrm{ST}} = \frac{1}{L}\left\lfloor \log_2 N_{\mathrm{t}}^L \right\rfloor + \log_2 M \quad [\text{bits/s/Hz}]. \tag{4.5}$$

4.2.3 Illustrative Example

Let $N_{\rm t} = 3$ and $M = 2$. The optimal data-rate as per (4.1) is $\overline{\eta}_{\rm SM} = 2.58$ bits/s/Hz, and the optimal rate to activate the $n^{\rm th}$ antenna based on the *index bits* is $P(n) = \frac{1}{N_{\rm t}}$. The achievable data-rate with SM (4.2) equals $\eta_{\rm SM} = 2$ bits/s/Hz, with antenna activation probabilities $P(1) = P(2) = 0.5$ and $P(3) = 0$. For SM with the proposed *space-time* mapping, when $L = 2$ we have $\eta_{\rm SM}^{\rm ST} = 2.5$ bits/s/Hz as per (4.5), and the antenna activation probabilities are $P(1) = P(2) = 3/8$ and $P(3) = 2/8$. Note that $\eta_{\rm SM} < \eta_{\rm SM}^{\rm ST} \approx \overline{\eta}_{\rm SM}$, for all $N_{\rm t} \neq 2^g$. For the considered parameters, the antenna activation vector $\mathbf{n}$ based on $b = 3$ *index bits* is presented in Table 4.1(a). The symbol vector $\mathbf{s}$ based on $d = 2$ *modulated bits* is shown in Table 4.1(b), and the possible codewords $\mathbf{X} = [\mathbf{x}_1,\ \mathbf{x}_2]$ are provided in Table 4.2.

4.2.4 Applicability in GSM and QSM Techniques

In the family of SM techniques, QSM [9, pp. 48] and GSM [9, pp. 44] are two prominent figures for improving data-rate. Fig. 4.1 shows the transmitter architecture of these techniques. In QSM, the in-phase and quadrature components of a M-APM symbol s_l can be jointly or independently transmitted. This helps in having a total of $R = N_{\rm t}^2 M$ distinct codewords. In GSM, multiple antennas are activated to transmit a symbol s_l, which results in a total of $M\binom{N_{\rm t}}{K} = M\frac{N_{\rm t}!}{(N_{\rm t}-K)!K!}$ codewords. A general expression for the total number of codewords with SM, GSM, and QSM techniques, under the conventional mapping ($L = 1$) and the *space-time* mapping ($L > 1$), is given by

$$R = M^L \binom{N_{\rm t}}{K}^{\alpha L}. \tag{4.6}$$

Based on (4.6), the data-rate performance of SM, QSM and GSM, can be evaluated using

$$\overline{\eta} = \log_2 R,\ \eta = \lfloor \log_2 R \rfloor,\ \eta^{\rm ST} = \frac{1}{L}\lfloor \log_2 R \rfloor, \tag{4.7}$$

where $\overline{\eta}$ represents an upper-bound on the data-rate, and where η and $\eta^{\rm ST}$ are the data-rate when the technique (SM, QSM or GSM) implements the conventional mapping or the *space-time* mapping, respectively.

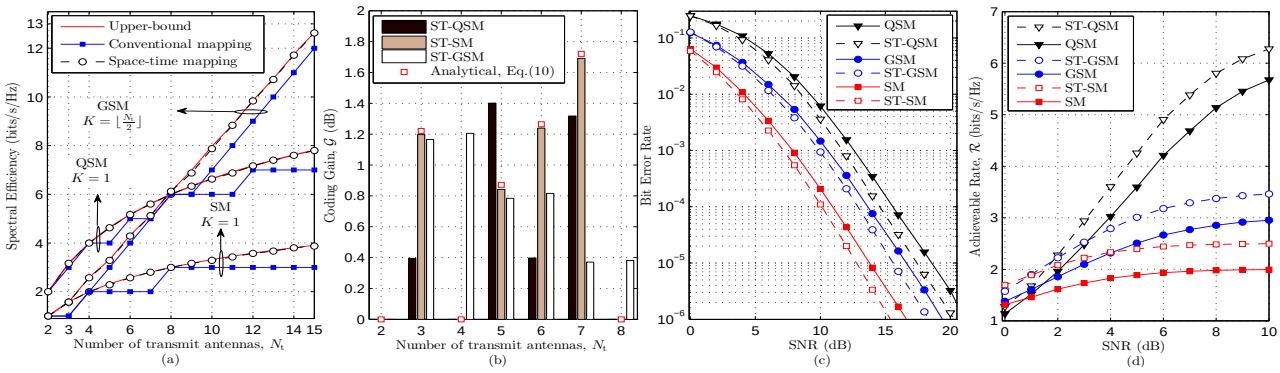

Figure 4.2: Comparison of the proposed space-time (ST) mapping against the conventional mapping in SM, QSM, and GSM: (a) data-rate; (b) Coding gain; (c) BER; and (d) Achievable rate.

Here, it is worth mentioning that the antenna activation in the GPSM [47], SQSM [48], and JSM [49] techniques is identical to that in GSM and SM techniques. Therefore, the proposed *space-time* mapping can be easily implemented in GPSM, SQSM, and JSM, to achieve near-optimal performances.

4.2.5 Optimal L

A choice of L which can activate the N_t antennas at a uniform rate is equally optimal in terms of data-rate and error rate performance. Therefore, the optimal choice is $L = 1$ when $R = 2^g$, due to the resulting $\overline{\eta} = \eta$. When $R \neq 2^g$, a brute-force search method is used, which is feasible since this is only required once.

For all $R \neq 2^g$, it can be easily shown that the data-rate of SM, QSM and GSM, satisfy $\eta < \eta^{\text{ST}} \approx \overline{\eta}$. The *space-time* method activates the N_t available transmit antennas as equally as possible, which yields a coding gain over the conventional mapping approach, as will be detailed shortly.

4.3 Performance Analysis

Bit Error rate and coding gain analysis when using space-time mapping in spatial modulation technique is detailed in Appendix C.1, where coding gain advantage of space-time mapping over the conventional mapping is provided.

4.4 Comparative Results and Concluding Remarks

Data-rate and Coding Gain: Figure 4.2(a) presents a comparison of the data-rates in (4.7) for SM, GSM, and QSM, versus the number of antennas. In the *space-time* mapping, optimal L for each value of $N_{\rm t}$ in all techniques is obtained according to Section 4.2.5, where a maximum of $L = 8$ was allowed. For clarity, we used $M = 1$ in (4.6) to isolate the common term, i.e., $d = \log_2 M$ in (4.7). The upper-bound and the actual data-rate achieved using conventional mapping in SM, GSM, and QSM, only match when $R = 2^g$, which is highly unlikely for most values of $N_{\rm t}$ in practical MIMO configurations. As shown in the figure, use of the proposed *space-time* mapping can yield near-optimal performance in data-rate. Fig. 4.2(b) depicts the coding advantage of *space-time* mapping over conventional mapping in SM, GSM, and QSM, for varying $N_{\rm t}$. The results correspond to a BER of 10^{-5} for all values of $N_{\rm t}$, and $N_{\rm r} = 4$ receive antennas. The coding gain is the result of the near-uniform activation of the transmit antennas via *space-time* mapping. No coding gain is noted when $R = 2^g$, in which case all antennas can be uniformly activated in each symbol period. Particularly, for $N_{\rm t} = 7$, a coding gain of 1.7 dB and 28% higher data-rate can be achieved in SM with *space-time* mapping compared to the conventional approach. As observed from Fig. 4.2(a-b), the maximum losses with conventional mapping in all techniques occur at the so-called severe condition of $R = 2^g - 1$. When $R = 2^g - 1$, nearly half of the antennas are left unused for transmission. This leads to maximum data-rate loss, $\overline{\eta} - \eta \approx 1$ bit/s/Hz, and maximum SNR loss. This argument is established for the discussion on detection complexity, presented shortly.

BER and Achievable Rates: We compare the BER performance with the proposed *space-time* mapping over the conventional one for three systems: SM with $N_{\rm t} = 3$ and $M = 2$, GSM with $N_{\rm t} = 4, K = 2$, and $M = 2$, and QSM with $N_{\rm t} = 5$ and $M = 4$. The number of receive antennas is always $N_{\rm r} = 4$. Here, $L = 2$ is used for the *space-time* mapping. The BER is depicted in Fig. 4.2(c). At a BER of 10^{-5}, the *space-time* method achieves a coding gain of 1.2 dB, 1.1 dB, and 1.3 dB, in SM, GSM, and QSM, respectively. Comparison of the achievable rates of these techniques with conventional mapping and *space-time* mapping is reported in Fig. 4.2(d). The achievable rate is calculated using $\mathcal{R} \leq \epsilon(1 + P_{\rm e}\log_2 P_{\rm e} + (1 - P_{\rm e})\log_2(1 - P_{\rm e}))$ bits/s/Hz [30], where $\epsilon = \eta$ for conventional mapping and $\epsilon = \eta^{\rm ST}$ when using *space-time* mapping. Here, $P_{\rm e}$ denotes the error probability of conventional- or *space-time* mapping assisted SM, GSM, or QSM. The gain in rate

performance of the SM techniques implementing *space-time* mapping is partly due to the coding gain (C.3), and partly to the gain in data-rate (4.7).

Detection Complexity: In terms of tradeoff, the coding and data-rate gains (cf. Fig. 4.2) with *space-time* mapping are achieved with an increment in detection complexity. Measuring detection complexity in terms of the number of complex multiplications required during each symbol period for the estimation of $\widehat{\mathbf{n}}$ and $\widehat{\mathbf{s}}$ according to (4.4), then as per [50] and (4.4), ratio of the detection complexity with *space-time* mapping over the conventional approach is $\frac{\delta^{\mathrm{ST}}}{\delta} = \frac{M^{L-1}}{L}\binom{N_{\mathrm{t}}}{K}^{\alpha(L-1)}$. The increment in complexity is exponential in L. However, choice of $L = 2$ can be easily shown in (4.7) to be sufficient in all techniques for achieving high performance for most values of R, especially at the severe condition defined earlier as $R = 2^g - 1$. Therefore, the increment in complexity is marginal. Detection complexities of SM, GSM, and QSM with conventional and *space-time* mappings considered in Fig. 4.2(c-d) are $\delta = [3, 6, 25]$ and $\delta^{\mathrm{ST}} = [4.5, 18, 312.5]$, respectively.

In conclusion, this chapter addressed the problem of irregular antenna activation in SM techniques, which causes high BER and losses in data-rate. A space-time mapping design in which the encoding procedure is extended to multiple symbol periods was proposed, and its merits were demonstrated in the well-known SM, GSM, and QSM techniques. Coding gain which arises from the near-uniform antenna activation was also analyzed. Use of the proposed space-time mapping can enable SM techniques to operate with near-optimal performance, making it a suitable candidate for B5G MIMO communications, where the number of antennas at devices can be highly constrained due to the size limitations. The reported gains were shown possible with a marginal increment in detection complexity. Moreover, the proposed mapping can be easily adopted in various other index modulation techniques.

Chapter 5

Information-Guided Antenna Selection and Activation for Spatial Modulation MIMO Systems

5.1 Introduction

In a SM based communication system, during each symbol period, the transmitter uses a block of information bits to choose one among a set of antennas for the transmission. The index of the activated antenna and the transmitted symbol carry useful information. Therefore, the SM technique can achieve higher data rate performance as compared to single-antenna transmission while avoiding the inter-carrier interference and inter-antenna synchronization problems of MIMO, making it suitable for many use cases in B5G.

Using SM, the probability of activating one among N_t available antennas is $\frac{1}{N_\mathrm{t}}$. As such, the weakest channel for transmission is chosen with the same probability of $\frac{1}{N_\mathrm{t}}$, which causes performance degradation. Antenna selection (AS) [51–57] and power allocation [58] are well-studied to combat this shortcoming. In the context of SM, the concept of AS is different from that of antenna activation (AA). The latter is performed based on the incoming information bits. For instance, the

[0]The contents of this chapter are extracted from a paper titled, "Information-Guided Antenna Selection and Activation for Spatial Modulation MIMO Systems" which was accepted on Feb. 2024 for publication in IEEE Transactions on Wireless Communications.

index of a transmit antenna is chosen based on the incoming information bits. The AS methods, on the other hand, are used to choose a subset of the available antennas for performance enhancement, say N_{t} out a total of N_{T} antennas. Usually, AS is performed based on the CSI. AS in SM is well investigated in [51–57] whereas, to the best of our knowledge, AA in SM is only investigated in [42], where CSI is assumed unavailable at the transmitter; but no studies investigated operations under CSI availability.

5.1.1 Problem Statement

Two problems associated with conventional U-AA and AS in SM techniques are identified. Firstly, U-AA uniformly activates each of the N_{t} antennas based on the information bits. The approach is ideal only when no CSI is available [42]. When CSI is available, U-AA is not an optimal strategy. Secondly, assume that a subset N_{t} out of a total of N_{T} antennas is chosen using any of the AS methods in [51–57]. Using conventional U-AA, it can be argued that the weakest channel pertaining to the chosen set of antennas will be activated with probability $\frac{1}{N_{\mathrm{t}}}$, causing performance degradation. Finally, in practical MIMO uplink communications, unlike on the downlink, the communications are facilitated by a limited number of antennas due to the small size of devices. While the methods in [51–57] are applicable to SM-assisted uplink communications, the power-constrained devices cannot satisfy the $N_{\mathrm{T}} > N_{\mathrm{t}}$ requirement to implement AS and handle the associated computational complexity and signalling overhead.

The above-mentioned problems motivate our proposal of the irregular antenna activation (I-AA) method for SM. Particularly, it will be shown that I-AA can use the better channels with higher probabilities, and the weaker channels with smaller probabilities, thereby leading to improvements in the data transmission rates and the error rates.

5.1.2 Related Work

The work in [51] was the first to study AS in SM. Therein, two techniques were proposed, namely, exhaustive search-based Euclidean distance optimized AS (EAS) and low-complexity AS (LAS), and both were shown to achieve performance improvements over SM without AS. AS methods based on antenna correlation were proposed in [52]. Cross-entropy based AS was reported in [53]. In [54],

the N_{T} antennas are divided into N_{t} groups, and the antenna with the best channel gain is chosen in each group, thus forming a subset of N_{t} antennas for transmission. The follow-up research on AS in SM mainly focused on reducing complexity (cf. [55–57] and references therein).

Recently, similarity among short bit-sequences of different users was exploited for data rate enhancement [59–62]. In [59], similarity in the message signals of users located in the same vicinity was exploited. Particularly, the message signal of a user is compressed based on its correlation with other users' message signals, and shown to reduce the required transmission rate. Exploiting similarity among the short information bit-sequences of different users in downlink non-orthogonal multiple access (NOMA) [60] and uplink NOMA [61] was shown to result in significant rate improvements over conventional NOMA. A superposition/puncturing strategy for reducing the impact of ultra-reliable low-latency communication traffic on that of enhanced mobile broadband by exploiting information similarity was proposed in [62], where up to 10 dB gains in the error rate performance were reported.

5.1.3 Contribution

The contributions of this paper and its findings are summarized as follows: *(i)* A novel method for AA in SM techniques is proposed, the so-called I-AA. The concept consists in assigning an integer value to consecutive equal information bits, and using the obtained value for AA. The applicability of I-AA is demonstrated for different variants of SM. *(ii)* For SM techniques with I-AA, two AS methods are proposed, namely, joint rate and Euclidean-distance optimized AS (REAS), and rate-optimized low-complexity AS (RLAS). *(iii)* Using order statistics, closed-form expressions for the pairwise error probability of SM implementing I-AA with/without the proposed REAS and RLAS methods are derived, considering transmissions over Rayleigh fading channels and single- or multiple-antenna reception. *(iv)* The main performance gains related to the use of I-AA in SM are twofold. Firstly, higher rates can be achieved as compared to SM with U-AA, particularly for small numbers of transmit antennas, making it a suitable candidate for uplink communications. Secondly, better error rates can be obtained as compared to SM with U-AA. Also, SM implementing I-AA without AS achieves even better error rate performance as compared to SM with U-AA and AS. Lastly, SM techniques implementing the proposed I-AA and AS methods are shown to outclass

SM implementing conventional U-AA and AS, i.e., EAS and LAS, with a negligible overhead in complexity and signalling.

5.2 Overview of Spatial Modulation

Consider a point-to-point SM-based MIMO communication system with N_{t} antennas at the transmitter and N_{r} antennas at the receiver. During each symbol period, the information bits are split into two blocks, *index bits* and *modulated bits*, of length b and d, respectively. The b *index bits* are used to activate one of the N_{t} antennas, and the d *modulated bits* are transmitted using the activated antenna after modulating them with M-APM. Therefore, the SM technique can achieve a rate of $\eta_{\mathrm{SM}} = b+d$ bits/s/Hz, thereby resulting in b bits/s/Hz gain over the counterpart single-input single-output (SISO) system. This gain depends on N_{t}, and on the method for mapping *index bits* to one of the N_{t} antennas. The existing method for mapping b *index bits* to an antenna index, the so-called U-AA, uniformly activates each antenna. The U-AA builds a one-to-one mapping which relates a natural number (index of a transmit antenna) to $b = \log_2 N_{\mathrm{t}}$ number of unique *index bits*. Hence, the achievable rate of SM implementing U-AA, in the unit of bps/Hz, is given by,[1]

$$\eta_{\mathrm{SM}}^{\mathrm{u}} = \lfloor \log_2 N_{\mathrm{t}} \rfloor + \log_2 M, \tag{5.1}$$

where $\lfloor . \rfloor$ is the floor function.

The received signal at the destination can be expressed as $\mathbf{y} = \sqrt{\rho^{\mathrm{u}}}\mathbf{h}_n s_m + \mathbf{w}$, where $\mathbf{y} \in \mathbb{C}^{N_{\mathrm{r}}}$, s_m $(m = 1, \cdots, M)$ is the m^{th} M-APM symbol of unit energy, $\mathbf{h}_n$ $(n = 1, \cdots, N_{\mathrm{t}})$ is the n^{th} column of the channel matrix $\mathbf{H} \in \mathbb{C}^{N_{\mathrm{r}} \times N_{\mathrm{t}}}$, and $\mathbf{w} \in \mathbb{C}^{N_{\mathrm{r}}}$ is the noise vector. Each entry of $\mathbf{H}$ follows $\mathcal{CN}(0, 1)$, and each element of $\mathbf{w}$ follows $\mathcal{CN}(0, \sigma^2)$. The average SNR per receive antenna is defined by $\rho^{\mathrm{u}} = \frac{1}{\sigma^2}$. Using the ML principle, estimation of the activated antenna index and the transmitted symbol under perfect CSI at the receiver is given by $[\widehat{n}, \widehat{m}] = \underset{n,m}{\arg\min} \|\mathbf{y} - \sqrt{\rho^{\mathrm{u}}}\mathbf{h}_n \; s_m\|^2$, and an

[1]The subscript in η is an indication of the SM variant. The superscript is an indication of the AA technique in use, namely, “u" for U-AA and “I" and “o" for I-AA and O-AA, respectively. The I-AA and O-AA techniques will be introduced shortly.

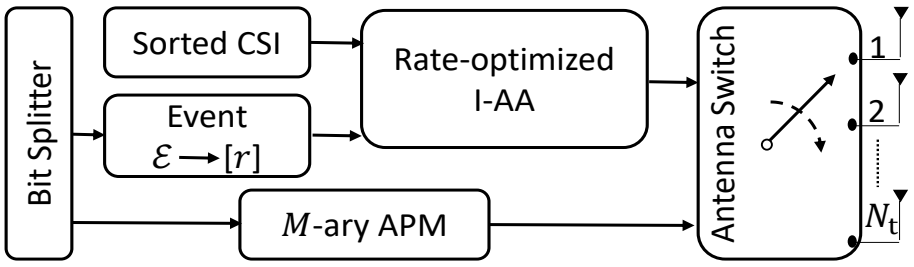

Figure 5.1: Block diagram of a spatial modulation transmitter implementing irregular antenna activation.

upper-bound on the BER is given by [51], as

$$P_{\mathrm{e}}(\widehat{n}) \leq \sum_{\substack{n=1 \\ n \neq n'}}^{N_{\mathrm{t}}} \sum_{\substack{m=1 \\ m'=1}}^{M} \frac{\mathrm{E}\left[\exp\left(\frac{-\rho^{\mathrm{u}}}{4}||\mathbf{h}_n s_m - \mathbf{h}_{n'} s_{m'}||^2\right)\right]}{2M^2 N_{\mathrm{t}}^2}, \tag{5.2a}$$

$$P_{\mathrm{e}}(\widehat{m}) \leq \sum_{n=1}^{N_{\mathrm{t}}} \sum_{\substack{m=1 \\ m' \neq m}}^{M} \frac{\mathrm{E}\left[\exp\left(\frac{-\rho^{\mathrm{u}}}{4}||\mathbf{h}_n||^2 |s_m - s_{m'}|^2\right)\right]}{2M^2 N_{\mathrm{t}}}, \tag{5.2b}$$

where $P_{\mathrm{e}}(\widehat{n})$ is the probability that the estimated antenna index is erroneous, and $P_{\mathrm{e}}(\widehat{m})$ is the probability that the estimated M-APM symbol is in error, with E[.] denoting expectation. During each transmission interval, $\min_n \|\mathbf{h}_n\|^2$ can occur at a uniform rate of $\frac{1}{N_{\mathrm{t}}}$, causing performance degradation in the estimation of the b and d bits as per (5.2a) and (5.2b), respectively.

The metrics (5.2a) and (5.2b) can be minimized by utilizing better channels for transmission, which is enabled in the literature by AS [51–57]. We take a different approach to minimize (5.2a) and (5.2b). The highlight of our proposal is as follows. First, assume that the columns of the channel matrix $\mathbf{H}$ satisfy $\|\mathbf{h}_1\|^2 > \cdots > \|\mathbf{h}_{N_{\mathrm{t}}}\|^2$.[2] Unlike U-AA, where the transmit antennas pertaining to $\mathbf{h}_1$ and $\mathbf{h}_{N_{\mathrm{t}}}$ are used for transmission at the uniform rate of $\frac{1}{N_{\mathrm{t}}}$, the proposed I-AA method can utilize $\mathbf{h}_1$ for transmission with a probability of $\frac{1}{2}$, and $\mathbf{h}_{N_{\mathrm{t}}}$ with a probability of $\frac{2}{2^{N_{\mathrm{t}}}}$, thereby enhancing the BER performance.

[2]For clarity, the assumption $\|\mathbf{h}_1\|^2 > \cdots > \|\mathbf{h}_{N_{\mathrm{t}}}\|^2$ will be recalled at several stages of this paper, and will be termed as "*Assumption-1*" for convenience.

5.3 Irregular Antenna Activation in Spatial Modulation

Next, the working principle of I-AA in SM-based system is presented. Then, an expression for the average rate of a SM-based system implementing the proposed I-AA is derived. The rate expression is then used to develop the method of rate-optimized I-AA. Finally, an illustrative example is presented.

5.3.1 The Working Principals of Irregular Antenna Activation

In this section, we first derive a closed form expression to determine the number of consecutively equal bits in a bit sequence of b bits where each bit is uniformly distributed with equal probability. More specifically, starting from the least-significant bit, we are interested in determining r number of consecutive equal bits, followed by q number of different consecutive equal bits in the bit sequence. For instance, we are interested in $r = 3$ consecutive equal bits follows by $q = 2$ consecutive equal bits, e.g., 00111. Then, based on the statistical likelihood of such sequences and the available full or partial CSI at transmitter, we will develop an antenna activation method for SM based systems, the so-called I-AA. For the sake of generalization, we extend the problem to finding r number of consecutive equal A-APM symbols followed by a different q number of consecutive equal A-APM symbol.

To begin, first denote a sequence of $b = W \log_2 A$ number of information bits as $G = [g_{1,a}, \cdots g_{W,a}] \in \mathbb{C}^W$, where $g_{w,a}$, for $w = 1, \cdots, W$ and $a = 1, \cdots, A$, is drawn from A-ary APM, and where W is the number of A-APM symbols in G. Hereinafter, for the sake of simplicity, we drop the subscript w from $g_{w,a}$. Each complex entry of G denotes $\log_2 A$ number of bits. Since the bits in G are uniformly distributed with equal probabilities, G is an outcome of permutations with repetition and the number of distinguishable outcomes in G is A^W. Among the outcomes of G, we are interested in finding the one outcomes with $1 \leq r \leq W$ number of consecutive equal elements g_a, followed by $1 \leq q \leq W$ number of consecutive equal elements $g_{a'}$, where $a' = 1, \cdots, A$, $a \neq a'$ and $r + q \leq W$. Based on the aforementioned sequences, the A^W outcomes of G can be arranged into 2^{W-1} groups. The grouping is explained using the following example.

Grouping Example: Let $A = 3$ and $W = 3$. This results in $A^W = 27$ outcomes of G, which can be arranged into $2^{W-1} = 4$ groups: $G_1 = [g_a, g_a, g_a] \in \mathbb{C}^{t_1 \times W}, G_2 = [g_a, g_a, g'_a] \in \mathbb{C}^{t_2 \times W}, G_3 =$

Tableau 5.1: A grouping example using $A = 3$ and $W = 3$: Group G_1 with 3 outcomes, G_2 and G_3 with 6 outcomes and G_4 with 12 outcomes

Group G_1		
g_1	g_1	g_1
g_2	g_2	g_2
g_3	g_3	g_3

Group G_2		
g_2	g_2	g_1
g_3	g_3	g_1
g_1	g_1	g_2
g_3	g_3	g_2
g_1	g_1	g_3
g_2	g_2	g_3

Group G_3		
g_1	g_2	g_2
g_1	g_3	g_3
g_2	g_1	g_1
g_2	g_3	g_3
g_3	g_1	g_1
g_3	g_2	g_2

Group G_4						
g_1	g_2	g_1		g_1	g_2	g_3
g_1	g_3	g_1		g_1	g_3	g_2
g_2	g_1	g_2		g_2	g_1	g_3
g_2	g_3	g_2		g_2	g_3	g_1
g_3	g_1	g_3		g_3	g_1	g_2
g_3	g_2	g_3		g_3	g_2	g_1

$[g_a, g_{a'}, g_{a'}] \in \mathbb{C}^{t_3 \times W}$, and $G_4 = [g_a, g_{a'}, g_a] \in \mathbb{C}^{t_4 \times W}$. The groups respectively contain $t_1 = 3$, $t_2 = 6$, $t_3 = 6$, and $t_4 = 12$ possible outcomes from G, and the corresponding sequences are as drawn in Table 1. In an example, for $N_\mathrm{t} = 2^{W-1} = 4$ transmit antennas, one naive strategy would be to map the group indices to the antenna indices for AA. Particularly, using one-to-one mapping, the outcomes in groups G_1, G_2, G_3, and G_4 can be used to activate the $1^{\mathrm{st}}, 2^{\mathrm{nd}}, 3^{\mathrm{rd}}$, and 4^{th} transmit antennas, respectively for the transmission of a M-APM modulation symbol. However, by doing so, note that upon reception of the signal, the receiver could only retrieve the group index and not the sequence index. To enable the receiver to retrieve the sequence index from the received signal, we re-arrange the M-APM constellation points at the transmitter, which will be discussed in Section D.1.1.

Based on the above example, it can be observed that the activation probability of the n^{th} antenna is $P(n : \text{active}) = \frac{t_n}{A^W}$, where $N_\mathrm{t} = 2^{W-1}$. From $P(n : \text{active})$, it can be noted that each of the N_t antennas will be activated with different probabilities, resulting in an I-AA. The proposed I-AA will be exploited for performance enhancement. Therefore, maximum I-AA is desirable, which can be achieved by maximizing the difference among the number of outcomes between different groups, i.e., when $\max_{n \neq n'} |t_n - t_{n'}|$ is satisfied. The latter rule can be satisfied when the number of groups is minimized, which can be achieved by introducing a constraint $2 \leq q \leq N_\mathrm{t}$ on the q number of consecutive equal symbols such that $r + q \leq W$. In the above example, this means that all outcomes in G_4 are added to G_3, resulting in $t_3 = 18$, which increases the difference in $P(n : \text{active})$ $\forall n$.

Recall that the index of an activated transmit antenna is chosen based on $r + q \leq W$ number of A-APM symbols. Therefore, the index of the activated antenna carries useful information. Next, the average number of transmitted bits in SM based system with I-AA using the active antenna indices is evaluated.

5.3.2 Average Number of Transmitted Bits

To evaluate the average number of transmitted bits of SM technique implementing the proposed I-AA, we are interested in the event probability of having r consecutive equal symbols g_a in G, followed by q consecutive equal symbols $g_{a'}$ therein, with $a \neq a'$. Such an event is denoted by $\mathcal{E} \rightarrow [r, q]$, and is derived in closed-form as

$$P\left(\mathcal{E} \rightarrow [r, q]\right) = \frac{2A^{q-1} - 1}{A(A^{r-1} - 1 + A^{q-1})}, \tag{5.3}$$

as detailed in the Appendix. The average number of transmitted bits of SM technique implementing I-AA, in the unit of bps/Hz, is then obtained as

$$\eta_{\text{SM}}^{\text{I}} = \sum_{i=1}^{2^{W-1}} P\left(\mathcal{E} \rightarrow [r, q]\right)(r + q)\log_2 A. \tag{5.4}$$

5.3.3 Illustrative Example ($A = 2$)

Conventional U-AA in SM is carried out at the bit level. We resort to the same approach by setting $A = 2$. In addition, only $1 \leq r \leq N_{\text{t}}$ consecutive equal bits are exploited for similarities. Based on r consecutive equal bits, the *index bits* can be arranged into N_{t} groups, each having $1, \cdots, N_{\text{t}}$ number of bits. In I-AA, first, starting from the least-significant bit of the $b = N_{\text{t}}$ *index bits*, $1 \leq r \leq N_{\text{t}}$ consecutive equal bits are identified; such an event is denoted by $\mathcal{E} \rightarrow [r]$, where r is the number of consecutive equal bits and termed as similarity-index. Based on this event, a transmit antenna can be activated, which is the main focus of this paper and will be detailed shortly. Using (5.3), it can be shown that r consecutive equal bits in a bit-sequence of length N_{t} occurs with probability

$$P\left(\mathcal{E} \rightarrow [r]\right) = \begin{cases} \frac{1}{2^r} & \text{if } 1 \leq r \leq N_{\text{t}} - 1, \\ \frac{2}{2^{N_{\text{t}}}} & \text{if } r = N_{\text{t}}. \end{cases} \tag{5.5}$$

Using (5.5), the number of transmitted bits of SM implementing I-AA can be expressed in the unit of bps/Hz as

$$\eta_{\text{SM}}^{\text{I}} = \sum_{r=1}^{N_{\text{t}}} r\ P\left(\mathcal{E} \rightarrow [r]\right) + \log_2 M = \sum_{r=1}^{N_{\text{t}}-1} \frac{r}{2^r} + \frac{2N_{\text{t}}}{2^{N\text{t}}} + \log_2 M. \tag{5.6}$$

Tableau 5.2: Antenna index selection and BPSK symbol mapping based on information bits

$\mathcal{E} \rightarrow [r]$	Antenna index and BPSK symbol mapping		
	bits	Antenna index	BPSK symbol
1	10	1	+1
2	100	2	+1
3	1000	3	+1
4	10000	4	+1
	00000	4	-j
1	01	1	-1
2	011	2	-1
3	0111	3	-1
4	01111	4	-1
	11111	4	+j

The working principles of an I-SM transmitter with $N_t = 4$ antennas and $M = 2$ binary phase shift keying (BPSK) modulation based on the proposed scheme is presented in Table II. Starting from the least significant bit (LSB), upto $N_t = 4$ consecutive equal bits can be identified. For instance, $\mathcal{E} \rightarrow [r = 4]$ for the event 00000. Starting from the LSB, the first four bits in this case determines the index of an active transmit antenna. The next bit is first modulated, phase shifted, and then transmitted using the activated antenna. Upon estimation of the BPSK symbol and the antenna index, the receiver can retrieve the information bits 00000. Next, a rate-optimized I-AA that maximizes the throughput is proposed.

5.3.4 Rate-Optimized Irregular Antenna Activation

During each symbol period, the SM technique implementing the proposed I-AA uses the events $\mathcal{E} \rightarrow [r]$ to activate one of the N_t antennas for the transmission of the *modulated bits*. The question is: based on a given event $\mathcal{E} \rightarrow [r]$, which antenna one may choose for transmission? An effective solution depends on the availability of CSI. Before addressing the problem, several features about U-AA and I-AA in SM techniques are highlighted:

- When full CSI is not available at the transmitter, the U-AA is an optimal strategy in terms of error rate performance [42].
- When full CSI or sorted CSI (sorted in ascending or descending order, e.g., as per *Assumption-1*), is available at the transmitter, I-AA is optimal in terms of BER and data rate performance as will be detailed shortly.

We assume that full CSI or sorted CSI is available at the transmitter. which is a valid assumption in both time division multiplexing (TDM) or frequency division multiplexing (FDM) in the New-Radio (NR) 5G CSI framework. In 5G NR TDM mode, the receiver send reference signals from each antenna to the transmitter and the transmitter estimates the CSI under the assumption of channel reciprocity. In 5G NR FDM mode, the transmitter sends reference signals to the receiver, the receiver estimates the CSI and reports a quantized CSI using one of the two uplink channel, namely physical uplink control channel or physical uplink shared channel. In both cases, the transmitter is able to obtain CSI for a coherence interval longer than the CSI estimation duration. If the coherence interval of the channel changes or is smaller than the time required to obtain CSI at transmitter, the transmitter (base station) performs link adaptation using outer loop link adaption (oLLA). Then, during the data transmission phase, a transmitter (base station) sends another reference signal to the receiver for the purpose of updating or to correct CSI information at receiver. For simplicity, in a given coherence interval, it is assumed that CSI at the transmitter obeys *Assumption-1.* The signalling overhead required to feedback the sorted CSI to the transmitter can be quantified as $\lceil \log_2 N_{\mathrm{t}}! \rceil$ bits per coherence interval, which will be used later for comparative studies.

Next, based on a given bit-similarity and available CSI at transmitter, an antenna index for transmission is determined under the constraint of maximizing the overall throughput performance.

Bit-Similarity to Antenna Index Mapping

The rate expression (5.6) in terms of different events $\mathcal{E} \to [r]$ is broken down as follows:

$$\eta_{\mathrm{SM}}^{\mathrm{I}} = \begin{cases} \frac{1}{2}\log_2 M & \text{if } r = 1, \\ \frac{1}{2^r}(r + \log_2 M) & \text{if } 2 \leq r < N_{\mathrm{t}}, \\ \frac{2}{2^{N_{\mathrm{t}}}}(N_{\mathrm{t}} + \log_2 M) & \text{if } r = N_{\mathrm{t}}. \end{cases} \tag{5.7}$$

Now, the index of a transmit antenna for a given event can be obtained using $n(\mathcal{E} \to [r]) = \arg\max_r(\eta_{\mathrm{SM}}^{\mathrm{I}}(r))$, where $n(r)$ denotes the chosen antenna index for a given event $\mathcal{E} \to [r]$. For clarifications, the mapping between events $\mathcal{E} \to [r]$ and antenna indices $n = 1, \cdots, N_{\mathrm{t}}$, is explained with the following two examples.

Tableau 5.3: One-to-one mapping between events $\mathcal{E} \to [r]$ and antenna indices $n = 1, \cdots, N_t$ based on sorted $\eta_{\mathrm{SM}}^{\mathrm{I}}$ in r (cf. 5.6) and exemplary CSI realizations.

M	N_t	CSI assumption	Rate, $\eta_{\mathrm{SM}}^{\mathrm{I}}(r)$, $r = 1, \cdots, N_t$	Event $\mathcal{E} \to [r]$	Antenna Index, n
1	3	$\|\mathbf{h}_1\|^2 > \|\mathbf{h}_2\|^2 > \|\mathbf{h}_3\|^2$	$\eta_{\mathrm{SM}}^{\mathrm{I}}(3) > \eta_{\mathrm{SM}}^{\mathrm{I}}(2) > \eta_{\mathrm{SM}}^{\mathrm{I}}(1)$	1	3
				2	2
				3	1
		$\|\mathbf{h}_3\|^2 > \|\mathbf{h}_2\|^2 > \|\mathbf{h}_1\|^2$		1	2
				2	1
				3	3
>1	3	$\|\mathbf{h}_1\|^2 > \|\mathbf{h}_2\|^2 > \|\mathbf{h}_3\|^2$	$\eta_{\mathrm{SM}}^{\mathrm{I}}(1) > \eta_{\mathrm{SM}}^{\mathrm{I}}(3) > \eta_{\mathrm{SM}}^{\mathrm{I}}(2)$	1	1
				2	3
				3	2
		$\|\mathbf{h}_2\|^2 > \|\mathbf{h}_3\|^2 > \|\mathbf{h}_1\|^2$		1	2
				2	1
				3	3
>1	>3	$\|\mathbf{h}_1\|^2 > \cdots > \|\mathbf{h}_{N_t}\|^2$	$\eta_{\mathrm{SM}}^{\mathrm{I}}(1) > \cdots > \eta_{\mathrm{SM}}^{\mathrm{I}}(N_t - 2) > \eta_{\mathrm{SM}}^{\mathrm{I}}(N_t) > \eta_{\mathrm{SM}}^{\mathrm{I}}(N_t - 1)$	1	1
				$\vdots$	$\vdots$
				$N_t - 2$	$N_t - 2$
				$N_t - 1$	N_t
				N_t	$N_1 - 1$

Example I

When $N_{\mathrm{t}} = 3$ and $M = 1$, (5.7) satisfies $\eta_{\mathrm{SM}}^{\mathrm{I}}(r = 3) > \eta_{\mathrm{SM}}^{\mathrm{I}}(r = 2) > \eta_{\mathrm{SM}}^{\mathrm{I}}(r = 1)$. Now, when channel gains are such that $\|\mathbf{h}_1\|^2 > \|\mathbf{h}_2\|^2 > \|\mathbf{h}_3\|^2$, then the antenna indexes $n = 1, n = 2$, and $n = 3$ are mapped to the events $\mathcal{E}_1 \to [3], \mathcal{E}_1 \to [2]$, and $\mathcal{E}_1 \to [1]$, respectively. Similarly, when the channel gains are such that $\|\mathbf{h}_1\|^2 > \|\mathbf{h}_3\|^2 > \|\mathbf{h}2\|^2$, then antenna indices $n = 1, n = 2$, and $n = 3$ are mapped to the events $\mathcal{E}_1 \to [3], \mathcal{E}_1 \to [2]$, and $\mathcal{E}_1 \to [1]$, respectively.

Example II

When $N_{\mathrm{t}} = 3$ and $M \geq 1$, (5.7) satisfies $\eta_{\mathrm{SM}}^{\mathrm{I}}(r = 1) > \eta_{\mathrm{SM}}^{\mathrm{I}}(r = 3) > \eta_{\mathrm{SM}}^{\mathrm{I}}(r = 2)$. Now, when channel gains are such that $\|\mathbf{h}_1\|^2 > \|\mathbf{h}_2\|^2 > \|\mathbf{h}_3\|^2$, the antenna indices $n = 1, n = 2$, and $n = 3$ are mapped to the events $\mathcal{E}_2 \to [1], \mathcal{E}_2 \to [3]$ and $\mathcal{E}_2 \to [2]$, respectively. Similarly, when the channel gains are such that $\|\mathbf{h}_1\|^2 > \|\mathbf{h}_3\|^2 > \|\mathbf{h}2\|^2$, then the antenna indices $n = 1, n = 2$, and $n = 3$ are mapped to the events $\mathcal{E}_2 \to [1], \mathcal{E}_2 \to [3]$, and $\mathcal{E}_2 \to [2]$, respectively.

In general, for $N_{\mathrm{t}} = 2$, we have $\eta_{\mathrm{SM}}^{\mathrm{I}}(r = 2) > \eta_{\mathrm{SM}}^{\mathrm{I}}(r = 1)$, whereas for $N_{\mathrm{t}} > 2$, it can be shown that (5.7) satisfies $\eta_{\mathrm{SM}}^{\mathrm{I}}(r = 1) > \cdots > \eta_{\mathrm{SM}}^{\mathrm{I}}(r = N_{\mathrm{t}} - 2) > \eta_{\mathrm{SM}}^{\mathrm{I}}(r = N_{\mathrm{t}}) > \eta_{\mathrm{SM}}^{\mathrm{I}}(r = N_{\mathrm{t}} - 1)$.

Therefore, using a one-to-one mapping, events $\mathcal{E} \rightarrow [1], \cdots, \mathcal{E} \rightarrow [N_\mathrm{t}-2], \mathcal{E} \rightarrow [N_\mathrm{t}], \mathcal{E} \rightarrow [N_\mathrm{t}-1]$ can be mapped to the N_t antennas based on the sorted CSI. Table 5.3 depicts a one-to-one mapping between events $\mathcal{E} \rightarrow r$ and antenna indices n for different M and N_t values. First, note that $M = 1$ is a case in which the information bits are only conveyed using the antenna indices, i.e., only *index bits* are transmitted and not the *modulated bits*, whereas $M > 1$ is a case in which both *index bits* and *modulated bits* are transmitted. Form the table, it can be observed that events that results in higher instantaneous rate, i.e., $\eta^{\mathrm{I}}_{\mathrm{SM}}(r)$ are mapped to channels with higher gain, whereas events that results in smaller instantaneous rate $\eta^{\mathrm{I}}_{\mathrm{SM}}(r)$ are mapped to channels with a smaller gain. Further, note that the one-to-one mapping will change when there is a change in the CSI realization, i.e., the mapping may change from one channel coherence interval to another. Now, a question is, how to ensure the same one-to-one mapping at the transmitter and receiver upon a change in the channel realization. As the sorted CSI is available at the transmitter and the receiver, change in the one-to-one mapping between the events and the antenna indices does not need to be exchanged between the receiver and the transmitter.

Assume that the index of an activated antenna is successfully estimated at the receiver. It is to be noted that the event $\mathcal{E} \rightarrow [r]$ can occur due to r consecutive 0's or 1's. Therefore, the correctly estimated antenna index cannot return the exact *index bits*. To address this issue, the symbol s_m is phase-shifted at the transmitter so that upon estimation of events at the receiver, the latter can correctly decide if a given event $\mathcal{E} \rightarrow [r]$ is indicating r consecutive 0's or r consecutive 1's. Such constellations rearrangement is detailed in Section. D.1.1 of Appendix

5.4 I-AA in Generalized Spatial Modulation

The achievable rate of SM with U-AA increases logarithmically with N_t. GSM was proposed to enhance the rate performance as compared to SM [9, pp. 44]. Higher transmission rate with GSM can be achieved by activating multiple antennas simultaneously [9]. Particularly, $b = \lfloor \log_2 \binom{N_\mathrm{t}}{K} \rfloor$ *index bits* get mapped to the indices of K $(2 \leq K < N_\mathrm{t})$ active antennas, where $\binom{N_\mathrm{t}}{K} = \frac{N_\mathrm{t}!}{(N_\mathrm{t}-K)!K!}$. The K activated antennas are then used for the transmission of M-APM symbol, yielding a rate of $\eta^{\mathrm{u}}_{\mathrm{GSM}} = \lfloor \log_2 \binom{N_\mathrm{t}}{K} \rfloor + \log_2 M$ bits/s/Hz. Rate improvements with GSM can be achieved by transmitting K independent M-APM symbols using the activated antennas, which results in rate $\eta^{\mathrm{u}}_{\mathrm{MASM}} = \lfloor \log_2 \binom{N_\mathrm{t}}{K} \rfloor + K \log_2 M$ bits/s/Hz. Such variant of GSM, known as MASM [36], was

proven to be capable of surpassing the rate performance of spatial multiplexing when the number of transmit antennas N_{t} and the modulation level M satisfy $N_{\mathrm{t}} > 2M$.

Next, the applicability of I-AA in GSM and MASM is presented for further rate and reliability enhancements.

First, in each symbol period, the incoming bits are split into three blocks: *sim bits*, *index bits*, and *modulated bits*, of length r, b, and d, respectively. For a given symbol period, the number of active antennas is set to the number of consecutive equal bits, i.e., $K = r$. Therefore, the number of activated antennas varies as per $1 \leq K \leq N_{\mathrm{t}}$ from one symbol period to another. The probability of having $K = r$ active antennas in a given symbol period, $P(K = r)$, is such that $P(K = r) = P(\mathcal{E} \to [r])$. The average number of active antennas per symbol period is

$$K_{\mathrm{avg}} = \sum_{r=1}^{N_{\mathrm{t}}} r \; P(K = r) = \sum_{r=1}^{N_{\mathrm{t}}-1} \frac{r}{2^r} + \frac{2N_{\mathrm{t}}}{2^{N^{\mathrm{t}}}}. \tag{5.8}$$

Moreover, $\lim_{N_{\mathrm{t}} \to \infty} K_{\mathrm{avg}} = 2$. Therefore, for a target rate performance, the required number of active antennas K_{avg} in GSM and MASM implementing the proposed I-AA is less than the required number of active antennas when these techniques implement U-AA.

Once the number of active antennas in a given symbol period using r *sim bits* is determined as $K = r$, $b = \lfloor \log_2 \binom{N_{\mathrm{t}}}{K} \rfloor$ *index bits* are used to choose indices of the K active antennas out of the N_{t} available ones. In GSM, the K active antennas transmit a M-APM symbol, whereas in MASM they transmit K independent M-APM symbols, yielding the following rates in bps/Hz:

$$\eta^{\mathrm{I}}_{\mathrm{GSM}} = \underbrace{\sum_{r=1}^{N_{\mathrm{t}}} [r \; P(K = r)]}_{\text{consecutive equal bits}} + \underbrace{\sum_{r=1}^{N_{\mathrm{t}}} \left[P(K = r) \left\lfloor \log_2 \binom{N_{\mathrm{t}}}{r} \right\rfloor \right]}_{\text{index bits}} + \underbrace{\log_2 M}_{\text{modulated bits}}, \tag{5.9a}$$

$$\eta^{\mathrm{I}}_{\mathrm{MASM}} = \underbrace{\sum_{r=1}^{N_{\mathrm{t}}} [r \; P(K = r)]}_{\text{consecutive equal bits}} + \underbrace{\sum_{r=1}^{N_{\mathrm{t}}} \left[P(K = r) \left\lfloor \log_2 \binom{N_{\mathrm{t}}}{r} \right\rfloor \right]}_{\text{index bits}} + \underbrace{\sum_{r=1}^{N_{\mathrm{t}}} r P(K = r) \log_2 M}_{\text{modulated bits}}. \tag{5.9b}$$

The constellation rearrangement detailed in Section D.1.1 is equally applicable to GSM and MASM implementing I-AA for distinguishing between the $K = r$ number consecutive equal 0's or $K = r$ number of consecutive equal 1's.

Next, a rate-optimized one-to-one mapping between the antenna indices and the $K = r$ number of consecutive equal bits in GSM and MASM is presented.

5.4.1 Rate-Optimized Irregular Antenna Activation in GSM

In GSM and MASM implementing the proposed I-AA, the indices of the $K = r$ active antennas are chosen based on the sorted CSI and the rate performance achieved at the events $\mathcal{E} \to [r]$ as given in (5.7). The rate in (5.9a) can be shown to satisfy $\eta^{\mathrm{I}}_{\mathrm{GSM}}(r = 1) > \cdots > \eta^{\mathrm{I}}_{\mathrm{GSM}}(r = N_{\mathrm{t}})$. The rate in (5.9b) can be shown to satisfy $\eta^{\mathrm{I}}_{\mathrm{MASM}}(r = 1) > \cdots > \eta^{\mathrm{I}}_{\mathrm{MASM}}(r = N_{\mathrm{t}})$ when $M = 1$, $\eta^{\mathrm{I}}_{\mathrm{MASM}}(r = 2) > \eta^{\mathrm{I}}_{\mathrm{MASM}}(r = 1)$ when $N_{\mathrm{t}} = 2$, $\eta^{\mathrm{I}}_{\mathrm{MASM}}(r = 3) > \eta^{\mathrm{I}}_{\mathrm{MASM}}(r = 1) > \eta^{\mathrm{I}}_{\mathrm{MASM}}(r = 2)$ when $N_{\mathrm{t}} = 3$, and $\eta^{\mathrm{I}}_{\mathrm{MASM}}(r = 1) > \cdots > \eta^{\mathrm{I}}_{\mathrm{MASM}}(r = N_{\mathrm{t}} - 2) > \eta^{\mathrm{I}}_{\mathrm{MASM}}(r = N_{\mathrm{t}}) > \eta^{\mathrm{I}}_{\mathrm{MASM}}(r = N_{\mathrm{t}} - 1)$ when $N_{\mathrm{t}} > 3$.

Based on the sorted CSI, a one-to-one mapping between the N_{t} antennas and the events $\mathcal{E} \to [r]$ can be developed as was shown in Section 5.3.4 for SM technique.

5.5 Irregular Antenna Activation with Antenna Selection

In this part, two AS methods for SM techniques implementing the I-AA are proposed.

5.5.1 Joint Rate and Euclidean-Distance Optimized Antenna Selection (REAS)

Assume $N_{\mathrm{T}} > N_{\mathrm{t}}$ antennas at the transmitter and N_{r} antennas at the receiver. The channel matrix $\tilde{\mathbf{H}} \in \mathbb{C}^{N_{\mathrm{r}} \times N_{\mathrm{T}}}$. The number of possible outcomes when choosing a subset of N_{t} antennas out of the N_{T} available is $\binom{N_{\mathrm{T}}}{N_{\mathrm{t}}}$. Let $\mathfrak{I}$ represent the set of all such outcomes. The REAS technique first maximizes the minimum Euclidean distance among the transmit vectors, conditioned on the channel matrix $\tilde{\mathbf{H}}$, according to

$$\hat{I} = \arg\max_{I \in \mathfrak{I}} \left\{ \min_{m \neq m'} \left\| \tilde{\mathbf{H}}(I)(s_m - s_{m'}) \right\|_2^2 \right\}, \tag{5.10}$$

where $\hat{I}$ denotes the N_{t} column indices of $\tilde{\mathbf{H}}$. The channel matrix after the antenna selection can be denoted as $\tilde{\mathbf{H}}(\hat{I}) \in \mathbb{C}^{N_{\mathrm{r}} \times N_{\mathrm{t}}}$. For simplicity, assume that the first N_{t} antennas out of the available N_{T} is chosen as per (5.10). Hence, $\hat{I} = 1, \cdots, N_{\mathrm{t}}$.

Next, sort the N_t columns of $\tilde{\mathbf{H}}(\hat{I})$ in descending order according to $\|\mathbf{h}_n\|^2$. For the sake of explanation, we assume that the sorted N_t columns of $\tilde{\mathbf{H}}(\hat{I})$ obey *Assumption-1*. The mapping of the events $\mathcal{E} \rightarrow [r]$ to transmit antenna indices is then performed as per Section 5.3.4 for the SM technique implementing I-AA, and as per Section 5.4.1 for the GSM and MASM techniques with I-AA.

The order of complexity in evaluating (5.10) is $\mathcal{O}\left(\binom{N_\mathrm{T}}{N_\mathrm{t}} N_\mathrm{t}^2 M^2\right)$. The order of complexity when sorting the CSI grows linearly with N_t. Hence, the overall complexity is $\mathcal{O}\left(\binom{N_\mathrm{T}}{N_\mathrm{t}} N_\mathrm{t}^2 M^2 + N_\mathrm{t}\right)$. Note that the receiver informs the transmitter once $\hat{I}$ is chosen and the CSI is sorted. The signaling overhead for reporting the chosen $\hat{I}$ from the receiver to the transmitter is $\lceil \log_2 \binom{N_\mathrm{T}}{N_\mathrm{t}} \rceil$ bits per coherence interval. The overhead in reporting the sorted CSI pertaining to the chosen $\hat{I}$ is $\lceil \log_2 N_\mathrm{t}! \rceil$. Therefore, the overall signalling overhead is $\lceil \log_2 \left(N_\mathrm{t}! \binom{N_\mathrm{T}}{N_\mathrm{t}}\right) \rceil$ bits per coherence interval.

5.5.2 Rate-Optimized Low-Complexity Antenna Selection (RLAS)

The higher complexity and signalling overhead of REAS in SM techniques implementing the proposed I-AA motivates the proposal of a less-complex AS method, namely RLAS. For a given coherence interval, let us assume that the channel gains satisfy $\|\mathbf{h}_1\|^2 > \cdots > \|\mathbf{h}_{N_\mathrm{t}}\|^2 > \cdots > \|\mathbf{h}_{N_\mathrm{T}}\|^2$. Based on the sorted CSI, first, the antennas $(1, \cdots, N_\mathrm{t})$ are chosen as part of the AS process. Then, a one-to-one mapping between the events $\mathcal{E} \rightarrow [r]$ and the N_t chosen antennas is performed, as per Section 5.3.4 for the I-AA assisted SM technique and Section 5.4.1 for the I-AA assisted GSM and MASM techniques.

When using RLAS, sorting CSI is the only associated complexity, given by $\mathcal{O}(N_\mathrm{T})$, whereas the signalling overhead is $\lceil \log_2 N_\mathrm{T}! \rceil$ bits per coherence interval.

Remark: Only I-AA allows joint optimization of the rate and Euclidean distance (cf. Section 5.5.1), or rate and better channel selection (cf. Section 5.5.2) for AS. The rate optimization cannot be exploited in U-AA. Therefore, the methods of REAS and RLAS are not applicable when implementing U-AA. Only the EAS and LAS, proposed in [51], can be implemented when using U-AA. In EAS, the set of the N_t out of N_T antennas, denoted by $\hat{I}$, is obtained using (5.10), whereas in LAS, the chosen set of N_t antennas pertains to the first N_t maximum order statistics of $\tilde{\mathbf{H}}$.

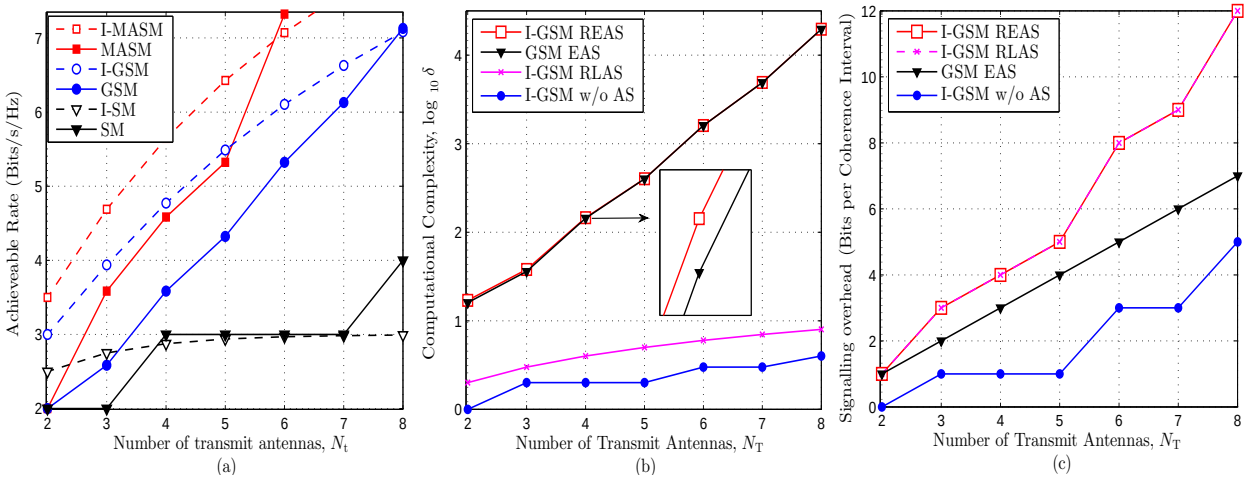

Figure 5.2: Performance comparison of U-AA and I-AA in different SM variants for various numbers of transmit antennas: (a) achievable rate, (b) computational complexity, (c) signalling overhead.

5.6 Performance Analysis

A closed-form upper-bound on the average BER of SM technique implementing I-AA with/without the proposed AS methods considering transmissions over Rayleigh fading channels and single- or multiple-antenna reception is derived in Appendix D.1. The computational complexity and signalling overhead associated with the use of I-AA and U-AA with/without AS is also presented. Hereafter, SM, GSM, and MASM implementing I-AA are denoted by I-SM, I-GSM, and I-MASM, whereas under U-AA, they are denoted by SM, GSM, and MASM.

5.6.1 Performance Overview

Figure 5.2(a) depicts the achievable rates of SM, GSM, MASM, I-SM, I-GSM, and I-MASM versus the total number of transmit antennas N_t, when using $M = 2$. As observed, I-SM, I-GSM, and I-MASM achieve higher rate performance as compared to SM, GSM, and MASM, particularly for small values of N_t, making SM with I-AA a suitable technique for uplink communications. The grouping method of parallel quadrature SM [63] can be adopted to increase the rate performance of I-AA when N_t is large.

Figure 5.2(b) shows the complexity of the proposed AS methods in I-GSM against GSM with EAS and I-GSM without AS. I-GSM with EAS demands $\mathcal{O}(N_t)$ additional complexity, which is negligible as compared to that of GSM with EAS. I-GSM with RLAS only requires sorting the

CSI and, thus, achieves a significantly smaller complexity as compared to GSM with EAS and also I-GSM with REAS. The complexity of I-GSM without AS is only $\mathcal{O}(N_\mathrm{t})$, making it suitable for computationally-constrained uplink communications.

The reported higher rate performance and smaller computational complexity of I-AA assisted SM techniques is achieved at the expense of signalling overhead. A comparison of the overhead is shown in Fig. 5.2(c). Note that I-GSM with REAS or RLAS requires the same signalling overhead, which is higher than the one of GSM with EAS, especially for high values of N_t, which is the trade-off when using I-AA along with AS. However, I-GSM without AS requires a much smaller overhead as compared to I-GSM and GSM with AS.

5.6.2 Numerical Results and Performance Verification

Figure D.1 illustrates a numerical verification of the derived average PEP expressions of SM, I-SM, and O-MIMO, and also shows the advantages of I-SM over SM in terms of average SNR and average PEP. The SNR results were obtained using (D.4) for SM without AS, (D.18) for SM with AS, (D.9) for I-SM without AS, (D.19) for I-SM with AS, and (D.10) for O-MIMO. The PEP results were obtained using (D.13a) for SM without AS, (D.21a) for SM with AS, (D.14) for I-SM without AS, (D.22a) for I-SM with AS, and (D.16) for O-MIMO. In Fig D.1, $\mathcal{C}_1$, $\mathcal{C}_2$, $\mathcal{C}_3$ and $\mathcal{C}_4$ are named cut-off points, whereas $\mathcal{D}_1, \mathcal{D}_2, \mathcal{D}_3, \mathcal{D}_4, \mathcal{D}_5$ and $\mathcal{D}_6$ are named convergence points. The significance of these points will be revealed shortly.

Figure D.1(a) shows a comparison of the average SNR versus the number of antennas N_t in SM, I-SM, and O-MIMO techniques. The average SNR is upper-bounded by the O-MIMO technique. The average SNR of SM without AS remains constant for all values of N_t, whereas the average SNR with I-SM without AS increases when increasing N_t. Particularly, I-SM achieves 3.5dB SNR gain over SM when $N_\mathrm{t} = 10$. When implementing AS, it can be seen that the average SNR achieved with SM decreases nearly linear as $N_\mathrm{T} - N_\mathrm{t}$ decreases, whereas the average SNR achieved with I-SM remains almost constant when $N_\mathrm{t} \geq 3$. I-SM is especially beneficial in terms of SNR at higher values of N_t.

Figure D.1(b) depicts the average PEP versus the number of antennas N_t in SM, I-SM, and O-MIMO techniques with and without AS, at $\frac{1}{\sigma^2} = 10$dB. The average PEP with and without

AS is upper-bounded by the O-MIMO technique. Without AS, the average PEP of SM and O-MIMO remains constant for all values of N_{t}. The average PEP performance of I-SM without AS decreases as N_{t} increases. When implementing AS, the average PEP performance of SM increases with increasing N_{t}, whereas that of I-SM remains nearly constant for $N_{\mathrm{t}} \geq 3$.

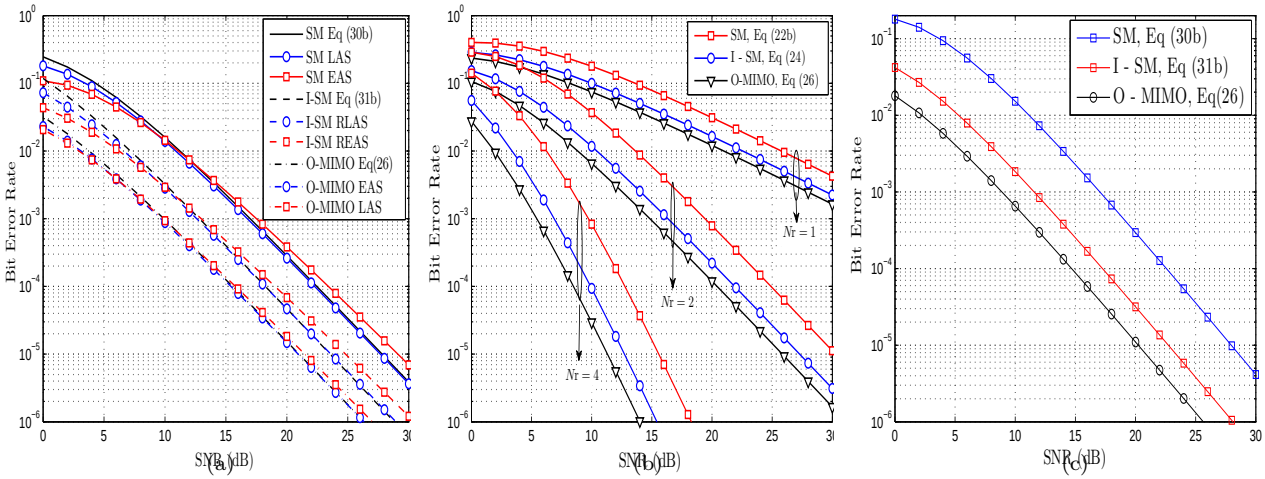

Figure 5.3: BER comparisons of SM, I-SM, and O-MIMO employing $N_{\mathrm{T}} = 10$ and $N_{\mathrm{t}} = 5$: (a) theoretical vs. simulation results when employing AS and $N_{\mathrm{r}} = 2$; (b) results without AS and different N_{r} settings; (c) results with AS and $N_{\mathrm{r}} = 2$.

The significance of the cut-off and convergence points (cf. Fig. D.1) is discussed as follows. $\mathcal{D}_1$: In terms of SNR, (D.10) and (D.9) converge to (D.4), whereas in terms of PEP, (D.16) and (D.14) converge to (D.13a). $\mathcal{D}_2$: In terms of SNR, (D.10) and (D.19) converges to (D.18), whereas in terms of PEP, (D.16) and (D.22a) converges to (D.21a). $\mathcal{D}_3$: In terms of SNR, (D.9) converges to (D.4), whereas in terms of PEP, (D.14) converges to (D.13a). $\mathcal{D}_4$: In terms of SNR, (D.14) is valid for O-MIMO with and without AS, whereas in terms of PEP, (D.16) is valid for O-MIMO with and without AS. $\mathcal{D}_5$: In terms of SNR, (D.19) converges to (D.9), whereas in terms of PEP, (D.22a) converges to (D.14). $\mathcal{D}_6$: In terms of SNR, (D.10) is valid for O-MIMO with and without AS, whereas in terms of PEP, (D.16) is valid for O-MIMO with and without AS.

The significance of each cut-off point is itemized as follows. $\mathcal{C}_1$: In terms of SNR, the use of I-SM with AS over SM with AS is only beneficial when $N_{\mathrm{t}} > 2$. In terms of PEP, I-SM with AS is superior to SM with AS only when $N_{\mathrm{t}} > 2$. In terms of rate performance, it will shortly be shown that I-SM outclasses SM even when $N_{\mathrm{t}} = 2$. $\mathcal{C}_2$: In terms of SNR and PEP, O-MIMO with $(N_{\mathrm{T}} = 4, N_{\mathrm{t}} = 1)$ outperforms SM with $(N_{\mathrm{T}} = 10, 4 \leq N_{\mathrm{t}} \leq 10)$, whereas I-SM at $(N_{\mathrm{T}} = 10, N_{\mathrm{t}} = 4)$ is superior to both SM and O-MIMO. $\mathcal{C}_3$: In terms of SNR and average PEP, I-SM with $(N_{\mathrm{T}} = 10, 5 \leq N_{\mathrm{t}} \leq 10)$

is only outclassed by O-MIMO with ($N_{\mathrm{T}} \geq 5, N_{\mathrm{t}} = 1$). $\mathcal{C}_4$: In terms of SNR, when $N_{\mathrm{t}} > 5$, I-SM without AS can outclass SM with AS when ($N_{\mathrm{T}} = 10, 5 \leq N_{\mathrm{t}} \leq 10$). In terms of PEP, for $N_{\mathrm{t}} > 5$ I-SM without AS can outclass SM with AS when ($N_{\mathrm{T}} = 10, 5 \leq N_{\mathrm{t}} \leq 10$).

The above results on convergence points clarify the correctness of the derived average SNR and average PEP expressions. The so-called cut-off points highlight the preference of I-SM over SM in a $N_{\mathrm{T}} = 10, 1 \leq N_{\mathrm{t}} \leq 10$ setting of a SM system. Next, comparative results are presented.

5.7 Comparative Results

The performances of I-SM, I-GSM and I-MASM are compared to SM, GSM and MASM, in terms of BER and achievable rate. The rate of O-MIMO is $\log_2 M$ bits/s/Hz, which is smaller compared to the rates of I-SM, I-GSM, and I-MASM, and their conventional counterparts. The BER results of O-MIMO are presented as benchmark to better highlight the advantages of I-AA over U-AA. All results were obtained considering transmissions over Rayleigh flat fading channels.

5.7.1 Bit Error Rate

In Fig. 5.3(a), we compare the impact of the antenna selection methods (EAS, REAS, LAS, and RLAS) in SM and I-SM. The following observations can be made: 1) The results obtained with (D.21b), (D.22b), and (D.17), for SM, I-SM, and O-MIMO, with AS, closely match the simulation results, thereby corroborating the derivations. 2) LAS outperforms EAS at higher SNRs. This point was also concluded in [51]. 3) As expected, I-SM outclasses SM, with a gain of 4dB at a BER of 10^{-4}. Considering the better BER performance and low complexity of LAS and RLAS compared to EAS and REAS, in the remaining part of this section we adopt RLAS when I-AA is implemented, and LAS when employing U-AA.

Figure 5.3(b) presents BER versus SNR comparison of SM and I-SM without AS, when $N_{\mathrm{t}} = 5$, $M = 2$ (BPSK), and $N_{\mathrm{r}} = 1,\ 2$ or 4. The BER performance of I-SM is close to that of O-MIMO. The following points can be observed. The SNR gain of I-SM over SM is 4dB when $N_{\mathrm{r}} = 1$, 3dB when $N_{\mathrm{r}} = 2$, and 2dB when $N_{\mathrm{r}} = 4$. The vanishing SNR gain when increasing N_{r} can be explained using the order statistics of matrices. Particularly, it can be shown that

$\lim_{N_\mathrm{r}\to\infty} \mathrm{E}_r[\sum_{n_\mathrm{r}=1}^{N_\mathrm{r}}(\mathbf{H}_{n_\mathrm{r}}), r+1] - \mathrm{E}[\sum_{n_\mathrm{r}=1}^{N_\mathrm{r}}(\mathbf{H}_{n_\mathrm{r}}), r] \approx 0$, $\forall n_\mathrm{t}$, where $\mathrm{E}_r[\sum_{n_\mathrm{r}=1}^{N_\mathrm{r}}(\mathbf{H}_{n_\mathrm{r}}), r]$ is the mean value of the r^{th} order statistic of $\sum_{n_\mathrm{r}=1}^{N_\mathrm{r}}(\mathbf{H}_{n_\mathrm{r}})$. Hence, in terms of BER, the I-SM is more beneficial under smaller number of receive antennas, especially when $N_\mathrm{r} = 1$.

Figure 5.3(c) compares the BER performance of SM, I-SM and O-MIMO for $N_\mathrm{T} = 10, N_\mathrm{t} = 5$, when $M = 2$ and $N_\mathrm{r} = 2$. At a BER of 10^{-4}, the SNR loss of SM and I-SM compared to O-MIMO is 8dB and 2dB, respectively. The said loss is explained as follows. The O-MIMO uses the best channel (pertaining to the 10^{th} order statistics of $\mathbf{H}$) for transmission with probability one, whereas SM uses the $1^{\mathrm{st}}, 2^{\mathrm{nd}}, 3^{\mathrm{rd}}, 4^{\mathrm{th}}$ and 5^{th} best channels, i.e., those pertaining to the $10^{\mathrm{th}}, 9^{\mathrm{th}}, 8^{\mathrm{th}}, 7^{\mathrm{th}}$ and 6^{th} order statistics of $\mathbf{H}$, with equal probability $\frac{1}{N_\mathrm{t}} = 0.2$. I-SM, on the other hand, uses the $1^{\mathrm{st}}, 2^{\mathrm{nd}}, 3^{\mathrm{rd}}, 4^{\mathrm{th}}$ and 5^{th} best channels with probabilities $0.5, 0.25, 0.125, 0.0625$ and 0.625, respectively, which results in a better received SNR and, hence, better BER performance.

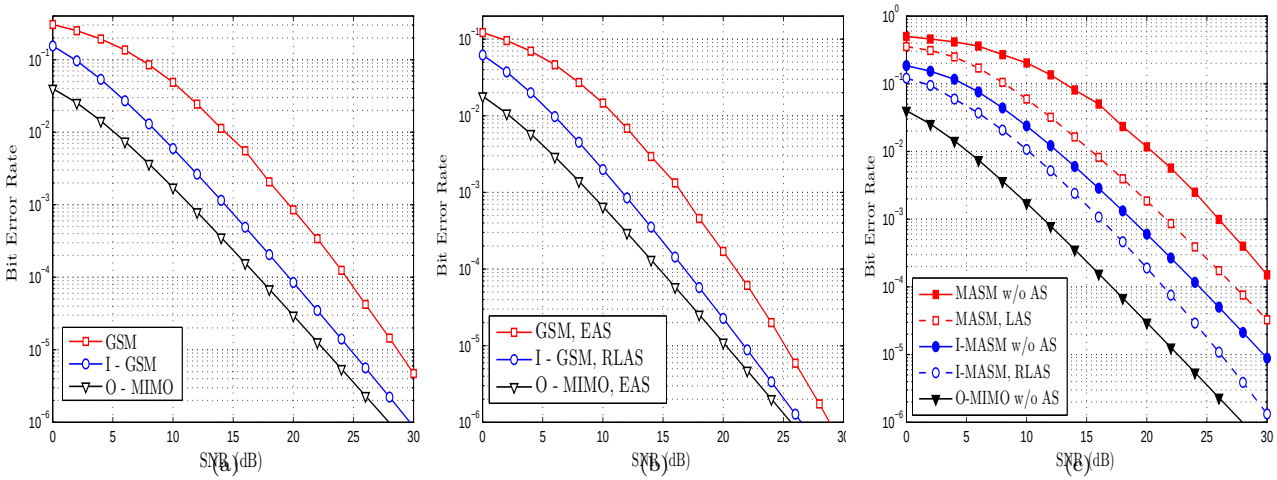

Figure 5.4: BER comparisons of GSM, I-GSM, MASM, I-MASM and O-MIMO employing $N_\mathrm{T} = 10$ and $N_\mathrm{t} = 5$: (a) results without AS and $N_\mathrm{r} = 2$, (b) results with AS and $N_\mathrm{r} = 2$, (c) results with/without AS and $N_\mathrm{r} = 2$.

In Fig. 5.4(a), the performances of GSM and I-GSM are compared when no AS is used. Here, $N_\mathrm{t} = 5$, $M = 2$ and $N_\mathrm{r} = 2$. At a BER of 10^{-4}, I-GSM achieves 4dB SNR gain over GSM. The SNR gain is more significant at medium values of SNR. From (5.8), the average number of active antennas in I-GSM is $K_\mathrm{av} = 1.9$, whereas GSM uses $K = 3$ active antennas. The use of a smaller number of active antennas in I-GSM ensures better channel utilization with higher probability, and yields better BER. Fig. 5.4(b) depicts the BER performance of GSM and I-GSM when implementing AS. Here, $N_\mathrm{T} = 10$, $N_\mathrm{t} = 5$, $M = 2$ and $N_\mathrm{r} = 2$. At a BER of 10^{-4}, I-GSM with RLAS achieves 4dB SNR gain over GSM with EAS. I-GSM with RLAS outclasses the computationally expensive GSM

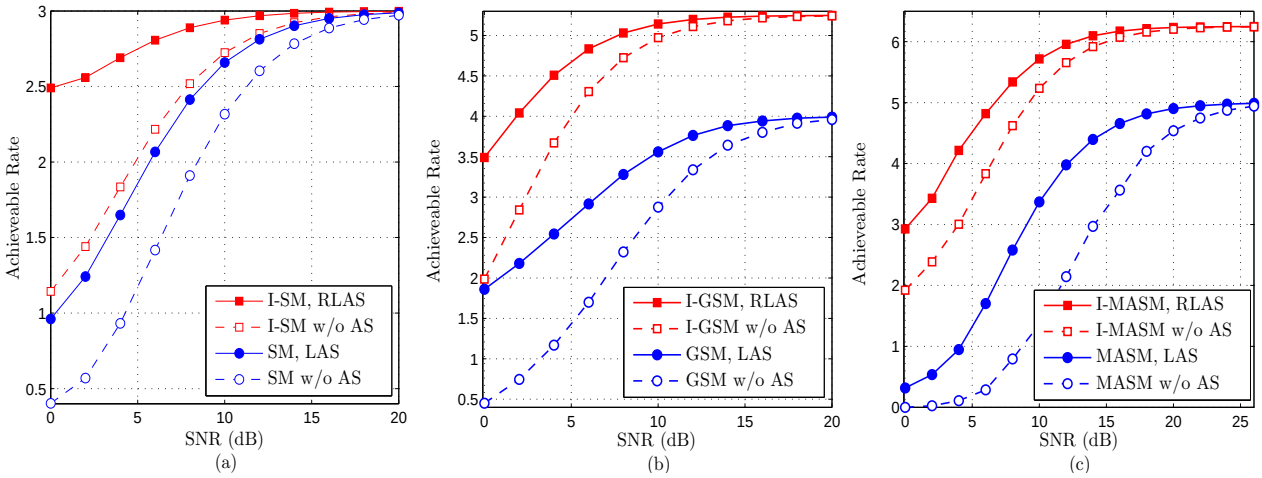

Figure 5.5: Achievable rate comparisons with/without AS: (a) SM vs. I-SM, (b) GSM vs. I-GSM, (c) MASM vs. I-MASM.

with EAS for all values of SNR. Comparing I-GSM without AS (cf. Fig. 5.4(a)) with GSM EAS (cf. Fig. 5.4(b)), it can be concluded that I-GSM without AS can outclass GSM with AS.

Figure 5.4(c) depicts a BER comparison of MASM and I-MASM with and without AS. I-MASM achieves 8dB gain over MASM when no AS is used, and 3dB gain over MASM with LAS. Moreover, I-MASM with RLAS achieves 10dB gain over MASM without AS, and 6dB gain over MASM with LAS.

5.7.2 Achievable Rate

For the comparisons, the achievable rate is calculated using $\mathcal{R} \leq \epsilon(1 + P_{\mathrm{e}} \log_2 P_{\mathrm{e}} + (1 - P_{\mathrm{e}}) \log_2(1 - P_{\mathrm{e}}))$ bits/s/Hz, where ϵ equals $\eta^{\mathrm{u}}_{\mathrm{SM}}$ for SM, $\eta^{\mathrm{I}}_{\mathrm{SM}}$ for I-SM, $\eta^{\mathrm{u}}_{\mathrm{GSM}}$ for GSM, $\eta^{\mathrm{I}}_{\mathrm{GSM}}$ for I-GSM, $\eta^{\mathrm{u}}_{\mathrm{MASM}}$ for MASM, and $\eta^{\mathrm{I}}_{\mathrm{MASM}}$ for I-MASM.

Figure 5.5(a) compares the rates of SM and I-SM with and without AS. As observed, the use of LAS with SM improves the achievable rate as compared to SM without AS. The I-SM technique without AS achieves higher rate as compared to SM with LAS. Significant rate improvements can be obtained when I-SM is used with RLAS.

Figure 5.5(b) shows the rate performance of GSM and I-GSM with and without AS, when $N_{\mathrm{t}} = 5$, $N_{\mathrm{T}} = 10$, $M = 2$, and $N_{\mathrm{r}} = 2$. The achievable rate of I-GSM is higher than that of GSM for the whole SNR range. The superiority is explained as follows. First, the rate performance of

I-GSM is higher than that of the GSM as shown in (5.9a), and also demonstrated in Fig. 5.2(a). Secondly, I-GSM has a better BER performance as compared to GSM. I-GSM with RLAS achieves up to 1.5, 1.8, and 1.25 bits/s/Hz gain over GSM with LAS, in the low, medium, and high SNR ranges, respectively. Moreover, I-GSM without AS outperforms GSM with LAS.

Figure 5.5(c) depicts the achievable rates of MASM and I-MASM with and without AS. Here, $N_{\mathrm{t}} = 5$, $N_{\mathrm{T}} = 10$, $M = 2$, and $N_{\mathrm{r}} = 2$. A similar trend as in Fig. 5.5(a) can be observed. In summary, whether AS is used or not, the rate performance of I-MASM is superior to that of MASM.

5.7.3 Applications in Other Domains and Extensions

The I-AA technique can be easily tailored for applications in various other communication domains, including the time-slot level, in the form of SCIM [11], CIM [64], and OFDM-IM [10]. Also, the proposed REAS and RLAS methods can be applied to the time, code, and subcarrier domains of SCIM, CIM, and OFDM-IM, respectively. Furthermore, the I-AA concept can be extended when the communication systems are aided with reconfigurable intelligent surfaces (RIS) [65] for rate and BER performance enhancements. The I-AA concept can be used to reduce the complexity and overhead associated with the selection of RIS elements, while at the same time achieving desirable received SNRs. The use of I-AA in massive MIMO and RIS is very appealing. Moreover, the use of the I-AA in simultaneous wireless information and power transfer can also result in better signal detection and better energy harnessing. The concept of I-AA can also enhance the physical-layer security due to its high flexibility in terms of information-similarity to antenna mapping. I-AA can find application in the mobility scenarios as well, e.g., the information-similarity to antenna mapping can be based on delay spread and/or Doppler spread in vehicle-to-vehicle and vehicle-to-everything communication systems including high-speed railway communication systems.

With I-AA, the transmission rate changes from one transmission period to another, which can cause error propagation. The use of bit-padding [45] and adaptive modulation can ensure constant transmission rate and overcome the error propagation, which is our main motivation for future work. Moreover, power allocation over both the temporal domain and the spatial domain of a MIMO system implementing I-AA is an interesting problem. Rate and energy efficiency maximization is another open research problem. Finally, identifying and investigating different use-cases for I-AA based MIMO transmissions is an interesting area as well.

5.7.4 Application of Spatial Modulation in Cell-free MIMO

In cell-free MIMO, a large number of antennas are distributed along a serving area to serve a number of users. Distribution of the antennas helps in reducing complexity and is shown to achieve promising gains in capacity. In cell-free MIMO, a UE can be served using more than one access point. Rel-17 and Rel-18 of 3GPP supports non-coherent (NC) and coherent (C) joint transmission (JT) schemes, where a single user is served by more than one transmission reception point (TRP), where a plurality of TRPs can form a cell. Loosely speaking, the concept of NCJT and CJT are closely align with cell-free MIMO. Both NCJT and CJT has been show to achieve superior throughput performance and has been specified for implementation by 3GPP in Rel-17 and Rel-18.

Based on the rate and reliability assessment of spatial modulation, it can be concluded that spatial modulation can further reduce the power consumption and complexity in cell-free MIMO. Particularly, the number of RF branches as well as the number of antenna needed for a target rate can be further reduced, which can help in further enhancing the performance of cell-free MIMO.

5.8 Concluding Remarks

This paper highlighted U-AA in SM-based communication systems as the main culprit behind severe performance losses when CSI is available. The novel method of I-AA was proposed, and its use in prominent variants of SM was shown to outshine U-AA in terms of rate and BER performances. Two AS methods, i.e., rate and Euclidean distance optimized AS, and rate-optimized low-complexity AS, were also proposed. The prominent variants of SM implementing I-AA without AS were shown to outclass their counterparts with U-AA and AS, in terms of rate and BER performances. SM-based MIMO communication implementing I-AA and RLAS was identified as a better scheme due to its better performance, lower complexity, and reduced signalling overhead. Also, applications of the I-AA concept in other domains were discussed.

Conclusion

Chapter 6

Conclusion

This thesis addressed the fundamental problems of spatial modulation, i.e., low data-rate and low reliability. The low data-rate problem was addressed in the first Part I and the reliability issues of spatial modulation were addressed in Part II of this thesis. A detailed summary of each part is presented as follows.

In Part I, we first systematically studied the low data-rate problem of IM techniques. It was proven that IM techniques can surpass the data-rate of traditional techniques under the constraint $N \geq 2M$ when properly selecting the design parameters (N, K, M). The OFDM-GIM$_1$ technique was shown to relax the $N \geq 2M$ condition of OFDM-IM by half, as it only requires $N \geq M-1$ subcarriers in a group to outperform classical OFDM. Unlike previous works, it was shown that OFDM-IM and OFDM-GIM$_1$ can surpass classical OFDM even at a high-rate transmission. OFDM-GIM$_2$ was designed for low data-rate communications demanding superior energy efficiency performance. The concept of IM, GIM and the proposed design guidelines, were shown to equally hold valid for IM techniques in other domains. The use of IM and GIM in the space, code, and time domains can outclass the BER, achievable rate, and energy efficiency performance of conventional MIMO (SMx), DSSS, and SC systems. Furthermore, under equal rate requirement, the use of IM can achieve savings of bandwidth in OFDM, antenna elements in MIMO, codes/bandwidth in DSSS, and time slots in a SC system. The use of GIM$_1$ allows to further relax the required conditions to achieve the mentioned gains in OFDM, MIMO, DSSS, and SC systems (cf. savings in the number of transmit and receive antennas in GSM over SMx [35]).

The second chapter of Part I first presented design guidelines to address the low data-rate problem of SM. It was proved that MASM requires fewer active transmit antennas N_{a} and fewer receive antennas N_{r} to surpass the data-rate of spatial multiplexing, or fewer number of transmit antennas N_{t}, N_{a} and N_{r} to match the said data-rate. MASM can deliver high data rates with fewer hardware units, low power and reduced inter-carrier interference, inter-antenna synchronization, cost, complexity, and device size, compared to spatial multiplexing. Also, the data-rate and diversity tradeoff of conventional MIMO can be overcome by the proposed Enhanced MASM technique.

In Part II of this thesis, we first addressed the problem of irregular antenna activation in SM techniques, which causes high BER and losses in data-rate. A space-time mapping design in which the encoding procedure is extended to multiple symbol periods was proposed, and its merits were demonstrated in the well-known SM, GSM, and QSM techniques. Coding gain which arises from the near-uniform antenna activation was also analyzed. Use of the proposed space-time mapping can enable SM techniques to operate with near-optimal performance, making it a suitable candidate for B5G MIMO communications, where the number of antennas at devices can be highly constrained due to the size limitations. The reported gains were shown possible with a marginal increment in detection complexity. Moreover, the proposed mapping can be easily adopted in various other index modulation techniques.

Finally, Chapter 5 of Part II first highlighted U-AA in SM-based communication systems as the main culprit behind severe performance losses when CSI is available. The novel method of I-AA was proposed, and its use in prominent variants of SM was shown to outshine U-AA in terms of rate and BER performances. Two AS methods, i.e., rate and Euclidean distance optimized AS, and rate-optimized low-complexity AS, were also proposed. The prominent variants of SM implementing I-AA without AS were shown to outclass their counterparts with U-AA and AS, in terms of rate and BER performances. SM-based MIMO communication implementing I-AA and RLAS was identified as a better scheme due to its better performance, lower complexity, and reduced signalling overhead. Also, applications of the I-AA concept in other domains were discussed.

This project resulted in the following publications.

- M. Irfan and S. Aïssa, "On the spectral efficiency of orthogonal frequency-division multiplexing with index modulation," in Proc. *IEEE Global Commun. Conf. (GLOBECOM), Abu Dhai, UAE*, Dec. 2018, pp. 1–6.

- M. Irfan and S. Aïssa, "Multiple active spatial modulation: A possibility of more than spatial multiplexing," *IEEE Wireless Commun. Lett.*, vol. 9, no. 3, pp. 294–297, Mar. 2019.
- M. Irfan and S. Aïssa, "Space-time mapping for equiprobable antenna activation in spatial modulation," *IEEE Commun Lett.*, vol. 24, no. 12, pp. 2961–2964, Dec. 2020.
- M. Irfan and S. Aïssa, "Generalization of index-modulation: Breaking the conventional limits on spectral and energy efficiencies," *IEEE Trans. Wireless Commun.*, vol. 20, no. 6, pp. 3911–3924, June 2021.
- M. Irfan and S. Aïssa, "Information-Guided Antenna Selection and Activation for Spatial Modulation MIMO Systems," *IEEE Trans. Wireless Commun.*, (in press, accepted Feb. 2024).

References

[1] V. Cisco, "Visual networking index: forecast and trends, 2017–2022," *White Paper*, 2018.

[2] A. S. Andrae and T. Edler, "On global electricity usage of communication technology: trends to 2030," *Challenges*, vol. 6, no. 1, pp. 117–157, 2015.

[3] X. Cheng, M. Zhang, M. Wen, and L. Yang, "Index modulation for 5G: Striving to do more with less," *IEEE Wireless Commun.*, vol. 25, no. 2, pp. 126–132, Apr. 2018.

[4] M. Wen, X. Cheng, and L. Yang, *Index modulation for 5G wireless communications*. Springer, 2017.

[5] E. Basar, U. Aygolu, E. Panayirci, and H. V. Poor, "Orthogonal frequency division multiplexing with index modulation," *IEEE Trans. Sig. Process.*, vol. 61, no. 22, pp. 5536–5549, Nov. 2013.

[6] M. Nakao, T. Ishihara, and S. Sugiura, "Single-carrier frequency-domain equalization with index modulation," *IEEE Commun. Lett.*, vol. 21, no. 2, pp. 298–301, Feb. 2017.

[7] A. Younis, N. Serafimovski, R. Mesleh, and H. Haas, "Generalised spatial modulation," in *Proc. Asilomar Conf. Sig., Sys. Comp., Pacific Grove, USA*, Nov. 2010, pp. 1498–1502.

[8] G. Kaddoum, Y. Nijsure, and H. Tran, "Generalized code index modulation technique for high-data-rate communication systems," *IEEE Trans. Veh. Technol.*, vol. 65, no. 9, pp. 7000–7009, Sep. 2016.

[9] R. Mesleh and A. Alhassi, *Space Modulation Techniques*. John Wiley & Sons, 2018.

[10] M. Irfan and S. Aïssa, "Generalization of index-modulation: Breaking the conventional limits on spectral and energy efficiencies," *IEEE Trans. Wireless Commun.*, vol. 20, no. 6, pp. 3911–3924, June 2021.

[11] R. Abu-alhiga and H. Haas, "Subcarrier-index modulation OFDM," in *Proc. 20th Int. Symp. Personal, Indoor. Mobile Radio Commun., Tokyo, Japan*, 2009, pp. 177–181.

[12] D. Tsonev, S. Sinanovic, and H. Haas, "Enhanced subcarrier index modulation (SIM) OFDM," in *Proc. IEEE Global Commun. Conf., Workshops, Tx., USA*, Dec. 2011, pp. 728–732.

[13] M. Wen, X. Cheng, M. Ma, B. Jiao, and H. V. Poor, "On the achievable rate of OFDM with index modulation," *IEEE Trans Sig. Process.*, vol. 64, no. 8, pp. 1919–1932, April 2016.

[14] T. M. et al., "Dual-mode index modulation aided OFDM," *IEEE Access*, vol. 5, pp. 50–60, Aug. 2017.

[15] M. Wen, E. Basar, Q. Li, B. Zheng, and M. Zhang, "Multiple-mode orthogonal frequency division multiplexing with index modulation," *IEEE Trans. Commun.*, vol. 65, no. 9, pp. 3892–3906, Sep. 2017.

[16] Q. Ma, P. Yang, Y. Xiao, H. Bai, and S. Li, "Error probability analysis of OFDM-IM with carrier frequency offset," *IEEE Commun. Lett.*, vol. 20, no. 12, pp. 2434–2437, Dec. 2016.

[17] E. Memisoglu, E. Basar, and H. Arslan, "Low complexity peak-to-average power ratio reduction in OFDM-IM," in *Proc. IEEE Int. Black Sea Conf. Commun. Net. (BlackSeaCom), Batumi, Georgia*, June 2018, pp. 1–5.

[18] K. Kim, "PAPR reduction in OFDM-IM using multilevel dither signals," *IEEE Commun. Lett.*, vol. 23, no. 2, pp. 258–261, Feb. 2019.

[19] A. I. Siddiq, "Effect of subcarrier activation ratio on the performance of OFDM-IM over Rayleigh fading channel," *IEEE Commun. Lett.*, vol. 21, no. 6, pp. 1293–1296, June 2017.

[20] N. H. Nguyen, B. Berscheid, and H. H. Nguyen, "Fast-OFDM with index modulation for NB-IoT," *IEEE Commun. Lett.*, vol. 23, no. 7, pp. 1157–1160, July 2019.

[21] M. Irfan and S. Aïssa, "On the spectral efficiency of orthogonal frequency-division multiplexing with index modulation," in *IEEE Global Commun. Conf., Abu Dhabi, UAE*, Dec. 2018, pp. 1–6.

[22] M. Wen, B. Ye, E. Basar, Q. Li, and F. Ji, "Enhanced orthogonal frequency division multiplexing with index modulation," *IEEE Trans. Wireless Commun.*, vol. 16, no. 7, pp. 4786–4801, July 2017.

[23] J. Li, S. Dang, M. Wen, X. Jiang, Y. Peng, and H. Hai, "Layered orthogonal frequency division multiplexing with index modulation," *IEEE Sys. J.*, vol. 13, no. 4, pp. 3793–3802, Dec. 2019.

[24] Y. Xiao, S. Wang, L. Dan, X. Lei, P. Yang, and W. Xiang, "OFDM with interleaved subcarrier-index modulation," *IEEE Commun. Lett.*, vol. 18, no. 8, pp. 1447–1450, Aug. 2014.

[25] S. Gao, X. Cheng, and L. Yang, "Spatial multiplexing with limited RF chains: Generalized beamspace modulation (GBM) for mmwave massive MIMO," *IEEE J. Sel. Areas Commun.*, vol. 37, no. 9, pp. 2029–2039, Sept. 2019.

[26] T. Mao, Q. Wang, and Z. Wang, "Generalized dual-mode index modulation aided OFDM," *IEEE Commun. Lett.*, vol. 21, no. 4, pp. 761–764, April 2017.

[27] M. Wen, Q. Li, E. Basar, and W. Zhang, "Generalized multiple-mode OFDM with index modulation," *IEEE Tran. Wireless Commun.*, vol. 17, no. 10, pp. 6531–6543, Oct. 2018.

[28] J. Jeganathan, A. Ghrayeb, L. Szczecinski, and A. Ceron, "Space shift keying modulation for MIMO channels," *IEEE Trans. Wireless Commun.*, vol. 8, no. 7, pp. 3692–3703, Jul. 2009.

[29] R. Fan, Y. J. Yu, and Y. L. Guan, "Generalization of orthogonal frequency division multiplexing with index modulation," *IEEE Trans. Wireless Commun.*, vol. 14, no. 10, pp. 5350–5359, Oct. 2015.

[30] F. A. Prisecaru, "Mutual information and capacity of spatial modulation systems," *Jacobs Univ. Bremen, Germany, Tech. Rep. BSC2007*, 2007.

[31] I. Al-Nahhal, E. Basar, O. A. Dobre, and S. Ikki, "Optimum low-complexity decoder for spatial modulation," *IEEE J. Sel. Areas. Commun.*, vol. 37, no. 9, pp. 2001–2013, Sep. 2019.

[32] E. Khorov, A. Kiryanov, A. Lyakhov, and G. Bianchi, "A tutorial on IEEE 802.11ax high efficiency WLANs," *IEEE Commun. Surveys Tut.*, vol. 21, no. 1, pp. 197–216, 2019.

[33] Y. Ghasempour, C. R. C. M. da Silva, C. Cordeiro, and E. W. Knightly, "IEEE 802.11ay: Next-generation 60 GHz communication for 100 Gb/s Wi-Fi," *IEEE Commun. Mag.*, vol. 55, no. 12, pp. 186–192, Dec. 2017.

[34] M. C. Caballe, A. C. Auge, E. Lopez Aguilera, E. Garcia-Villegas, I. Demirkol, and J. P. Aspas, "An alternative to IEEE 802.11ba: Wake-up radio with legacy IEEE 802.11 transmitters," *IEEE Access*, vol. 7, pp. 48 068–48 086, April 2019.

[35] J. Wang, S. Jia, and J. Song, "Generalised spatial modulation system with multiple active transmit antennas and low complexity detection scheme," *IEEE Trans. Wireless Commun.*, vol. 11, no. 4, pp. 1605–1615, Apr. 2012.

[36] M. Irfan and S. Aïssa, "Multiple active spatial modulation: A possibility of more than spatial multiplexing," *IEEE Wireless Commun. Lett.*, vol. 9, no. 3, pp. 294–297, Mar. 2019.

[37] R. Y. Mesleh, H. Haas, S. Sinanovic, C. W. Ahn, and S. Yun, "Spatial modulation," *IEEE Trans. Veh. Technol.*, vol. 57, no. 4, pp. 2228–2241, Jul. 2008.

[38] R. Mesleh, S. S. Ikki, and H. M. Aggoune, "Quadrature spatial modulation," *IEEE Trans. Veh. Technol.*, vol. 64, no. 6, pp. 2738–2742, June 2015.

[39] T. Datta and A. Chockalingam, "On generalized spatial modulation," in *Proc. IEEE Wireless Commun. Network. Conf., Shanghai, China*, Apr. 2013, pp. 2716–2721.

[40] L. Zheng and D. N. C. Tse, "Diversity and multiplexing: a fundamental tradeoff in multiple-antenna channels," *IEEE Trans. Info. Theo.*, vol. 49, no. 5, pp. 1073–1096, May 2003.

[41] M. Irfan and S. Y. Shin, "Robust Walsh–Hadamard transform-based spatial modulation," *Digital Sig. Processing*, vol. 64, pp. 1–7, May 2017.

[42] M. Irfan and S. Aïssa, "Space-time mapping for equiprobable antenna activation in spatial modulation," *IEEE Commun Lett.*, vol. 24, no. 12, pp. 2961–2964, Dec. 2020.

[43] L. Xiao et al., "Single-RF and twin-RF spatial modulation for an arbitrary number of transmit antennas," *IEEE Trans. Veh. Technol.*, vol. 67, no. 7, pp. 6311–6324, July 2018.

[44] N. Serafimovski et al., "Fractional bit encoded spatial modulation (FBE-SM)," *IEEE Commun. Lett.*, vol. 14, no. 5, pp. 429–431, May 2010.

[45] Y. Yang and S. Aïssa, "Bit-padding information guided channel hopping," *IEEE Commun. Lett.*, vol. 15, no. 2, pp. 163–165, Feb. 2011.

[46] M. Wen et al., "Equiprobable subcarrier activation method for OFDM with index modulation," *IEEE Commun. Lett.*, vol. 20, no. 12, pp. 2386–2389, Dec. 2016.

[47] J. Luo, S. Wang, F. Wang, and W. Zhang, "Generalized precoding-aided spatial modulation via receive antenna transition," *IEEE Wireless Commun. Lett.*, vol. 8, no. 3, pp. 733–736, June 2019.

[48] A. M. Abu-Hudrouss, M. O. E. Astal, A. H. Al Habbash, and S. Aïssa, "Signed quadrature spatial modulation for MIMO systems," *IEEE Trans. Veh. Technol.*, vol. 69, no. 3, pp. 2740–2746, Mar. 2020.

[49] J. Luo, S. Wang, and F. Wang, "Joint transmitter-receiver spatial modulation design via minimum euclidean distance maximization," *IEEE J. Sel. Areas. Commun.*, vol. 37, no. 9, pp. 1986–2000, Sep. 2019.

[50] C. Xu et al., ""Near-perfect" finite-cardinality generalized space-time shift keying," *IEEE J. Sel. Areas. Commun.*, vol. 37, no. 9, pp. 2146–2164, Sep. 2019.

[51] R. Rajashekar et al., "Antenna selection in spatial modulation systems," *IEEE Commun. Lett.*, vol. 17, no. 3, pp. 521–524, Mar. 2013.

[52] Z. Zhou, N. Ge, and X. Lin, "Reduced-complexity antenna selection schemes in spatial modulation," *IEEE Commun. Lett.*, vol. 18, no. 1, pp. 14–17, Jan. 2014.

[53] Z. Sun, Y. Xiao, L. You, L. Yin, P. Yang, and S. Li, "Cross-entropy-based antenna selection for spatial modulation," *IEEE Commun. Lett.*, vol. 20, no. 3, pp. 622–625, Mar. 2016.

[54] Y. He, S. Atapattu, C. Tellambura, and J. S. Evans, "Opportunistic group antenna selection in spatial modulation systems," *IEEE Trans. Commun.*, vol. 66, no. 11, pp. 5317–5331, Nov. 2018.

[55] K. Ntontin, M. Di Renzo, A. I. Perez-Neira, and C. Verikoukis, "A low-complexity method for antenna selection in spatial modulation systems," *IEEE Commun. Lett.*, vol. 17, no. 12, pp. 2312–2315, Dec. 2013.

[56] P. Yang, Y. Xiao, Y. L. Guan, S. Li, and L. Hanzo, "Transmit antenna selection for multiple-input multiple-output spatial modulation systems," *IEEE Tran. Commun.*, vol. 64, no. 5, pp. 2035–2048, May 2016.

[57] Z. Sun, Y. Xiao, P. Yang, S. Li, and W. Xiang, "Transmit antenna selection schemes for spatial modulation systems: Search complexity reduction and large-scale MIMO applications," *IEEE Tran. Veh. Technol.*, vol. 66, no. 9, pp. 8010–8021, Sep. 2017.

[58] Y. Shi, M. Ma, Y. Yang, and B. Jiao, "Optimal power allocation in spatial modulation systems," *IEEE Trans. Wireless Commun.*, vol. 16, no. 3, pp. 1646–1655, Jan. 2017.

[59] C. Zhou and E. Schulz, "Cross-device signaling channel for cellular machine-type services," in *Proc. IEEE Veh. Technol. Conf., Vancouver, Canada*, Sep. 2014, pp. 1–5.

[60] M. Chraiti, A. Ghrayeb, and C. Assi, "A NOMA scheme exploiting partial similarity among users bit sequences," *IEEE Tran. Commun.*, vol. 66, no. 10, pp. 4923–4935, Oct. 2018.

[61] ——, "A spectrally efficient uplink transmission scheme exploiting similarity among short bit blocks," *IEEE Trans. Commun.*, vol. 67, no. 10, pp. 7114–7125, Oct. 2019.

[62] M. Hamood, M. Chraiti, A. Arfaoui, C. Assi, A. Ghrayeb, and A. Alloum, "A downlink puncturing scheme for simultaneous transmission of URLLC and eMBB traffic by exploiting data similarity," *IEEE Tran. Veh. Technol.*, vol. 70, no. 12, pp. 13 087–13 100, Dec. 2021.

[63] G. Huang, C. Li, S. Aïssa, and M. Xia, "Parallel quadrature spatial modulation for massive MIMO systems with ICI avoidance," *IEEE Access*, vol. 7, pp. 154 750–154 760, Oct. 2019.

[64] G. Kaddoum, M. F. A. Ahmed, and Y. Nijsure, "Code index modulation: A high data rate and energy efficient communication system," *IEEE Commun. Lett.*, vol. 19, no. 2, pp. 175–178, Dec. 2015.

[65] A. Bhowal, S. Aïssa, and R. Singh Kshetrimayum, "RIS-assisted spatial modulation and space shift keying for ambient backscattering communications," in *Proc. IEEE Int. Conf. Commun., Montreal, Canada*, June 2021, pp. 1–6.

[66] I. Mezo and A. Baricz, "On the generalization of the lambert W function," *Trans. American Math. Soc.*, vol. 369, no. 11, pp. 7917–7934, 1 2017.

[67] S. Gao, M. Zhang, and X. Cheng, "Precoded index modulation for multi-input multi-output OFDM," *IEEE Trans. Wireless Commun.*, vol. 17, no. 1, pp. 17–28, Jan. 2018.

[68] B. Zheng, F. Chen, M. Wen, F. Ji, H. Yu, and Y. Liu, "Low-complexity ML detector and performance analysis for OFDM with in-phase/quadrature index modulation," *IEEE Commun. Lett.*, vol. 19, no. 11, pp. 1893–1896, Nov. 2015.

[69] B. Zheng, M. Wen, E. Basar, and F. Chen, "Multiple-input multiple-output OFDM with index modulation: Low-complexity detector design," *IEEE Trans. Sig. Process.*, vol. 65, no. 11, pp. 2758–2772, June 2017.

[70] Y. Yang and S. Aïssa, "Bit-padding information guided channel hopping," *IEEE Commun. Lett.*, vol. 15, no. 2, pp. 163–165, Feb. 2011.

[71] J. W. Craig, "A new, simple and exact result for calculating the probability of error for two-dimensional signal constellations," in *Proc IEEE MIL., Commun., VA., USA*, Nov. 1991, pp. 571–575.

[72] M. S. Alouini and A. J. Goldsmith, "A unified approach for calculating error rates of linearly modulated signals over generalized fading channels," *IEEE Trans. Commun.*, vol. 47, no. 9, pp. 1324–1334, Sep. 1999.

[73] L. Xiao, Y. Xiao, L. You, P. Yang, S. Li, and L. Hanzo, "Single-RF and twin-RF spatial modulation for an arbitrary number of transmit antennas," *IEEE Tran. Veh. Technol.*, vol. 67, no. 7, pp. 6311–6324, July 2018.

Résumé en Français

Conception et analyse de la modulation spatiale spectrale et économe en énergie

par

Mohammad Irfan

Sommaire

Le projet de partenariat de génération 3rd (3GPP) a commencé à travailler sur les spécifications de la 5G-Advanced sous la forme de la Release-18. Les systèmes multi-antennes sont considérés comme essentiels pour activer diverses fonctionnalités et cas d'utilisation dans la 5G-Advanced et au-delà. Cependant, les systèmes MIMO (multiple-input multiple-output) existants présentent des limites de mise en œuvre importantes, notamment une consommation d'énergie élevée, des interférences inter-porteuses (ICI) et une synchronisation inter-antennes (IAS) qui entraînent de grandes complexités de mise en œuvre, de fonctionnement et de détection. . Ces problèmes surviennent en raison de l'activation simultanée de toutes les antennes d'émission pour la transmission. Les limitations susmentionnées sont encore plus importantes dans les implémentations MIMO massives, ce qui est essentiel pour répondre aux exigences de service de la 5G-Advanced et au-delà. Les lacunes des systèmes MIMO peuvent être résolues dans une large mesure en adoptant le concept récemment développé, largement connu sous le nom de modulation spatiale (SM). Contrairement aux techniques MIMO existantes, la SM offre un bon compromis en termes d'efficacité spectrale, d'efficacité énergétique et de complexité, ce qui la rend attrayante pour de nombreux cas d'utilisation.

Cette thèse vise la conception et la modélisation de techniques SM spectrales et énergétiquement efficaces. Cette thèse peut être globalement divisée en deux parties basées sur deux problèmes majeurs de SM. La faible efficacité spectrale du SM par rapport au multiplexage spatial conventionnel (SMx) est un problème majeur. Deuxièmement, la fiabilité ou la performance du taux d'erreur binaire (BER) du SM est un autre problème majeur. L'efficacité spectrale limitée du SM est due au résultat d'une modélisation inefficace, tandis que les problèmes de fiabilité se posent en raison du mécanisme d'activation de l'antenne du SM. Plus précisément, la partie 1 de cette thèse comprend deux chapitres 2 et chapitre 3, qui se concentrent sur les améliorations de l'efficacité spectrale. La partie 2 de cette thèse comprend le chapitre 4 et le chapitre 5, qui se concentrent sur l'amélioration des performances de fiabilité des techniques SM.

La technique SM fait partie de la famille plus large de la modulation d'indice (IM). L'IM a trouvé d'immenses applications dans divers domaines, notamment au niveau de la sous-porteuse du multiplexage par répartition orthogonale de la fréquence (OFDM), au niveau du symbole d'un système à porteuse unique, au niveau de l'antenne d'un système MIMO et au niveau du code de la séquence directe. étaler le spectre. Les problèmes d'efficacité spectrale et de fiabilité existent dans toutes les techniques IM. Bien que l'objectif principal de cette thèse soit le SM, les solutions proposées ici pour l'amélioration de l'efficacité spectrale dans la partie 1 et les améliorations de la fiabilité dans la partie 2 sont également applicables à toutes les techniques IM et sont mises en évidence tout au long de cette thèse.

En particulier, dans la partie I, chapitre 2, étudiez d'abord systématiquement les raisons de la faible efficacité spectrale des techniques IM. Ensuite, des directives de conception explicites sont proposées afin d'améliorer l'efficacité spectrale et l'efficacité énergétique des techniques IM. En utilisant à la fois les résultats de simulation et l'analyse théorique, il est démontré que les lignes directrices proposées contribuent à améliorer l'efficacité spectrale, l'efficacité énergétique et les performances de fiabilité des techniques IM. Les lignes directrices proposées dans le chapitre 2 sont étendues à la technique SM dans le chapitre 3 pour montrer la supériorité de la technique SM sur les techniques MIMO existantes en termes d'efficacité spectrale, d'efficacité énergétique, de fiabilité et de complexité. Puis dans la partie II, chapitre 4 étudier le problème de l'activation optimale de l'antenne dans les techniques SM lorsque l'information sur l'état du canal (CSI) n'est pas disponible à l'émetteur du SM. Il est montré que l'activation équiprobable de l'antenne est une stratégie optimale lorsque CSI n'est pas disponible à l'émetteur de SM. De plus, une méthode de cartographie spatio-temporelle pour permettre l'activation d'antenne équiprobable dans les techniques SM est développée au chapitre 4. À l'aide de simulations et d'analyses théoriques, il est démontré que la méthode proposée peut améliorer la fiabilité des techniques SM. Enfin, le chapitre 5 étudie le problème d'activation d'antenne dans les techniques SM lorsque CSI est disponible à l'émetteur de SM. Dans le chapitre 5, il est montré qu'une activation d'antenne au maximum irrégulière est souhaitable. Une méthode simple basée sur les similitudes entre les bits d'information est proposée au chapitre 5 pour permettre une activation d'antenne au maximum irrégulière. En utilisant à la fois les résultats de simulation et l'analyse théorique, il est montré que l'utilisation de l'activation d'antenne irrégulière proposée dans les techniques SM peut permettre d'obtenir des améliorations de fiabilité plus élevées. En un mot, les solutions détaillées dans cette thèse répondent à deux limitations majeures de la technique SM, à savoir l'efficacité spectrale et la fiabilité.

Sommaire

Des rapports récemment publiés indiquent le taux d'augmentation rapide du trafic mondial de données [1]. Le trafic Internet mondial, qui était de 1,5 ZB par an en 2017, devrait atteindre 4,8 ZB d'ici 2022, le trafic de données provenant d'appareils sans fil et mobiles représentant plus de 71% de CISCO [1]. Outre une efficacité spectrale élevée, une efficacité énergétique élevée est une autre exigence fondamentale des futurs systèmes de communication sans fil. En effet, la part de la consommation mondiale totale d'énergie relative aux technologies de l'information et de la communication, y compris le sans fil, qui était de 4,7% en 2012, devrait atteindre 14% en 2020 et contribuer jusqu'à 23% des émissions mondiales de gaz à effet de serre d'ici 2030 [2]. L'optimisation conjointe de la SE et de l'EE des systèmes de communication sans fil est cependant une tâche difficile ; et des avancées significatives dans la recherche seraient nécessaires avant que les exigences de haute efficacité puissent être satisfaites dans les systèmes B5G (au-delà de la 5G).

Le concept de modulation d'indice (IM) promet d'importantes économies d'énergie [3, 4]. Par rapport aux systèmes de communication classiques, les systèmes basés sur la messagerie instantanée utilisent moins d'éléments de ressources pour la transmission d'informations. En particulier, un sous-groupe de sous-porteuses en OFDM, un sous-groupe d'antennes en entrées multiples sorties multiples (MIMO), un sous-groupe de codes en spectre étalé à séquence directe et un sous-groupe de créneaux temporels dans les systèmes à porteuse unique peuvent être utilisés pour transmettre des informations utiles. [5]. L'utilisation partielle des éléments de ressource conduit à des économies d'énergie en raison de l'utilisation de moins de blocs de communication, y compris des convertisseurs, des amplificateurs, des déphaseurs et des filtres. Cependant, la SE maximale des systèmes basés sur la messagerie instantanée est généralement inférieure à la limite d'un système de communication classique avec les mêmes paramètres [3, 4]. Un système de communication classique avec des sous-porteuses N en cas d'OFDM, des antennes d'émission N en cas de multiplexage spatial MIMO, des codes N en spectre étalé à séquence directe et des créneaux temporels N dans un système monoporteuse, fonctionnant avec un schéma de modulation de niveau M, peut atteindre un maximum de $N \log_2 M$ bits par transmission [3, 4]. Bien que les communications basées sur la messagerie instantanée promettent des améliorations dans l'EE, la faible efficacité spectrale et la fiabilité de ces techniques restent un problème difficile.

Le projet de partenariat de 3e génération (3GPP) a roulé les spécifications pour la nouvelle radio (NR) dans sa quinzième version. Le haut débit mobile amélioré (eMBB) et la communication à faible latence ultra-fiable (URLLC) sont deux exigences de service majeures de NR. Les versions ultérieures de NR ont également introduit une nouvelle exigence de service appelée capacité réduite (RedCap). Un équipement utilisateur (UE) RedCap nécessite des opérations à faible consommation d'énergie avec des performances de débit et de fiabilité plus élevées. Les systèmes basés sur la messagerie instantanée avec un bon compromis entre l'efficacité spectrale et l'efficacité énergétique et

ses performances de fiabilité supérieures par rapport aux systèmes de communication conventionnels en font un candidat approprié pour les UE RedCap en NR. Cependant, l'utilisation de systèmes basés sur la messagerie instantanée dans la RN est loin de la réalité en raison d'un certain nombre de problèmes non résolus. Deux problèmes majeurs des systèmes de communication basés sur la messagerie instantanée sont sa faible efficacité spectrale par rapport aux systèmes de communication existants et ses performances de fiabilité plus faibles. La performance de fiabilité des systèmes basés sur la messagerie instantanée est supérieure à celle des systèmes de communication existants dans la littérature disponible [3, 4]. Cependant, en raison du manque de directives de conception appropriées, la fiabilité des systèmes basés sur la messagerie instantanée peut être encore améliorée. La mauvaise fiabilité des techniques IM est causée par l'activation aléatoire de sous-porteuses, d'antennes, de créneaux temporels ou de codes. Dans les techniques de messagerie instantanée, un sous-ensemble des ressources susmentionnées est activé indépendamment de la connaissance du canal. En fait, ces ressources sont activées sur la base de bits d'information, ce qui entraîne une activation quasi uniforme des sous-porteuses, des antennes, des tranches de temps ou des codes, entraînant ainsi une dégradation des performances. La motivation principale de cette thèse est de proposer des solutions pour améliorer l'efficacité spectrale et la fiabilité des techniques IM, qui sont les deux facteurs limitants des techniques IM en pratique. La résolution de ces problèmes peut rapprocher les techniques de GI de leur application dans la RN.

6.1 Problèmes de recherche

Le concept de modulation d'indice a trouvé une immense application dans plusieurs domaines de communication, y compris le domaine des créneaux temporels des systèmes de communication à porteuse unique, le domaine spatial du MIMO, le niveau de sous-porteuse de l'OFDM et le domaine du code du spectre étalé à séquence directe. Les principes de fonctionnement de la messagerie instantanée dans tous ces domaines mentionnés en termes de mappage des bits d'information sur les ressources temporelles, d'antenne, de sous-porteuse et de code au niveau de l'émetteur et de récupération des bits d'information au niveau du récepteur sont identiques. La quantité de bits d'information qui peuvent être mappés à une ressource de temps, d'antenne, de sous-porteuse et de code et l'efficacité avec laquelle elle peut être récupérée au niveau du récepteur définissent l'efficacité spectrale et les performances de fiabilité d'une technique IM. Ce problème de mappage des bits d'information aux ressources est à l'origine de plusieurs problèmes dans la conception et le fonctionnement des systèmes basés sur la messagerie instantanée. La cartographie des bits d'information aux ressources et son effet sur plusieurs mesures de performance est un problème ouvert et n'est pas bien traité dans la littérature disponible.

Les avantages des techniques de messagerie instantanée par rapport aux techniques de communication conventionnelles en termes d'efficacité énergétique, de fiabilité et de complexité ont été largement étudiés dans la littérature disponible au cours de la dernière décennie. Grâce aux gains susmentionnés des techniques de GI et à son compromis supérieur entre différentes mesures de performance, plusieurs domaines d'application de ces techniques ont été identifiés et étudiés au cours de la dernière décennie. Au lieu de trouver des domaines d'application pour les techniques de messagerie instantanée, la majorité des solutions présentées dans cette thèse tournent principalement autour du problème de la cartographie des bits d'information aux ressources, puis de l'étude de son effet sur plusieurs mesures de performance clés. Plus précisément, cette thèse vise à améliorer

les performances d'efficacité spectrale et de fiabilité des techniques IM. Les problèmes de recherche abordés dans cette thèse sont classés comme suit.

6.1.1 Efficacité spectrale des techniques de modulation d'indice

La littérature existante a bien étudié l'efficacité spectrale des techniques IM. Les techniques IM utilisent partiellement les créneaux temporels, les sous-porteuses, les antennes et les ressources de code disponibles. Cet argument est largement utilisé dans la littérature disponible pour justifier l'affirmation selon laquelle l'efficacité spectrale des techniques IM est inférieure à celle des techniques de communication conventionnelles. Les performances d'efficacité spectrale marginales des techniques IM, qui surviennent en raison du mappage binaire d'informations inefficace au niveau de l'émetteur, ont vilipendé les techniques IM en termes d'efficacité spectrale. L'utilisation dite partielle des techniques de messagerie instantanée peut être explorée pour améliorer l'efficacité spectrale des techniques de messagerie instantanée au-delà des techniques de communication conventionnelles, ce qui est la principale motivation du chapitre 2 et du chapitre 3. En particulier, la faible efficacité spectrale de l'OFDM avec IM est abordée au chapitre 2 et la faible efficacité spectrale lors de la mise en œuvre de la technique IM dans le domaine spatial de MIMO, connue sous le nom de modulation spatiale, est abordée au chapitre 3 . Les méthodologies utilisées pour résoudre le problème de faible efficacité spectrale des techniques IM dans les chapitres 2 et chapitre 3 sont présentées dans la section. 6.3.1.

6.1.2 Fiabilité des techniques de modulation d'indice

L'utilisation de l'utilisation partielle des ressources lors de l'utilisation des techniques de messagerie instantanée nous permet d'augmenter le niveau de puissance au niveau des ressources de créneau temporel, de sous-porteuse, d'antenne et de code correspondantes utilisées pour la transmission, ce qui conduit à une meilleure qualité de signal au niveau du récepteur. Cela contribue à améliorer les performances du taux d'erreur, ce qui est un autre attrait derrière l'utilisation des techniques de messagerie instantanée. Alors que la fiabilité des techniques de messagerie instantanée s'avère supérieure par rapport aux systèmes de communication conventionnels, les principes de fonctionnement derrière l'activation des ressources dans les techniques de messagerie instantanée entraînent une perte de performances de fiabilité. Différentes stratégies d'activation des ressources dans les techniques IM sont efficaces en termes de performances de fiabilité. Le choix d'une stratégie optimale dépend de la disponibilité des informations sur l'état du canal (CSI) au niveau de l'émetteur. Une méthode d'activation d'antenne optimale pour la technique SM est conçue au chapitre 4 lorsque CSI n'est pas disponible au niveau de l'émetteur. De plus, une méthode d'activation d'antenne quasi-optimale est proposée au Chapitre 5 pour le cas où le CSI est disponible à l'émetteur. Les méthodologies détaillées derrière le Chapitre 4 et le Chapitre 5 sont respectivement présentées dans la Section. 6.3.2.

6.2 Objectifs de recherche

Les principaux problèmes de recherche des techniques IM, c'est-à-dire la faible efficacité spectrale et la faible fiabilité des techniques IM, ont été mentionnés dans la section précédente. Un aperçu

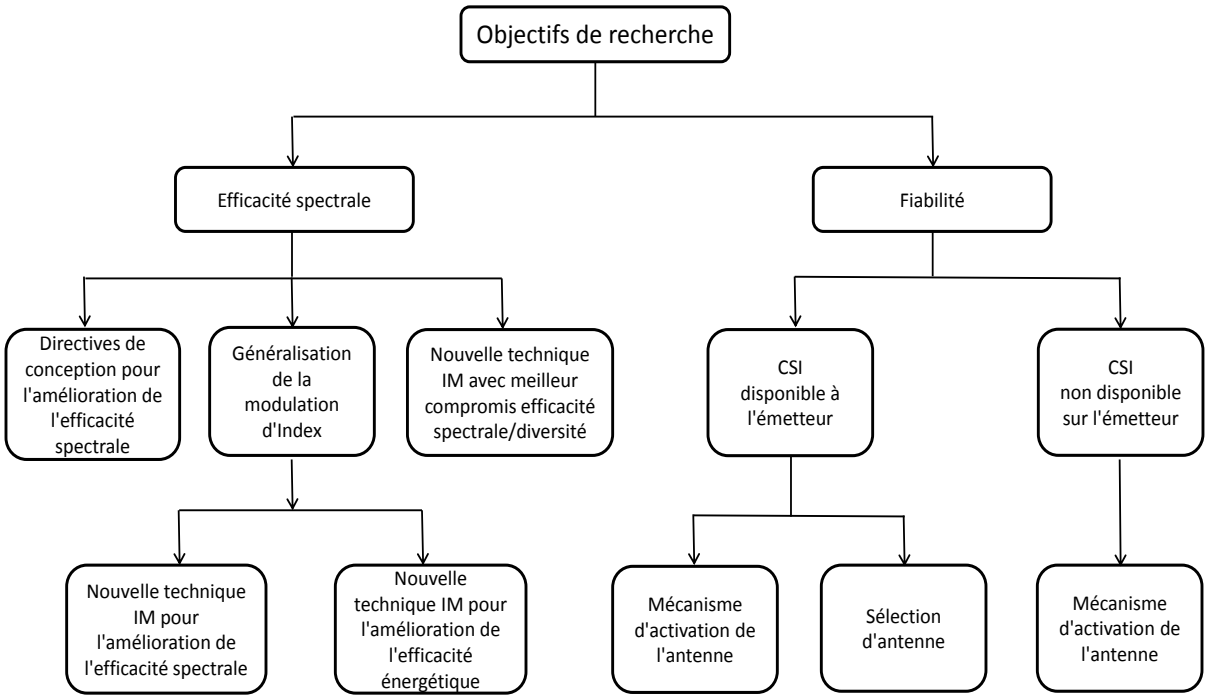

Figure 6.1: Un aperçu de haut niveau des objectifs de recherche

détaillé des objectifs de recherche et de chacun des objectifs de recherche sont expliqués dans cette section. Un aperçu de haut niveau des objectifs de recherche est fourni à la Fig. 6.1. Sur la base des enjeux majeurs de la MN, les objectifs de recherche peuvent être divisés en deux catégories, à savoir l'efficacité spectrale et la fiabilité.

Comme mentionné précédemment, la littérature disponible affirme que l'efficacité spectrale d'une technique IM est plus faible par rapport aux techniques de communication conventionnelles [9]. En fait, il est largement admis que l'application de la technique IM dans différents domaines, c'est-à-dire les améliorations SM, SC-IM, CIM et OFDM-IM, peut améliorer l'efficacité énergétique et les performances d'erreur au détriment d'une perte d'efficacité spectrale. Par conséquent, le meilleur compromis entre l'efficacité spectrale et l'efficacité énergétique offert par les techniques IM par rapport aux techniques de communication conventionnelles est considéré comme l'avantage le plus attrayant des techniques IM [9]. Cependant, en observant les principes de fonctionnement des techniques IM au niveau de la modulation en bande de base, on peut conclure que l'idée des techniques IM est en fait une extension du concept de modulation en bande de base existant. En fait, le concept des techniques IM peut être vu comme une généralisation de très haut niveau des modulations en bande de base existantes. Cependant, cette soi-disant généralisation de haut niveau des modulations en bande de base en est à ses balbutiements en raison du manque de directives de conception complètes. Par conséquent, pour améliorer l'efficacité spectrale, l'efficacité énergétique et les performances d'erreur des techniques IM, notre objectif de recherche est de concevoir un ensemble de directives de conception complètes en résolvant des problèmes d'optimisation complexes et une analyse probabiliste. De plus, de nouvelles techniques IM sont également proposées pour améliorer les performances d'efficacité spectrale, d'efficacité énergétique et de fiabilité.

Dans les techniques IM, l'efficacité spectrale, l'efficacité énergétique et les performances d'erreur (fiabilité) dépendent principalement du bit à ressource (sous-porteuse en cas d'OFDM, antenne en cas de MIMO, créneau temporel en cas de système à porteuse unique et code en cas d'étalement de spectre) indices des techniques IM. Dans le contexte des techniques SM, nous étudions l'effet de la cartographie des indices bit à antenne sur l'efficacité spectrale, l'efficacité énergétique et l'analyse des performances d'erreur. En fait, les performances d'erreur et l'efficacité spectrale des techniques SM dépendent de plusieurs facteurs, notamment le nombre d'antennes d'émission disponibles à l'émetteur et la disponibilité de CSI à l'émetteur. La disponibilité de CSI au niveau de l'émetteur est un facteur crucial dans le choix d'une méthode de mappage des bits aux indices d'antenne, également connue sous le nom d'activation d'antenne tout au long de cette thèse. Par conséquent, sur la base de la disponibilité de CSI au niveau de l'émetteur, des méthodes d'activation d'antenne sont proposées pour résoudre le mappage inefficace existant et pour surmonter les pertes de performances associées. Le problème de l'activation des antennes en SM est traité au Chapitre 4 et au Chapitre 5.

Sur la base de la discussion de haut niveau ci-dessus sur les objectifs de recherche, la contribution de cette thèse est classée en quatre chapitres et les objectifs de recherche détaillés de chaque chapitre sont présentés comme suit.

6.2.1 Multiplexage par répartition orthogonale de la fréquence avec modulation d'indice

L'objectif du Chapitre 2, dans le contexte de l'OFDM-IM est de résoudre le problème bien connu de la faible efficacité spectrale des techniques IM en général et de l'OFDM-IM en particulier. Le problème de faible efficacité spectrale de la technique OFDM-IM a été résolu en dérivant le nombre minimum requis de sous-porteuses par groupe, et le nombre minimum de sous-porteuses actives dans chaque groupe, de la technique OFDM-IM conventionnelle. Il est prouvé que lorsque le nombre de sous-porteuses par groupe et le nombre de sous-porteuses actives par groupe satisfont les limites dérivées, l'OFDM-IM peut fournir des efficacités spectrales et énergétiques supérieures à celles de l'OFDM classique. Les gains d'efficacité spectrale de l'OFDM-IM se font au détriment d'une complexité de détection accrue. Par conséquent, une technique OFDM avec IM généralisée (OFDM-GIM) est présentée, où un nombre variable de sous-porteuses par groupe peut être activé. Ensuite, deux variantes d'OFDM-GIM sont conçues sur la base du schéma d'activation des sous-porteuses : la première atteint une efficacité spectrale supérieure avec une complexité de détection réduite par rapport à l'OFDM-IM, et la seconde est adaptée aux communications à faible débit de données avec une efficacité énergétique plus élevée. conditions. Outre la détection optimale du maximum de vraisemblance, un détecteur sous-optimal moins complexe a été proposé. Une expression sous forme fermée pour le taux d'erreur binaire (BER) de l'OFDM-IIM et des deux variantes de l'OFDM-GIM est dérivée, en tenant compte des transmissions sur les canaux d'évanouissement de Nakagami et de la réception à antennes multiples. Enfin, OFDM-IM et OFDM-GIM sont comparés à des techniques de pointe pour valider leur supériorité en termes de BER, de taux réalisable et d'efficacité énergétique.

6.2.2 Modulation spatiale active multiple

Le problème de faible efficacité spectrale de la technique SM est abordé au Chapitre 3. Il est largement admis que les performances d'efficacité spectrale de la technique SM sont inférieures à

celles de SMx. Le chapitre 3 remet en question ce mythe et prouve qu'une variante de la technique SM peut surpasser les performances d'efficacité spectrale de SMx. En particulier, nous cherchons à justifier les deux énoncés suivants à l'aide de dérivations mathématiques. Tout d'abord, par rapport à SMx et vaguement basé sur la découverte du chapitre 2, il est prouvé que la technique MASM peut atteindre une efficacité spectrale similaire à SMx mais avec un plus petit nombre d'antennes d'émission, un plus petit nombre d'antennes actives, et moins d'antennes de réception. Deuxièmement, il est prouvé que lorsque le MASM et le SMx fonctionnent avec le même nombre d'antennes d'émission, la technique MASM peut atteindre une efficacité spectrale plus élevée tout en utilisant moins d'antennes d'émission actives et moins d'antennes de réception. En outre, le problème de faible efficacité spectrale et de compromis de diversité du MASM est mis en évidence, et une proposition d'une technique MASM améliorée (E-MASM) est présentée pour obtenir un meilleur compromis entre l'efficacité spectrale et la diversité par rapport au SMx. Enfin, par rapport au SMx, il est démontré que l'E-MASM permet d'obtenir un meilleur compromis entre l'efficacité spectrale et la diversité.

L'amélioration de l'efficacité spectrale de l'OFDM avec IM et MASM est détaillée dans les chapitres 2 et chapitre 3, respectivement. En particulier, au chapitre 2, il est prouvé que l'OFDM-IM peut surpasser l'OFDM classique en termes d'efficacité spectrale. De plus, dans le Chapitre 3, il est prouvé que la technique MASM peut surpasser les performances d'efficacité spectrale de SMx. Les deux autres chapitres de cette thèse traitent des problèmes de fiabilité des techniques SM. Les objectifs de recherche de chacun des chapitres restants sont détaillés comme suit.

6.2.3 Activation d'antenne équiprobable en modulation spatiale

Dans la technique SM, lorsque le nombre d'antennes n'est pas une puissance entière de deux, l'activation de l'antenne devient difficile. Dans un tel cas, seul un sous-ensemble des antennes d'émission disponibles dont la cardinalité est une puissance entière de deux est utilisé. Cela conduit à une activation de l'antenne avec une probabilité inégale, ce qui entraîne des taux d'erreur élevés et des pertes d'efficacité spectrale. Les mêmes limitations et pertes de performances existent également dans la modulation spatiale en quadrature (QSM) et la modulation spatiale généralisée (GSM), les deux principales variantes de SM. Dans le chapitre 4, contrairement à l'approche classique d'activation d'antenne dans chaque période de symbole, une méthode de mappage de bits spatio-temporel dans laquelle la procédure de sélection d'antenne est étendue à plusieurs périodes de symbole est proposée. L'utilisation de la méthode proposée dans les techniques SM, QSM et GSM permet d'atteindre des performances proches de leur plein potentiel pour un nombre donné d'antennes d'émission, avec seulement une augmentation marginale de la complexité de détection.

6.2.4 Activation d'antenne irrégulière et sélection d'antenne dans la modulation spatiale

Chaque antenne d'émission dans une communication basée sur SM est activée de manière uniforme, ce qui peut conduire à de mauvais canaux de transmission, entraînant une dégradation des performances. Bien que la sélection d'antenne puisse être utilisée pour résoudre ce problème d'activation d'antenne uniforme (U-AA), elle nécessite des éléments d'antenne supplémentaires, une complexité de calcul élevée et une surcharge de signalisation. Dans le Chapitre 5, nous proposons une technique d'activation d'antenne irrégulière (I-AA). Premièrement, pendant chaque période de symbole, un

nombre entier r, qui peut prendre une valeur comprise entre zéro et le nombre total d'antennes d'émission, est affecté à des bits égaux consécutifs. Ensuite, la séquence de r bits égaux consécutifs est utilisée pour choisir la ou les antennes pour la transmission, ce qui donne I-AA. Un I-AA à débit optimisé est développé pour utiliser de meilleurs canaux de transmission. Dans les principales variantes de SM, l'utilisation de l'I-AA s'avère produire des débits de données plus élevés et des taux d'erreur plus faibles par rapport aux opérations avec l'U-AA conventionnel. De plus, une sélection d'antenne conjointe optimisée en débit et en distance euclidienne (REAS) et un AS à faible complexité optimisé en débit (RLAS) pour SM avec I-AA sont proposés. Il a été démontré que l'utilisation de l'I-AA proposé sans AS dans des variantes importantes de la technique SM permet d'obtenir de meilleures performances en matière de taux d'erreur par rapport à l'U-AA avec AS. En outre, l'utilisation de l'I-AA dans les REAS et RLAS proposés améliore les débits de données et les taux d'erreur par rapport à l'U-AA avec l'AS, avec une complexité supplémentaire et une surcharge de signalisation négligeables.

6.3 Méthodologie

Dans cette section, nous décrivons comment les objectifs fixés dans la section précédente sont atteints.

6.3.1 Améliorations de l'efficacité spectrale

L'amélioration de l'efficacité spectrale de l'OFDM basé sur l'IM, connu sous le nom d'OFDM avec modulation d'indice et du MIMO basé sur l'IM, connu sous le nom de modulation spatiale, a été réalisée. Les méthodologies sous-jacentes à chacun des systèmes basés sur la messagerie instantanée mentionnés ci-dessus sont présentées comme suit.

Amélioration de l'efficacité spectrale de l'OFDM avec modulation d'indice

Les principes de fonctionnement des techniques de messagerie instantanée sont étudiés pour mieux comprendre ses principes de fonctionnement, ce qui facilite la résolution du problème de faible efficacité spectrale des techniques de messagerie instantanée par rapport aux systèmes de communication conventionnels. En particulier, le principe de fonctionnement des techniques IM est décomposé dans le contexte de la modulation en bande de base. Il a été conclu que le concept IM est une extension des schémas de modulation existants. Explicitement, le concept IM est une généralisation des techniques de modulation en bande de base existantes. Cela nous a permis de prouver mathématiquement que le concept IM peut atteindre une efficacité spectrale plus élevée que les systèmes de communication conventionnels. La preuve a été largement facilitée par la théorie de l'optimisation. Nous avons utilisé les résultats de la preuve pour proposer des directives de conception complètes. Les lignes directrices aident à mieux comprendre le potentiel de l'IM en termes d'efficacité spectrale, d'efficacité énergétique et de complexité. De telles lignes directrices manquaient dans la littérature existante. De plus, un concept généralisé d'IM a été proposé avec des directives de conception complètes pour le choix de divers paramètres du système. Les compromis entre l'efficacité spectrale, l'efficacité énergétique et la complexité de la détection ont été analysés en profondeur.

Après avoir prouvé le potentiel élevé de l'IM en termes d'efficacité spectrale et d'efficacité énergétique, la théorie des probabilités a été utilisée pour étudier les performances de fiabilité de l'OFDM avec modulation d'indice. Une expression de taux d'erreur binaire (BER) sous forme fermée a été dérivée. Ensuite, une expression des performances de débit a été dérivée. À l'aide de Matlab, des simulations de Monte Carlo ont été effectuées pour étudier les performances de fiabilité d'OFDM-IM. L'expression dérivée du BER a été vérifiée à l'aide des résultats de la simulation. En particulier, des gains plus élevés ont été démontrés lorsque les paramètres de ressources de l'OFDM-IM ont été choisis conformément aux directives de conception proposées. Sur la base de l'étude comparative, plusieurs domaines d'application de l'OFDM-IM dans les systèmes de communication pratiques ont été identifiés. Notre contribution détaillée est résumée comme suit.

- Le nombre minimum de ressources, en termes de nombre de sous-porteuses par groupe, et le nombre de sous-porteuses actives au sein d'un groupe, sont dérivés sous un niveau de modulation contraint, dans le but de maximiser l'efficacité spectrale et l'efficacité énergétique de l'OFDM- IM au-delà des limites conventionnelles de l'OFDM classique.
- La recherche de SE et EE plus élevés avec OFDM-IIM augmente l'espace de recherche d'un détecteur à maximum de vraisemblance (ML) et, par conséquent, la complexité de la détection. Une nouvelle technique OFDM-GIM (OFDM avec généralisation IM) a été proposé. Deux variantes ont été développées sur la base du modèle d'activation des sous-porteuses, où la première variante s'est avérée atteindre une efficacité spectrale plus élevée et la deuxième variante a été montrée pour atteindre une efficacité spectrale plus faible avec des performances d'efficacité énergétique supérieures.
- Une expression BER de forme fermée a été dérivée en tenant compte des transmissions sujettes à l'évanouissement de Nakagami et à la réception d'antennes multiples. Il a été démontré que les résultats d'analyse et de simulation du BER correspondent étroitement dans la plage SNR de l'intérêt. Fait important, par rapport à l'OFDM classique et à d'autres techniques OFDM-IM, il a été démontré que les deux variantes proposées d'OFDM-GIM atteignent efficacité spectrale et efficacité énergétique supérieures avec des performances BER supérieures.

Amélioration de l'efficacité spectrale de la modulation spatiale active multiple

Le concept d'IM dans MIMO est connu sous le nom de modulation spatiale. Le potentiel de SM en termes de gains de performances n'est pas un secret. En fait, une bonne quantité de littérature est disponible sur le potentiel de la modulation spatiale, notamment en termes d'efficacité énergétique, de complexité et de fiabilité. Ce qui n'est pas non plus un secret, c'est le mythe de la faible efficacité spectrale du SM. En particulier, dans la littérature disponible, il est largement admis que SM ne peut pas surpasser les performances d'efficacité spectrale du multiplexage spatial bien connu (SMx). La deuxième partie de cette thèse s'oppose à ce mythe. En utilisant la théorie de l'optimisation, il a été prouvé qu'une variante de SM peut surpasser les performances d'efficacité spectrale de SMx. La preuve a été utilisée pour développer des directives de conception pour la technique SM. Ensuite, en utilisant la théorie des probabilités, une expression de la performance de fiabilité de la technique SM a été dérivée. L'expression dérivée a également été utilisée pour analyser la performance du taux. À l'aide de Matlab, une simulation de Monte Carlo a été effectuée pour montrer l'efficacité de la technique SM, à la fois en termes de fiabilité et de performances de débit. Il a été vérifié qu'une variante de la technique SM a le potentiel de surpasser les performances de taux de SMx.

Le compromis entre l'efficacité spectrale et la diversité de la technique SM a également été analysé et il a été observé que l'efficacité spectrale par rapport aux performances de diversité des techniques SM sont médiocres par rapport à SMx. Une technique SM améliorée a été proposée pour obtenir un meilleur compromis entre l'efficacité spectrale et la diversité. Il a été démontré que les techniques SM améliorées peuvent atteindre une efficacité spectrale et un compromis de diversité supérieurs par rapport au SMx. En utilisant la théorie des probabilités, les performances de taux et de fiabilité de la technique SM améliorée proposée ont été analysées. Ensuite, à l'aide de simulations de Monte Carlo, les performances de débit et de fiabilité plus élevées de la technique SM améliorée proposée ont été vérifiées.

Les contributions de cette partie se résument comme suit

- Il a été prouvé que la technique SM nécessite moins de chaînes de radiofréquences (RF) actives et d'antennes de réception pour surpasser les performances d'efficacité spectrale de SMx.
- Il a été prouvé que la technique SM nécessite moins d'antennes d'émission et d'antennes de réception pour correspondre aux performances d'efficacité spectrale de SMx.
- Il a été démontré que le compromis entre l'efficacité spectrale et la diversité de SMx peut être surmonté par la technique SM améliorée proposée.

6.3.2 Améliorations de la fiabilité

L'amélioration de la fiabilité des systèmes basés sur la messagerie instantanée a été étudiée dans le domaine MIMO, c'est-à-dire que l'amélioration de la fiabilité de la technique SM et de sa variante a été étudiée. En particulier, une étude approfondie du mécanisme d'activation de l'antenne dans la technique SM et de ses variantes a été réalisée. Il a été conclu que le mécanisme d'activation d'antenne de la technique SM et ses variantes provoque une grave dégradation des performances. En guise de réflexion rapide, il a été conclu que l'activation uniforme de l'antenne est optimale lorsque les informations sur l'état du canal (CSI) ne sont pas disponibles au niveau de l'émetteur et qu'une activation irrégulière de l'antenne est optimale lorsque le CSI est connu au niveau de l'émetteur. Chacun de ces deux cas est présenté dans les sous-sections suivantes.

Améliorations de la fiabilité de la modulation spatiale sans CSI au niveau de l'émetteur

Comme mentionné ci-dessus, il est optimal d'activer chaque antenne d'émission de la technique SM et ses variantes avec une probabilité égale lorsque le CSI n'est pas disponible au niveau de l'émetteur. Les techniques SM existantes utilisent une méthode combinatoire basée sur un bloc de bits d'information au niveau de l'émetteur pour l'activation de l'antenne. Cela permet une activation d'antenne équiprobable uniquement lorsque le nombre d'antennes d'émission est une puissance de deux, ce qui est un cas rare, en particulier dans les systèmes pratiques. Lorsque le nombre d'antennes n'est pas une puissance de deux, les antennes disponibles sont activées avec des probabilités inégales. Une telle activation d'antenne inégale se traduit par une protection largement inégale des bits transmis, affectant ainsi les performances de fiabilité. De plus, l'activation non uniforme de l'antenne dans les techniques SM est également responsable d'une perte d'efficacité spectrale. Les pertes d'efficacité spectrale de fiabilité augmentent lorsque le nombre d'antennes

d'émission augmente, ce qui en fait un problème plus grave pour l'application de la technique SM en NR.

Pour activer l'activation d'antenne équiprobable dans les techniques SM, nous étendons le processus d'activation d'antenne de la technique SM et ses variantes sur les domaines spatial et temporel. Cela permet une activation d'antenne presque équiprobable. Le nombre optimal de tranches de temps pour l'extension de l'activation de l'antenne a été dérivé. En utilisant la théorie des probabilités, une expression du BER a été dérivée. Une expression pour coder les avantages de gain de l'utilisation d'une activation d'antenne équiprobable par rapport à l'activation d'antenne conventionnelle dans la technique SM a également été dérivée. À l'aide de Matlab, des simulations de Monte Carlo ont été effectuées et les gains de performance en termes d'amélioration de l'efficacité spectrale et de fiabilité lors de l'utilisation d'une activation d'antenne équiprobable ont été vérifiés.

La contribution de cette partie se résume comme suit

- Le problème de l'activation de l'antenne entraînant une dégradation des performances en termes d'efficacité spectrale et de fiabilité dans les techniques SM a été étudié en profondeur.
- Une conception de mappage espace-temps dans laquelle la procédure de codage est étendue à plusieurs périodes de symboles a été proposée et il a été démontré que le mappage proposé peut améliorer les performances de débit et de fiabilité.

Améliorations de la fiabilité de la modulation spatiale avec CSI à l'émetteur

La sélection d'antenne et l'allocation de puissance ont été largement étudiées lorsque CSI est disponible à l'émetteur d'un système basé sur SM. Après une analyse approfondie du mécanisme d'activation de l'antenne, nous avons montré que l'activation équiprobable de l'antenne n'est pas une stratégie optimale lorsque le CSI est disponible à l'émetteur d'un système basé sur SM. Au lieu de cela, l'activation irrégulière maximale de l'antenne est optimale lorsque le CSI est disponible au niveau de l'émetteur. Cela nous a motivés à développer une nouvelle méthode d'activation d'antenne pour les techniques SM, appelée activation d'antenne irrégulière.

Les similitudes entre les bits d'information courts au niveau de l'émetteur ont été exploitées. Il a été montré que différentes séquences de bits d'information basées sur des similitudes consécutives avec la séquence au niveau de l'émetteur se produisent naturellement avec des probabilités différentes. Une expression de ces probabilités a été dérivée, qui a ensuite été utilisée pour dériver une expression de la performance de débit de la technique SM mettant en œuvre l'activation d'antenne irrégulière proposée. À l'aide de l'expression du débit et des probabilités d'événement, une cartographie entre les événements et les indices d'antenne a été développée afin que le débit global puisse être amélioré. Ensuite, en utilisant la théorie des probabilités et les statistiques d'ordre, une expression du BER de la technique SM mettant en œuvre l'activation d'antenne irrégulière proposée a été développée. À l'aide de Matlab, des simulations de Monte Carlo ont été effectuées pour vérifier les gains de fiabilité de l'utilisation d'une activation d'antenne irrégulière par rapport à une activation d'antenne équiprobable.

La sélection d'antenne a également été étudiée lors de l'utilisation d'une activation d'antenne irrégulière. Une méthode de sélection d'antenne a été développée. En utilisant la théorie des probabilités et les statistiques d'ordre, une expression de forme fermée pour le BER de la technique

SM mettant en œuvre une activation d'antenne irrégulière et la sélection d'antenne proposée a été dérivée. À l'aide de Matlab, des simulations de Monte Carlo ont été effectuées pour vérifier les gains de fiabilité de l'utilisation d'une activation d'antenne irrégulière avec sélection d'antenne par rapport à une activation d'antenne équiprobable avec sélection d'antenne.

Les principales contributions de cette partie sont résumées comme suit

- Une nouvelle méthode d'activation d'antenne dans les techniques SM est proposée. Le concept consiste à attribuer une valeur entière à des bits d'information égaux consécutifs, et à utiliser les valeurs obtenues pour l'activation de l'antenne.
- Deux méthodes de sélection d'antenne optimisée en débit, à savoir la sélection d'antenne optimisée en débit et en distance euclidienne et la sélection d'antenne à faible complexité optimisée en débit ont été proposées. À l'aide des statistiques d'ordre, une expression de forme fermée pour le BER de SM mettant en œuvre une activation d'antenne irrégulière a été dérivée avec/sans les méthodes de sélection d'antenne a été dérivée pour la transmission soumise aux canaux d'évanouissement de Rayleigh et à la réception à une ou plusieurs antennes.
- Les principaux gains de performances liés à l'utilisation d'une activation d'antenne irrégulière dans la technique SM se sont avérés doubles. Tout d'abord, il a été démontré que des taux plus élevés peuvent être atteints par rapport au SM avec une activation d'antenne équiprobable. Deuxièmement, de meilleurs taux d'erreur peuvent être obtenus par rapport au SM avec une activation d'antenne équiprobable. Il a été démontré que SM mettant en œuvre une activation d'antenne irrégulière sans sélection d'antenne permet d'obtenir des performances de taux d'erreur encore meilleures par rapport à SM avec une activation d'antenne uniforme avec sélection d'antenne. Enfin, les techniques SM mettant en œuvre les méthodes d'activation et de sélection d'antenne irrégulières proposées sont présentées comme surclassant les SM mettant en œuvre une activation et une sélection d'antenne équiprobables avec un surcoût négligeable en termes de complexité et de signalisation.

6.4 Chapitre 2: Résultats Comparatifs

Maintenant, nous présentons des résultats numériques pour le BER, le taux réalisable et la performance d'efficacité énergétique. Pour simplifier, nous supposons $P_{\mathrm{t}} = \log_2 M$ W, de sorte que l'énergie par bit $E_{\mathrm{b}} = \frac{E_{\mathrm{s}}}{\log_2 M} = 1$J , où E_{s} est l'énergie du symbole. Selon les hypothèses, un système OFDM classique peut atteindre un débit maximal de $\eta_{\mathrm{c}} = \log_2 M$ bits/s/Hz, avec une efficacité énergétique maximale $\mathrm{EE}_{\mathrm{c}} = 1$ bit /J. Dans le reste de l'article, les triplets appartenant aux tracés de OFDM-IM et OFDM-IIM désignent (N, K, M), alors que dans OFDM-GIM$_1$ ils représentent (N_1, B_1, M). Tout d'abord, une comparaison des performances BER de l'OFDM-IIM et de l'OFDM-GIM par rapport à l'OFDM classique est présentée.

Figure. 2.2(a) illustre une comparaison de P_{a} (A.27), P_{c} (A.23) et P_{e_1} (A.32), par rapport aux résultats de la simulation Monte-Carlo pour montrer l'efficacité des expressions dérivées. Les résultats de performance BER dans un environnement d'évanouissement plat de Rayleigh ($n = 0$) sont comparés pour $(N_1, B_1, M) = (2, 3, 2)$. Les résultats théoriques et de simulation pour les taux d'erreur P_{a}, P_{c} et P_{e_1} correspondent étroitement sous les détecteurs ML et LC pour différentes valeurs du nombre de recevoir des antennes L_{r}, confirmant les expressions dérivées. Les résultats

du BER ont également été vérifiés pour OFDM-IIM et OFDM-GIM$_2$. Ensuite, la performance BER de l'OFDM-IIM et de l'OFDM-GIM$_1$ sous les politiques PSP et PRP est comparée à l'OFDM classique.

BER sous la politique d'économie d'énergie

Selon (A.27), sous la politique PSP, la probabilité d'erreur de l'OFDM classique P_{b} et la probabilité d'erreur de l'activité de sous-porteuse P_{a} sont telles que $P_{\mathrm{b}} < P_{\mathrm{a}}$ pour $M = 2$ et $P_{\mathrm{a}} < P_{\mathrm{b}}$ pour $M > 4$. Par conséquent, selon (A.24), $P_{\mathrm{b}} < P_{\mathrm{e}_\lambda}$ pour des valeurs plus petites du niveau de modulation M. En utilisant OFDM-IIM avec $n = 0$ et $L = 1$ dans (A.24), nous avons trouvé des pertes SNR de 3dB, 1.5dB, 0.5dB et 0.2dB avec OFDM-IIM contre OFDM classique pour $M = 2$, $M = 4$, $M = 16$ et $M = 64$, respectivement. Cependant, en augmentant le facteur Nakagami n et/ou le nombre d'antennes de réception L_{r}, la différence $P_{\mathrm{b}} - P_{\mathrm{e}_\lambda}$ diminue et peut même satisfaire $P_{\mathrm{b}} - P_{\mathrm{e}_\lambda} < 0$ sous PSP pour des valeurs supérieures de M, comme le montre la Fig. 2.2(b-c) , et discuté en détail comme suit.

BER sous la politique de réallocation de puissance

La figure 2.2(b) illustre les performances du BER par rapport au facteur Nakagami lorsque l'antenne de réception $L_{\mathrm{r}} = 1$ est utilisée. Sous de meilleurs canaux (valeurs plus élevées de n), les techniques OFDM-IIM et OFDM-GIM$_1$ peuvent toutes deux surpasser l'OFDM classique sous PSP et PRP. La figure 2.2(c) représente le BER pour un nombre variable d'antennes de réception L_{r}. Les techniques OFDM-IIM et OFDM-GIM$_1$ peuvent surpasser l'OFDM classique, et leur gain de performance BER augmente avec un nombre croissant d'antennes de réception L_{r} et/ou le facteur Nakagami n. Un BER plus petit à des valeurs plus élevées de n et/ou L_{r} sous PSP est dû au $\frac{b_\lambda}{N_\lambda \eta_\lambda} P_{\mathrm{a}}$ terme dans (A.24). Sous PRP, les gains sont en partie dus au terme mentionné dans (A.24) et à la puissance d'émission élevée liée au rapport $\frac{N_\lambda}{K_\lambda}$. Ensuite, le taux réalisable et l'efficacité énergétique de l'OFDM-IIM et de l'OFDM-GIM$_1$ par rapport à l'OFDM classique sont discutés.

6.4.1 Taux réalisable et efficacité énergétique

Le nombre de bits correctement estimés pouvant être récupérés sur une sous-porteuse donnée est considéré comme une mesure de débit, donnée par $\xi_\lambda = \eta_\lambda \ (1 + P_{\mathrm{e}_\lambda} \log_2 P_{\mathrm{e}_\lambda} + (1 - P_{\mathrm{e}_\lambda}) \log_2 (1 - P_{\mathrm{e}_\lambda}))$ bits/s/Hz [30], et l'efficacité énergétique est donnée par $E_\lambda = \frac{\xi_\lambda}{P_{\mathrm{t}}}$ bits/J. Les deux expressions sont valables pour OFDM-IIM et OFDM-GIM.

Remarque 2

Il est largement admis que les techniques IM peuvent surpasser l'OFDM classique en termes de BER et de taux réalisable uniquement lorsque $M \leq 4$ [5,13]. Les techniques OFDM-IIM et OFDM-GIM$_1$ peuvent également surpasser l'OFDM classique pour $M \leq 4$. Par exemple, à un débit cible de 1 bit/s/Hz, nous avons constaté que OFDM-GIM$_2$ avec $(N_2, B_2, M) = (9, 3, 2)$ peut atteindre un gain SNR de 2dB, 50% de taux plus élevé et EE 270% plus élevé que l'OFDM classique. Selon

la proposition 3 et l'équation. (A.15b), OFDM-IIM et OFDM-GIM$_1$ peuvent surpasser l'OFDM classique pour toutes les valeurs de M. Cependant, à des valeurs plus élevées de M, le gain de performances de débit d'OFDM-IIM et d'OFDM-GIM$_1$ par rapport à l'OFDM classique est tel que $\lim_{M\to\infty} \frac{log_2(M+1) - \log_2 M}{\log_2 M} = 0$. Par conséquent, pour des valeurs inférieures de M, généralement pour $M \leq 16$, les améliorations du taux et de l'EE dans OFDM-IIM et OFDM-GIM$_1$ sont dominées par η_λ, alors que pour M $geq16$ les gains sont dominés par P_{e_λ}. Ensuite, le BER, le taux réalisable et les performances EE de l'OFDM-IIM et de l'OFDM-GIM$_1$ sont évalués pour $M = 16$ et $M = 64$ afin de démontrer leur supériorité sur un système OFDM classique à des valeurs plus élevées de M.

6.4.2 Comparaison des performances pour des niveaux de modulation plus élevés

La figure 2.3(a) présente la comparaison du BER des techniques IM considérées lorsque $M = 16$. OFDM-IIM et OFDM-GIM$_1$ obtiennent un BER légèrement meilleur par rapport à l'OFDM classique, même sous PSP. Sous PRP, OFDM-GIM$_1$ et OFDM-IIM atteignent respectivement des gains SNR de 2dB et 2,5dB par rapport à l'OFDM classique à un BER de 10^{-5}. Pour exploiter la diversité de fréquence, nous avons utilisé le mappage de sous-porteuses entrelacées proposé à l'origine dans le contexte de l'OFDM-IM dans [24]. Les techniques OFDM-IIM et OFDM-GIM$_1$ mettant en œuvre le mappage de sous-porteuses entrelacées sont respectivement désignées par I-OFDM-IIM et I-OFDM-GIM$_1$. Les techniques I-OFDM-IIM et I-OFDM-GIM$_1$ atteignent respectivement un gain SNR de 4dB et 4,3dB par rapport à l'OFDM classique à un BER de 10^{-5}. La figure 2.3(b) montre les résultats de taux réalisables des techniques IM considérées dans la figure 2.3(a). Premièrement, OFDM-IIM et OFDM-GIM$_1$ peuvent surpasser l'OFDM classique même sous PSP pour SNR$\geq$ 1dB, grâce à leur faible BER et à leur SE plus élevé. Sous PRP, OFDM-GIM$_1$ et OFDM-IIM obtiennent de nouvelles améliorations grâce à leurs gains SNR de 2 dB et 2,5 dB par rapport à l'OFDM classique. La performance à haut débit de I-OFDM-IIM et I-OFDM-GIM$_1$ est le résultat de leur plus petit BER par rapport aux autres techniques à l'étude. La figure 2.3(c) représente les résultats EE des techniques IM considérées dans la figure 2.3(a) et la figure 2.3(b). OFDM-IIM et OFDM-GIM$_1$ surpassent l'OFDM classique en raison de leur SE plus élevé et de leur BER plus petit. Un gain supplémentaire de performance EE d'OFDM-IIM et OFDM-GIM$_1$ peut être obtenu en utilisant PSP et/ou I-OFDM-IIM et I-OFDM-GIM$_1$.

La figure 2.4(a) présente la comparaison du BER de l'OFDM-IIM, de l'I-OFDM-IIM, de l'OFDM-GIM$_1$ et de l'I-OFDM-GIM$_1$ par rapport à l'OFDM classique lorsque $M = 64$. Les techniques OFDM-IIM et OFDM-GIM$_1$ sous PSP obtiennent un BER légèrement meilleur par rapport à OFDM. Sous PRP, OFDM-GIM$_1$ et OFDM-IIM atteignent respectivement un gain SNR de 1dB et 1,2dB sur OFDM. I-OFDM-GIM$_1$ et I-OFDM-IIM atteignent respectivement un gain SNR de 3 dB et 3,1 dB par rapport à l'OFDM classique. La figure 2.4(b) montre les performances de débit des techniques considérées dans la figure 2.4(a). Grâce au SE élevé et au faible BER d'OFDM-IIM, I-OFDM-IIM, OFDM-GIM$_1$ et I-OFDM-GIM$_1$, les techniques considérées surpassent l'OFDM classique pour SNR>2dB. La performance EE est illustrée dans la Fig. 2.4(c). On peut observer que l'OFDM-IIM, l'I-OFDM-IIM, l'OFDM-GIM$_1$ et l'I-OFDM-GIM$_1$ atteignent un EE plus élevé que l'OFDM classique.

Les gains rapportés sont obtenus au détriment de la complexité de détection lors de l'utilisation du détecteur ML. Les complexités de détection de l'OFDM-IIM et de l'OFDM-GIM$_1$ sous les détecteurs ML et LC, avec les paramètres de ressource considérés dans les Figs. 2.3 et 2.4 sont fournies

dans le Tableau 2.1. La complexité de I-OFDM-IIM est égale à OFDM-IIM et celle de I-OFDM-GIM$_1$ est égale à OFDM-GIM$_1$. Bien que la complexité de détection de l'OFDM-GIM$_1$ sous le détecteur ML soit nettement inférieure à celle de l'OFDM-IIM, elle n'est toujours pas réalisable sur le plan informatique dans les systèmes pratiques. Par conséquent, le détecteur LC et les méthodes de [31] peuvent être utilisés pour des détections de faible complexité.

6.4.3 Application d'OFDM-IIM et d'OFDM-GIM dans IEEE 802.11

IEEE 802.11ax peut prendre en charge 2048 sous-porteuses avec $M = 1024$ et se concentre sur l'amélioration des performances dans les environnements denses [32]. IEEE 802.11be est un nouvel amendement qui s'appuie sur IEEE 802.11ax ciblant des débits extrêmement élevés, avec des applications telles que les bureaux distants, le cloud computing, la réalité augmentée (AR), la réalité virtuelle (VR) et les appels vidéo [32]. Grâce à l'ICI moins sévère [16], au PAPR réduit [17,18], au taux plus élevé et à la meilleure fiabilité des techniques OFDM-IIM et OFDM-GIM$_1$, elles peuvent offrir d'autres améliorations de performances dans IEEE 802.11 hache/être. La prise en charge de 2048 sous-porteuses et $M = 1024$ dans IEEE 802.11ax/be s'aligne bien avec les exigences minimales d'OFDM-IIM et OFDM-GIM$_1$ pour obtenir des performances supérieures. En particulier, le paramètre de conception B_1 de OFDM-GIM$_1$ peut être utilisé pour ajuster le nombre souhaité de sous-porteuses actives pour réduire l'ICI et le PAPR dans des environnements denses tout en maintenant les performances de débit souhaitées. La norme IEEE 802.11ay avec des économies d'énergie avancées comme caractéristique clé et un débit de pointe de 20 Gbit/s fonctionnant à 60 GHz est en cours de développement pour les communications à très courte portée [33]. Les cas d'utilisation de l'IEEE 802.11ay incluent le déchargement mobile, la station d'accueil au bureau, le sans fil fixe, les appareils portables, la réalité augmentée et la réalité virtuelle. Les performances de débit et de fiabilité supérieures de l'OFDM-IIM et de l'OFDM-GIM$_1$, en particulier dans les canaux de meilleure qualité, peuvent encore améliorer les performances de débit et de fiabilité de l'IEEE 802.11ay. En particulier, les deux techniques peuvent offrir des performances améliorées avec des économies d'énergie améliorées, en particulier dans le cadre de la politique PSP. Enfin, la radio de réveil IEEE 802.11ba servira de commutateur pour la radio principale dans une maison intelligente, un entrepôt ou un appareil portable, afin d'améliorer l'efficacité énergétique des stations. La partie radio de réveil de l'IEEE 802.11ba devrait consommer moins d'un milliwatt de puissance dans un état actif et utilisera une simple modulation On-Off-Keying (OOK) dans une bande passante étroite avec des transmissions à courte portée [34]. L'OFDM-GIM$_2$ à faible débit et économe en énergie utilise également la modulation OOK et est donc un candidat intéressant pour la transmission de paquets de réveil pour allumer la radio principale dans IEEE 802.11ba.

6.5 Chapitre 3: Résultats Comparatifs

Taux d'erreur binaire

La performance BER des SMT avec $N_a > 1$, c'est-à-dire MASM, E-MASM, GSM et SMx, est évaluée en annexe. B.0.2. Les résultats sont présentés comme suit.

La figure 3.6(a) montre le BER des systèmes comparés pour un débit de 6 bits/s/Hz. Tout d'abord, une différence de SNR de 7dB est observée entre les deux configurations SM, SM sous-

optimale(2,1,32,6) et SM optimale(32,1,2,6), à un BER de 10^{-4}. Le BER minimum avec les SMT n'est réalisable qu'à $\max(N_\mathrm{t})$, $\min(N_\mathrm{a})$ et $\min(M)$ (cf. SSK(64,1,0 ,6) sur la figure 3(a)). Deuxièmement, l'E-MASM proposé avec $\alpha = 2$ permet d'obtenir des performances BER plus proches du cas optimal SM(32,1,2,6) et SSK(64,1,0,6), avec un plus petit nombre d'antennes d'émission N_t. À un BER de 10^{-5}, le gain SNR avec E-MASM est de 2 dB sur MASM et GSM, 2,5 dB sur SMx, 3,5 dB sur GSSK, 5,5 dB sur QSM et 6 dB sur le SM sous-optimal (2,1,32,6).

Efficacité spectrale

La SE réalisable des SMT en fonction du SNR (ρ) sous M contraint est $R \leq \lambda(1 + P_\mathrm{e} \log_2 P_\mathrm{e} + (1 - P_\mathrm{e}) \log_2(1 - P_\mathrm{e}))$ bits/s/Hz [30], qui sous $P_\mathrm{t} = 1$ représente également le EE réalisable donné par R bits/J.

La figure 3.6(b) présente la comparaison des performances SE/EE par rapport au SNR. Tout d'abord, pour $N_\mathrm{t} = 10$, les techniques SM, GSM, SSK, GSSK et QSM n'atteignent pas les objectifs de 10 bits/s/Hz et 10 bits/J fixés par SMx et sont donc exclus de la comparaison. Deuxièmement, MASM avec (10,6,2,10) active 4 chaînes RF de moins N_a que SMx, tout en obtenant des gains de 3 bits/s/Hz et 3 bits/J à des SNR plus élevés. De même, MASM avec (10,6,2,6) utilise 4 chaînes RF de moins et 4 antennes de réception de moins N_r que SMx, tout en obtenant des gains de 3 bits/s/Hz et 3 bits/J à SNR plus élevés. Troisièmement, les configurations (8,4,2,10) et (8,4,2,4) de MASM correspondent aux performances SE et EE de SMx à des valeurs SNR plus élevées mais avec moins d'antennes d'émission et de chaînes RF. Cette dernière configuration nécessite même 4 antennes de réception en moins N_r par rapport à SMx. Enfin, même si MASM ne peut pas atteindre une SE similaire à SMx à faible SNR, l'E-MASM proposé avec $\alpha = 2$ est capable d'atteindre une SE supérieure à SMx pour un SNR supérieur à 2dB, grâce à son compromis SE/diversité notable.

6.6 Chapitre 4: Résultats Comparatifs

Efficacité spectrale et gain de codage : La figure 4.2(a) présente une comparaison des efficacités spectrales en (4.7) pour SM, GSM et QSM, par rapport au nombre d'antennes. Dans le mappage *espace-temps*, le L optimal pour chaque valeur de N_t dans toutes les techniques est obtenu selon la Section 4.2.5, où un maximum de $L = 8$ était autorisé. Pour plus de clarté, nous avons utilisé $M = 1$ dans (4.6) pour isoler le terme commun, c'est-à-dire $d = \log_2 M$ dans (4.7). La limite supérieure et l'efficacité spectrale réelle obtenues à l'aide de la cartographie conventionnelle dans SM, GSM et QSM ne correspondent que lorsque $R = 2^g$, ce qui est très peu probable pour la plupart des valeurs de N_t en pratique Configurations MIMO. Comme le montre la figure, l'utilisation de la cartographie *espace-temps* proposée peut donner des performances quasi optimales en termes d'efficacité spectrale. La figure 4.2(b) illustre l'avantage de codage de la cartographie *espace-temps* par rapport à la cartographie conventionnelle dans SM, GSM et QSM, pour faire varier N_t. Les résultats correspondent à un BER de 10^{-5} pour toutes les valeurs de N_t, et $N_\mathrm{r} = 4$ antennes de réception. Le gain de codage est le résultat de l'activation quasi-uniforme des antennes d'émission via la cartographie *espace-temps*. Aucun gain de codage n'est noté lorsque $R = 2^g$, auquel cas toutes les antennes peuvent être activées uniformément à chaque période symbole. En particulier, pour $N_\mathrm{t} = 7$, un gain de codage de $1,7$ dB et une efficacité spectrale supérieure de 28% peuvent être obtenus en SM avec une cartographie *espace-temps* par rapport à l'approche conventionnelle.

Comme observé sur la Fig. 4.2(a-b), les pertes maximales avec la cartographie conventionnelle dans toutes les techniques se produisent à la condition dite sévère de $R = 2^g - 1$. Lorsque $R = 2^g - 1$, près de la moitié des antennes sont laissées inutilisées pour la transmission. Cela conduit à une perte d'efficacité spectrale maximale, $\overline{\eta} - \eta \approx 1$ bit/s/Hz, et à une perte SNR maximale. Cet argument est établi pour la discussion sur la complexité de la détection, présentée brièvement.

BER et taux réalisables : Nous comparons les performances du BER avec la cartographie *espace-temps* proposée par rapport à la cartographie conventionnelle pour trois systèmes : SM avec $N_{\mathrm{t}} = 3$ et $M = 2$, GSM avec $N_{\mathrm{t}} = 4, K = 2$ et $M = 2$, et QSM avec $N_{\mathrm{t}} = 5$ et $M = 4$. Le nombre d'antennes de réception est toujours $N_{\mathrm{r}} = 4$. Ici, $L = 2$ est utilisé pour le mappage *espace-temps*. Le BER est illustré à la Fig. 4.2(c). À un BER de 10^{-5}, la méthode *espace-temps* atteint un gain de codage de 1,2 dB, 1,1 dB et 1,3 dB, respectivement en SM, GSM et QSM. La comparaison des taux réalisables de ces techniques avec la cartographie conventionnelle et la cartographie *espace-temps* est rapportée dans la Fig. 4.2(d). Le taux réalisable est calculé en utilisant $\mathcal{R} \leq \epsilon(1 + P_{\mathrm{e}} \log_2 P_{\mathrm{e}} + (1 - P_{\mathrm{e}}) \log_2(1 - P_{\mathrm{e}}))$ bits/s/Hz [30], où $\epsilon = \eta$ pour le mappage conventionnel et $\epsilon = \eta^{\,\mathrm{ST}}$ lors de l'utilisation du mappage *espace-temps*. Ici, P_{e} désigne la probabilité d'erreur d'un SM, GSM ou QSM assisté par cartographie conventionnelle ou *espace-temps*. Le gain de performance en débit des techniques SM implémentant la cartographie *espace-temps* est en partie dû au gain de codage (C.3), et en partie au gain d'efficacité spectrale (4.7).

Complexité de détection : En termes de compromis, les gains d'efficacité de codage et spectrale (cf. Fig. 4.2) avec la cartographie *espace-temps* sont obtenus avec une augmentation de la complexité de détection. Mesurer la complexité de la détection en termes de nombre de multiplications complexes nécessaires pendant chaque période de symbole pour l'estimation de $\widehat{\mathbf{n}}$ et $\widehat{\mathbf{s}}$ selon eqrefeqml1, puis selon [50] et (4.4), le rapport de la complexité de détection avec la cartographie *espace-temps* sur l'approche conventionnelle est $\frac{\delta^{\mathrm{ST}}}{\delta} = \frac{M^{L-1}}{L}\binom{N_{\mathrm{t}}}{K}^{\alpha(L-1)}$. L'incrément de complexité est exponentiel en L. Cependant, le choix de $L = 2$ peut être facilement démontré dans (4.7) comme étant suffisant dans toutes les techniques pour atteindre des performances élevées pour la plupart des valeurs de R, en particulier dans la condition sévère définie précédemment comme $R = 2^g - 1$. Par conséquent, l'augmentation de la complexité est marginale. Les complexités de détection de SM, GSM et QSM avec des mappages conventionnels et *espace-temps* considérés dans la Fig. 4.2(c-d) sont $\delta = [3, 6, 25]$ et $\delta^{\mathrm{ST}} = [4, 5, 18, 312, 5]$, respectivement.

6.7 Chapitre 5: Résultats Comparatifs

Les performances de I-SM, I-GSM et I-MASM sont comparées à celles de SM, GSM et MASM, en termes de BER et de débit réalisable. Le débit d'O-MIMO est de $\log_2 M$ bits/s/Hz, ce qui est inférieur aux débits d'I-SM, I-GSM et I-MASM, et de leurs homologues conventionnels. Les résultats du BER de l'O-MIMO sont présentés comme référence pour mieux mettre en évidence les avantages de l'I-AA par rapport à l'U-AA. Tous les résultats ont été obtenus en considérant les transmissions sur les canaux à évanouissement plat de Rayleigh.

6.7.1 Taux d'erreur binaire

Dans la Fig. 5.3(a), nous comparons l'impact des méthodes de sélection d'antenne (EAS, REAS, LAS et RLAS) dans SM et I-SM. Les observations suivantes peuvent être faites : 1) Les résultats obtenus avec (D.21b), (D.22b) et (D.17), pour SM, I-SM et O-MIMO, avec AS, correspondent étroitement aux résultats de simulation, corroborant ainsi les dérivations. 2) LAS surpasse EAS à des SNR plus élevés. Ce point a également été conclu dans [51]. 3) Comme prévu, I-SM surclasse SM, avec un gain de 4dB à un BER de 10^{-4}. Compte tenu des meilleures performances BER et de la faible complexité de LAS et RLAS par rapport à EAS et REAS, dans la partie restante de cette section, nous adoptons RLAS lorsque I-AA est mis en œuvre, et LAS lors de l'utilisation de U-AA.

La figure 5.3(b) présente une comparaison entre le BER et le SNR de SM et I-SM sans AS, lorsque $N_{\mathrm{t}} = 5$, $M = 2$ (BPSK) et $N_{rmr} = 1,\ 2$ ou 4. La performance BER d'I-SM est proche de celle d'O-MIMO. Les points suivants peuvent être observés. Le gain SNR de I-SM sur SM est de 4dB lorsque $N_{\mathrm{r}} = 1$, 3dB lorsque $N_{\mathrm{r}} = 2$ et 2dB lorsque $N_{\mathrm{r}} = 4$. La disparition du gain SNR lors de l'augmentation de N_{r} peut être expliquée à l'aide des statistiques d'ordre des matrices. En particulier, on peut montrer que $\lim_{N_{\mathrm{r}}\to\infty} \mathrm{E}_r[\sum_{n_{\mathrm{r}}=1}^{N_{\mathrm{r}}}(\mathbf{H}_{n_{\mathrm{r}}}), r+1] - \mathrm{E}[\sum_{n_{\mathrm{r}}=1}^{N_{\mathrm{r}}}(\mathbf{H}_{n_{\mathrm{r}}}), r] \approx 0$, $\forall n_{\mathrm{t}}$, où $\mathrm{E}_r[\sum_{n_{\mathrm{r}}=1}^{N_{\mathrm{r}}}(\mathbf{H}_{n_{\mathrm{r}}}), r]$ est la valeur moyenne de r^{th} statistique d'ordre de $\sum_{n_{\mathrm{r}}=1}^{N_{\mathrm{r}}}(\mathbf{H}_{n_{\mathrm{r}}})$. Par conséquent, en termes de BER, l'I-SM est plus avantageux avec un plus petit nombre d'antennes de réception, en particulier lorsque $N_{\mathrm{r}} = 1$.

La figure 5.3(c) compare les performances BER de SM, I-SM et O-MIMO pour $N_{\mathrm{T}} = 10, N_{\mathrm{t}} = 5$, quand $M = 2$ et $N_{\mathrm{r}} = 2$. À un BER de 10^{-4}, la perte de SNR de SM et I-SM par rapport à O-MIMO est respectivement de 8 dB et 2 dB. Ladite perte s'explique comme suit. L'O-MIMO utilise le meilleur canal (relatif aux statistiques d'ordre 10^{th} de $\mathbf{H}$) pour la transmission avec probabilité un, tandis que SM utilise le $1^{\mathrm{st}}, 2^{\mathrm{nd}}, 3^{\mathrm{rd}}, 4^{\mathrm{th}}$ et 5^{th} meilleurs canaux, c'est-à-dire ceux concernant les $10^{\mathrm{th}}, 9^{\mathrm{th}}, 8^{\mathrm{th}}, 7^{\mathrm{th}}$ et 6^{th} ordonnent des statistiques de $\mathbf{H}$, avec une probabilité égale $\frac{1}{N_{\mathrm{t}}} = 0,2$. I-SM, d'autre part, utilise les $1^{\mathrm{st}}, 2^{\mathrm{nd}}, 3^{\mathrm{rd}}, 4^{\mathrm{th}}$ et 5^{th} meilleurs canaux avec des probabilités de 0,5 $, 0,25, 0,125, 0,0625$ et 0,625, respectivement, ce qui se traduit par un meilleur SNR reçu et, par conséquent, de meilleures performances BER.

Dans la Fig. 5.4(a), les performances du GSM et de l'I-GSM sont comparées lorsqu'aucun AS n'est utilisé. Ici, $N_{\mathrm{t}} = 5$, $M = 2$ et $N_{\mathrm{r}} = 2$. Avec un BER de 10^{-4}, l'I-GSM atteint un gain SNR de 4 dB sur le GSM. Le gain SNR est plus significatif à des valeurs moyennes de SNR. D'après (5.8), le nombre moyen d'antennes actives dans l'I-GSM est $K_{\mathrm{av}} = 1,9$, alors que le GSM utilise $K = 3$ antennes actives. L'utilisation d'un plus petit nombre d'antennes actives dans l'I-GSM garantit une meilleure utilisation des canaux avec une probabilité plus élevée et un meilleur BER. La figure 5.4(b) illustre les performances du BER du GSM et de l'I-GSM lors de la mise en œuvre de l'AS. Ici, $N_{\mathrm{T}} = 10,\ N_{\mathrm{t}} = 5$, $M = 2$ et $N_{\mathrm{r}} = 2$. Avec un BER de 10^{-4}, I-GSM avec RLAS atteint un gain SNR de 4 dB sur GSM avec EAS. I-GSM avec RLAS surclasse le GSM coûteux en calcul avec EAS pour toutes les valeurs de SNR. En comparant I-GSM sans AS (cf. Fig. 5.4(a)) avec GSM EAS (cf. Fig. 5.4(b)), on peut conclure que I-GSM sans AS peut surclasser GSM avec AS.

La figure 5.4(c) représente une comparaison du BER de MASM et I-MASM avec et sans AS. I-MASM atteint un gain de 8 dB sur MASM lorsqu'aucun AS n'est utilisé, et un gain de 3 dB sur MASM avec LAS. De plus, I-MASM avec RLAS atteint un gain de 10 dB sur MASM sans AS et un gain de 6 dB sur MASM avec LAS.

6.7.2 Taux réalisable

Pour les comparaisons, le taux réalisable est calculé en utilisant $\mathcal{R} \leq \epsilon(1+P_{\mathrm{e}}\log_2 P_{\mathrm{e}}+(1-P_{\mathrm{e}})\log_2(1-P_{\mathrm{e}}))$ bits/s/Hz, où ϵ est égal à $\eta^{\mathrm{u}}_{\mathrm{SM}}$ pour SM, $\eta^{\mathrm{I}}_{\mathrm{SM}}$ pour I-SM, $\eta^{\mathrm{u}}_{\mathrm{GSM}}$ pour GSM, $\eta^{\mathrm{I}}_{\mathrm{GSM}}$ pour I-GSM, $\eta^{\mathrm{u}}_{\mathrm{MASM}}$ pour MASM et $\eta^{\mathrm{I}}_{\mathrm{MASM}}$ pour I-MASM.

La figure 5.5(a) compare les taux de SM et I-SM avec et sans AS. Comme observé, l'utilisation de LAS avec SM améliore le taux réalisable par rapport à SM sans AS. La technique I-SM sans AS atteint un taux plus élevé par rapport à SM avec LAS. Des améliorations de taux significatives peuvent être obtenues lorsque I-SM est utilisé avec RLAS.

La figure 5.5(b) montre les performances de débit du GSM et de l'I-GSM avec et sans AS, lorsque $N_{\mathrm{t}} = 5$, $N_{\mathrm{T}} = 10$, $M = 2$ et $N_{\mathrm{r}} = 2$. Le débit réalisable de l'I-GSM est supérieur à celui du GSM pour toute la gamme SNR. La supériorité s'explique comme suit. Premièrement, les performances de débit de l'I-GSM sont supérieures à celles du GSM, comme indiqué dans (5.9a), et également démontré dans la Fig. 5.2(a). Deuxièmement, I-GSM a une meilleure performance BER par rapport au GSM. I-GSM avec RLAS atteint jusqu'à 1,5, 1,8 et 1,25 bits/s/Hz de gain sur GSM avec LAS, respectivement dans les plages SNR faible, moyen et élevé. De plus, I-GSM sans AS surpasse GSM avec LAS.

La figure 5.5(c) représente les taux réalisables de MASM et I-MASM avec et sans AS. Ici, $N_{\mathrm{t}} = 5$, $N_{\mathrm{T}} = 10$, $M = 2$ et $N_{\mathrm{r}} = 2$. Une tendance similaire à celle de la Fig. 5.5(a) peut être observée. En résumé, que l'AS soit utilisé ou non, les performances de débit de l'I-MASM sont supérieures à celles du MASM.

6.7.3 Applications dans d'autres domaines et extensions

La technique I-AA peut être facilement adaptée pour des applications dans divers autres domaines de communication, y compris le niveau des tranches de temps, sous la forme d'une modulation d'indice à porteuse unique (SCIM) [11], le domaine de code de l'étalement en séquence directe spectre (CIM) [64], et le niveau de sous-porteuse du multiplexage par répartition orthogonale de la fréquence avec modulation d'indice (OFDM-IM) [10]. En outre, les méthodes REAS et RLAS proposées peuvent être appliquées aux domaines temporel, code et sous-porteuse de SCIM, CIM et OFDM-IM, respectivement. De plus, le concept I-AA peut être étendu lorsque les systèmes de communication sont aidés par des surfaces intelligentes reconfigurables (RIS) [65] pour des améliorations de débit et de performances BER. Le concept I-AA peut être utilisé pour réduire la complexité et le temps système associés à la sélection des éléments RIS, tout en obtenant en même temps les SNR reçus souhaitables. L'utilisation de l'I-AA dans le MIMO massif et le RIS est très attrayante. De plus, l'utilisation de l'I-AA dans les informations sans fil simultanées et le transfert de puissance peut également entraîner une meilleure détection du signal et une meilleure exploitation de l'énergie. Le concept d'I-AA peut également améliorer la sécurité de la couche physique en raison de sa grande flexibilité en termes de similitude des informations avec le mappage d'antenne. L'I-AA peut également trouver une application dans les scénarios de mobilité, par exemple, la similitude des informations avec la cartographie d'antenne peut être basée sur la propagation du retard et/ou la propagation Doppler dans les systèmes de communication de véhicule à véhicule et de véhicule à tout, y compris les systèmes à haut débit. systèmes de communication ferroviaire à grande vitesse.

Avec I-AA, le débit de transmission change d'une période de transmission à une autre, ce qui peut provoquer une propagation d'erreurs. L'utilisation du bit-padding [45] et de la modulation adaptative peut assurer un taux de transmission constant et surmonter la propagation des erreurs, ce qui est notre principale motivation pour les travaux futurs. De plus, l'allocation de puissance à la fois dans le domaine temporel et dans le domaine spatial d'un système MIMO implémentant I-AA est un problème intéressant. La maximisation du débit et de l'efficacité énergétique est un autre problème de recherche ouvert. Enfin, l'identification et l'étude de différents cas d'utilisation pour les transmissions MIMO basées sur I-AA est également un domaine intéressant.

6.8 Remarques Finales

Cette thèse a abordé les problèmes fondamentaux de la modulation spatiale, c'est-à-dire une faible efficacité spectrale et une faible fiabilité. Le problème de la faible efficacité spectrale a été abordé au Chapitre 2 et au Chapitre 3, tandis que les problèmes de fiabilité de la modulation spatiale ont été abordés au Chapitre 4 et au Chapitre 5. Un résumé de chaque chapitre de cette thèse est présenté comme suit.

Le chapitre 2 a étudié systématiquement le problème de faible efficacité spectrale des techniques IM. Il a été prouvé que les techniques IM peuvent surpasser l'efficacité spectrale des techniques traditionnelles sous la contrainte $N \geq 2M$ en sélectionnant correctement les paramètres de conception (N, K, M). Il a été démontré que la technique OFDM-GIM$_1$ assouplit de moitié la condition $N \geq 2M$ d'OFDM-IM, car elle ne nécessite que $N \geq M-1$ sous-porteuses dans un groupe pour surpasser l'OFDM classique. Contrairement aux travaux précédents, il a été montré que l'OFDM-IM et l'OFDM-GIM$_1$ peuvent surpasser l'OFDM classique même à une transmission à haut débit. OFDM-GIM$_2$ a été conçu pour les communications à faible débit de données exigeant des performances d'efficacité énergétique supérieures. Le concept d'IM, GIM et les directives de conception proposées se sont avérés également valables pour les techniques d'IM dans d'autres domaines. L'utilisation de l'IM et du GIM dans les domaines de l'espace, du code et du temps peut surclasser le BER, le taux réalisable et les performances d'efficacité énergétique des systèmes MIMO (SMx), DSSS et SC conventionnels. De plus, à débit égal, l'utilisation de la messagerie instantanée peut permettre des économies de bande passante en OFDM, d'éléments d'antenne en MIMO, de codes/bande passante en DSSS et de tranches de temps dans un système SC. L'utilisation de GIM$_1$ permet d'assouplir davantage les conditions requises pour atteindre les gains mentionnés dans les systèmes OFDM, MIMO, DSSS et SC (cf. économies du nombre d'antennes d'émission et de réception en GSM sur SMx [35]).

Le chapitre 3 a d'abord présenté des directives de conception pour résoudre le problème de faible efficacité spectrale du SM. Il a été prouvé que MASM nécessite moins d'antennes d'émission actives N_{a} et moins d'antennes de réception N_{r} pour surpasser l'efficacité spectrale du multiplexage spatial, ou moins d'antennes d'émission N_{t}, N_{a} et N_{r} pour correspondre à ladite efficacité spectrale. MASM peut fournir des débits de données élevés avec moins d'unités matérielles, une faible puissance et une réduction des interférences inter-porteuses, de la synchronisation inter-antennes, du coût, de la complexité et de la taille de l'appareil, par rapport au multiplexage spatial. En outre, le compromis entre l'efficacité spectrale et la diversité du MIMO conventionnel peut être surmonté par la technique MASM améliorée proposée.

Le chapitre 4 a abordé le problème de l'activation irrégulière de l'antenne dans les techniques SM, qui entraîne un BER élevé et des pertes d'efficacité spectrale. Une conception de mappage espace-temps dans laquelle la procédure de codage est étendue à plusieurs périodes de symboles a été proposée, et ses mérites ont été démontrés dans les techniques SM, GSM et QSM bien connues. Le gain de codage qui résulte de l'activation quasi-uniforme de l'antenne a également été analysé. L'utilisation de la cartographie spatio-temporelle proposée peut permettre aux techniques SM de fonctionner avec des performances quasi optimales, ce qui en fait un candidat approprié pour les communications B5G MIMO, où le nombre d'antennes sur les appareils peut être fortement limité en raison des limitations de taille. Les gains rapportés se sont avérés possibles avec une augmentation marginale de la complexité de détection. De plus, la cartographie proposée peut être facilement adoptée dans diverses autres techniques de modulation d'indice.

Le chapitre 5 a d'abord mis en évidence l'U-AA dans les systèmes de communication basés sur SM comme le principal responsable des graves pertes de performances lorsque CSI est disponible. La nouvelle méthode d'I-AA a été proposée, et son utilisation dans des variantes importantes de SM s'est avérée supérieure à l'U-AA en termes de débit et de performances BER. Deux méthodes d'AS, à savoir l'AS optimisée en débit et en distance euclidienne, et l'AS à faible complexité optimisée en débit, ont également été proposées. Il a été démontré que les principales variantes de SM mettant en œuvre I-AA sans AS surpassent leurs homologues avec U-AA et AS, en termes de performances de débit et de BER. La communication MIMO basée sur SM mettant en œuvre I-AA et RLAS a été identifiée comme un meilleur schéma en raison de ses meilleures performances, de sa complexité moindre et de sa surcharge de signalisation réduite. En outre, les applications du concept I-AA dans d'autres domaines ont été discutées.

Appendix

Appendix A

Generalization of Index-Modulation: Breaking the Conventional Limits on Data-rate and Energy Efficiency

A.1 Data-rate Enhancement of OFDM with Index-Modulation

The data-rate expression in (2.2) is rewritten in terms of the Sterling formula, $Z! = \sqrt{2\pi}\exp(-Z)Z^{Z+\frac{1}{2}}$ and $\lfloor \log_2 \binom{N}{K} \rfloor = \log_2 \binom{N}{K} - \theta$, with $0 \leq \theta < 1$, as follows:

$$\eta = \frac{-1}{N \ln 2}\left[\ln\sqrt{2\pi} + \ln K\left(K+\frac{1}{2}\right) - \ln N\left(N+\frac{1}{2}\right) + \ln(N-K)\left(N-K+\frac{1}{2}\right) - K\ln M - \theta\ln 2\right], \quad \text{(A.1)}$$

where $\theta = 0$ points to an upper-bound on (A.1). Taking the first- and second-order derivatives of (A.1) w.r.t. K yields

$$\eta'(K) \leq \frac{\ln\left(\frac{MN-MK}{K}\right) - \frac{1}{2}\left(\frac{1}{K} - \frac{1}{N-K}\right)}{N\ln 2}, \quad \text{(A.2a)}$$

$$\eta''(K) \leq \frac{\frac{1}{2(N-K)^2} + \frac{1}{2K^2} - \frac{1}{N-K} - \frac{1}{K}}{N\ln 2}, \quad \text{(A.2b)}$$

where the inequality in (A.2a) and (A.2b) are the results of vanishing θ. Since $K \geq 1$ and $N-K \geq 1$, then in (A.2b) we have $\frac{1}{2(N-K)^2} < \frac{1}{(N-K)^2} \leq \frac{1}{(N-K)}$ and $\frac{1}{2K^2} < \frac{1}{K^2} \leq \frac{1}{K}$. Hence, $\eta''(K) \leq 0$ and, as such, (A.2a) is a decreasing function of K. Accordingly, $\min\{\eta'(K)\} = \eta'(N-1)$ and $\max\{\eta'(K)\} = \eta'(1)$ are given by

$$\min\left\{\eta'(K)\right\} = \frac{1}{N\ln 2}\left[\ln M - \ln(N-1) + \frac{1}{2}\left(1 - \frac{1}{N-1}\right)\right], \quad \text{(A.3a)}$$

$$\max\left\{\eta'(K)\right\} = \frac{1}{N\ln 2}\left[\ln M + \ln(N-1) + \frac{1}{2}\left(\frac{1}{N-1} - 1\right)\right]. \quad \text{(A.3b)}$$

Since $\ln(N-1)+\frac{1}{2}\left(\frac{1}{N-1}-1\right)\geq 0$, then $\max\{\eta'(K)\}\geq 0$ and, hence, (A.3b) is an increasing function of K. Now, making use of $\frac{N}{2}\geq M$ into (A.3a) results in

$$\min\{\eta'(K)\}\leq \frac{1}{N\ln 2}\underbrace{\left[\ln\left(\frac{N}{2N-2}\right)+\frac{1}{2}\left(1-\frac{1}{N-1}\right)\right]}_{\rho(N)}. \tag{A.4}$$

Differentiating $\rho(N)$ w.r.t. N yields

$$\rho'(N)=\frac{1}{N-1}\left(\frac{1}{2(N-1)}-\frac{1}{N}\right)\leq 0, \tag{A.5}$$

where $\frac{1}{2(N-1)}\leq\frac{1}{N}$, due to the fact that $N\geq 2$. Hence, $\rho(N)$ is a decreasing function of N. Therefore, $\rho(N)\leq\max\{\rho(N)\}=\rho(2)=0$, and (A.4) shows that $\min\{\eta'(K)\}\leq 0$, which concludes that $\eta'(K)$ is a decreasing function of K. Also, $\min\{\eta'(K)\}\leq\eta'(K)\leq\max\{\eta'(K)\}$ and $\min\{\eta'(K)\}\leq 0$. This leads to the result that $\eta'(K)=0$ has only one root, and that the objective function in (A.1) is an increasing function of K for $N\leq 2M$, and a first increasing and then decreasing function w.r.t. K for $N\geq 2M$.

Now, the optimal solutions in terms of data-rate, i.e., K^* and N^*, are obtained by first equating $\eta'(K)=0$, which, after some algebraic manipulation, yields

$$\exp\left(\frac{1}{2K}-\frac{1}{2(N-K)}\right)=\frac{M(N-K)}{K}, \tag{A.6}$$

the optimal solution of which lies in the region defined by $1\leq K\leq\frac{N}{2}$ and $\frac{MN}{M+1}\leq K\leq N-1$. Equation (A.6) can be further simplified as follows:

$$Q=\frac{-1}{2K}\exp\left(\frac{-1}{2K}\right)=\frac{-1}{2M(N-K)}\exp\left(\frac{-1}{2(N-K)}\right). \tag{A.7}$$

A closed-form solution cannot be obtained directly due to the transcendental nature of (A.7). However, an implicit solution can be obtained by using the Lambert W function, which for a transcendental equation of the form $z\exp(z)=x$ is given by $f^{-1}(z\exp(z))=W(x)$, where $W(x)$ represents the corresponding solution [66]. Using the Lambert W function, the implicit solution of (A.7) is given by

$$\underline{K}=-\frac{1}{2W(Q)};\quad \underline{N}=-\frac{1}{2}\left(\frac{1}{W(Q)}+\frac{1}{W(MQ)}\right) \tag{A.8}$$

where $\underline{K}\in\mathbb{R}^+$, whereas $1\leq K\in\mathbb{Z}^+\leq N-1$, and where $\underline{N}\in\mathbb{R}^+$, while $N\in\mathbb{Z}^+$. Therefore, the optimal solution is

$$N^*=\lfloor\underline{N}\rfloor;\quad K^*=\begin{cases}\lfloor\underline{K}\rfloor, & \text{if } \eta(\lfloor\underline{K}\rfloor)\geq\eta(\lceil\underline{K}\rceil)\\ \lceil\underline{K}\rceil, & \text{if } \eta(\lfloor\underline{K}\rfloor)<\eta(\lceil\underline{K}\rceil)\end{cases}. \tag{A.9}$$

The above discussion clarifies the effect of N and K on the data-rate shown in (A.1). Also, N^* and K^* as per (A.9) satisfy (2.6a) and (2.6c), but do not necessarily satisfy (2.6b), which is the main point of discussion and a well-known problem of IM. In the following, the conclusion drawn above is used to determine the minimum limits on N and K to satisfy (2.6b). We start by comparing the

data-rate of a classical OFDM system, i.e., $\log_2 M$ bits/s/Hz, to (2.2), as follows:

$$\frac{1}{N}\left(K\log_2 M + \left\lfloor \log_2 \binom{N}{K} \right\rfloor\right) \geq \log_2 M, \tag{A.10a}$$

$$\mathfrak{g}\left(\binom{N}{K}^{\frac{1}{N-K}}\right) \geq M, \tag{A.10b}$$

where (A.10b) is obtained from (A.10a) after some algebraic manipulations.[1] Now, we use (A.10b) to satisfy (2.6b) using the following three propositions [21].

Theorem 1. *For $N < M$, the data-rate of OFDM-IM compared to classical OFDM is such that*

$$\max_{\forall(N<M, K<M-1)}(\eta) \;<\; \log_2 M. \tag{A.11}$$

Proof. Recall that the objective function in (A.1) is a first increasing and then decreasing function w.r.t. K for $N > 2M$. Also, (A.1) is an only increasing function of K till $N = 2M$. Similarly, it can be shown that $\max\{\eta'(N)\}$ is an increasing function, and the objective function (A.1) is an only increasing function in terms of N. Therefore, as per the restrictions set by the proposition, i.e., $N < M$, $\max(\eta)$ should occur at $N = M - 1$ and $K = N - 1 = M - 2$. Substituting these values into the left-hand-side (LHS) of (A.10b) results in $\mathfrak{g}(M-1)$, where $\mathfrak{g}(M-1) < M$. Therefore, according to (A.10b), $\max(\eta) < \log_2 M$. □

Theorem 2. *For $M \leq N < 2M$,*

$$\max_{\forall(M\leq N<2M,\; K<2M-1)}(\eta) \;=\; \log_2 M. \tag{A.12}$$

Proof. As the objective function in (A.1) is an only increasing function w.r.t. N, two boundary values of N, i.e., $N = M$ and $N = 2M - 1$, are considered. Also, the objective function (A.1) is an only increasing function of K till $N = 2M$. Therefore, for the considered limit of N in Proposition 5, $\max(\eta)$ occurs at $(N = M, K = M - 1)$ and $(N = 2M - 1, K = 2M - 2)$. Substituting these values into the LHS of (A.10b) results in $\mathfrak{g}(M)$ for the first case, and in $\mathfrak{g}(2M-1)$ for the latter. As $\mathfrak{g}(M) = \mathfrak{g}(2M-1) = M$, then as per (A.10b), this points to the fact that $\max(\eta) = \log_2 M$ when $M \leq N < 2M$. □

Theorem 3. *For $N \geq 2M$,*

$$\max_{\forall(N\geq 2M, K<N)}(\eta) \;>\; \log_2 M. \tag{A.13}$$

Proof. The function (A.1) is an only increasing function in terms of N, and a first increasing and then decreasing function of K when $N \geq 2M$. Therefore, $\min(N)$, i.e., $N = 2M$, is considered to prove the proposition. Substituting $N = 2M$ and $K = 2M - 1$ into the LHS of (A.10b) results in $\mathfrak{g}(2M) = 2M > M$, which points to the fact that IM in general and OFDM-IM in particular have the ability to outclass the data-rate and energy efficiencies of classical OFDM system. The upper limit on the data-rate of OFDM-IIM, i.e., $\eta \leq \log_2(M+1)$, is realizable by further increasing N beyond $2M$. □

[1] For $M = 2^r, r \in \mathbb{Z}^+$, and some variable x such that $2^r < x < 2^{r+1}$, we have $\mathfrak{g}(x) = 2^r$ and $\mathfrak{s}(x) = 2^{r+1}$.

A.2 OFDM with Generalized Index Modulation

A.2.1 Low Complexity Conditions

A target data-rate with OFDM-GIM$_1$ can be achieved with several settings of N_1 and B_1, resulting in different values of m_1 (cf. Eq. (2.7)). As the detection complexity of ML detector is proportional to the size of its code-book $\mathbf{S}_1$, different values of m_1 will result in different sizes of $\mathbf{S}_1$ and, hence, different detection complexities. Therefore, $\min(N_1)$ and $\min(m_1)$, satisfying a target data-rate, will achieve the minimum complexity.

In OFDM-GIM$_1$, $\max(m_1) = 2^{N_1}$, $\max(b_1) = N_1$ and $\min(d_1) = \frac{N_1}{2}\log_2 M$ occur at $B_1 = N_1{+}1$. Similarly, $\min(m_1) = N_1 + 1$, $\min(b_1) = \lfloor \log_2(N_1+1) \rfloor$ and $\max(d_1) = \frac{N_1^2}{2^{\lfloor \log_2(N_1+1) \rfloor}}\log_2 M$ occur at $B_1 = 2$. Also, at higher M, the contribution of d_1 in (2.10) is higher than b_1. To reduce N_1, m_1 and, hence, the complexity of the ML detection, N_1, K_1, M^{K_1} and $\binom{N_1}{K_1}$ are minimized such that a minimum target data-rate of $\log_2 M$ bits/s/Hz is attained. Due to the integer nature of such optimization problem, the latter is solved under $B_1 = 2$, which would ensure the $\min(N_1)$, $\min(K_1)$, $\min(M^{K_1})$ and $\min\binom{N_1}{K_1}$ for a given data-rate requirement. The data-rate of OFDM-GIM$_1$ under $B_1 = 2$ and that of classical OFDM are compared as follows:

$$\frac{1}{N_1}\left[\left(N_1 - 1 + \frac{1}{2^{b_1}}\right)\log_2 M + b_1\right] \geq \log_2 M, \tag{A.14a}$$

$$\frac{N_1+1}{N_1}\log_2(N_1+1) \geq \log_2 M, \tag{A.14b}$$

where (A.14b) is obtained by manipulating (A.14a). The LHS of (A.14b) solely depends on the choice of N_1. Several values of N_1 can satisfy (A.14b) with different detection complexities, but the minimum complexity is ensured by $\min(N_1)$. The inequalities in (A.15a) and (A.15b) are used to determine the minimum complexity conditions in terms of N_1 under a minimum data-rate requirement of $\log_2 M$ bits/s/Hz. These are given by:

$$\max_{\forall(N_1<M-1)}(\eta_1) \geq \log_2 M, \qquad \text{if } M \leq 4, \tag{A.15a}$$

$$\max_{\forall(N_1\geq M-1)}(\eta_1) \geq \log_2 M, \qquad \text{if } M > 4. \tag{A.15b}$$

Proof. Similar to the data-rate of OFDM-IM (A.1), it can be shown that η_1 is an only increasing function in terms of N_1 for $N_1 < M-1$ and a first increasing, and then decreasing function of N_1 for $N_1 \geq M-1$. Substituting $N_1 = M-2$ into (A.14b) yields $\frac{M-1}{M-2}\log_2(M-1) \geq \log_2 M$, which only holds for $M \leq 4$, and satisfies (A.15a). Similarly, substituting $N_1 = M-1$ into (A.14b) yields $M > M-1$, which satisfies (A.15b). Unlike [29], OFDM-GIM$_1$ can outperform classical OFDM for all values of the modulation level M. □

A.2.2 Data-rate

Similar to OFDM-IIM, where the data-rate η approaches $\log_2(M+1)$ bits/s/Hz by increasing N (cf. Eq. (A.3b)), in OFDM-GIM$_1$ the data-rate η_1 also tends to $\log_2(M+1)$ bits/s/Hz with increasing N_1 and/or B_1. The formulation of optimal (N_1, B_1) in terms of data-rate is a challenging task given

that N_1 and $B_1 \in \mathbb{Z}^+$. Therefore, we determine optimal N_1 in terms of data-rate for fixed B_1 and M. To proceed, we assume that $N_1 \notin \mathbb{Z}^+$ but that $N_1 \in \mathbb{R}^+$, and use N_1' to denote the optimal N_1 in terms of data-rate η_1. To find N_1', the upper-bound on the data-rate η_1^{up} is maximized for chosen B_1 and M. For instance, the optimal group size N_1' for the case of $B_1 = M = 2$ is found by maximizing $\eta_1^{\text{up}} = \frac{N_1}{N_1+1} + \frac{\ln(N_1+1)}{N_1 \ln 2}$. Here, $\frac{\partial \eta_1^{\text{up}}}{\partial N_1} = 0$ results in $N_1' = 0.67$. Then, a digitized or actual optimal group size N_1^* in terms of data-rate for $N_1 \in \mathbb{Z}^+$ is obtained as:

$$N_1^* = \begin{cases} \mathfrak{g}(N_1') - 1, & \text{if } \eta_1(\mathfrak{g}(N_1') - 1) \geq \eta_1(\mathfrak{s}(N_1') - 1) \\ \mathfrak{s}(N_1') - 1, & \text{otherwise.} \end{cases} \tag{A.16}$$

As per the above rule, the digitized group size for the example of $B_1 = M = 2$ and $N_1' = 0.67$ is $N_1^* = 1$. Similarly, for $B_1 = 2$ and $M = 4$, $N_1' = 5.06$ and the optimal group size is $N_1^* = 7$. Similar to the $B_1 = M = 2$ and the $B_1 = 2, M = 4$ examples discussed earlier, (A.16) can be easily shown to be valid for all possible values of B_1 and M. For illustration, the effect of the group size N_1 on the data-rate η_1 is shown in Fig. A.1(a-b), for $B_1 = 2, 3$ and $M = 2, 4$. The figure also plots the $\log_2 M$ bits/s/Hz limit of classical OFDM. The plots clearly show a mismatch at some points between the upper bound and the actual values of data-rate, for both cases of M. The upper-bound data-rate and the actual data-rate match when the total number of patterns satisfies $m_1 = 2^r, r \in \mathbb{Z}^+$, in which case the length of *index bits* is $b_1 = \log_2 m_1$. For $B_1 = 2$, all groups of size $N_1 = 2^r - 1$ subcarriers result in a total of $m_1 = 1 + N_1$ patterns, hence the perfect match with the upper-bound data-rate. The optimal group sizes we obtained earlier agree with the results of Fig. A.1(a-b) and yield superior data-rate compared to classical OFDM.

As observed from Fig. A.1(a-b), further gain in η_1 is achievable when increasing B_1. Indeed, an increment of B_1 increases the total available patterns m_1 in (2.7), leading to the transmission of more *index bits* of length b_1 per group of N_1 subcarriers and, hence, enhanced data-rate. However, increasing B_1 increases the required N_1 for achieving higher data-rate. Particularly, increasing B_1 by one increases the required N_1 for achieving higher data-rate by a factor of $\frac{M}{2}$. The data-rate percentage gain of OFDM-GIM$_1$ for $M = 2, 4$ and varying B_1 is plotted in Fig. A.1(c). As will be detailed later in Section A.4, the trade-off or limiting factor of such gain in data-rate is the increasing receiver complexity (cf. Section A.2.1 and Fig. A.1(d)).

A.2.3 Energy Efficiency

Recalling OFDM-GIM$_1$, Fig. A.1(c) shows that its data-rate (2.10) increases as a function of B_1. Under fixed N_1, the required K_1 decreases with increasing B_1 and reduces to the minimum $\frac{N_1}{2}$ at $B_1 = N_1 + 1$. Also, for higher B_1, a larger N_1 is required as compared to the conditions defined by (A.15a) and (A.15b) to achieve $\eta_1 \geq \log_2 M$. The ratio $\frac{N_1}{K_1}$ increases with increasing B_1. Therefore, $\max(\text{EE}_1^{\text{PSP}})$ occurs at $B_1 = N_1 = \infty$. However, operation under such settings is impractical and associated with enormous detection complexity δ_1^{ML}. Therefore, we consider a joint EE_1^{PSP} maximization and δ_1^{ML} minimization such that $\eta_1 \geq \log_2 M$.

As per (A.15a) and (A.15b), the minimum complexity occurs at $B_1 = 2$. Also, (2.3) is dominated by $\frac{N_1}{K_1}$ for $M \leq 4$, whereas for $M \geq 8$, (2.3) is dominated by η_1 as $\frac{N_1}{K_1}$ reduces to $\frac{M}{M-1} \approx 1$, especially for large values of M. Therefore, the conditions for $\max(\text{EE}_1^{\text{PSP}})$ and $\min(\delta_1^{\text{ML}})$ are

$$\begin{cases} N_1 = 1, & \text{if } M < 8, \\ N_1 = M - 1, & \text{if } M \geq 8. \end{cases} \tag{A.17}$$

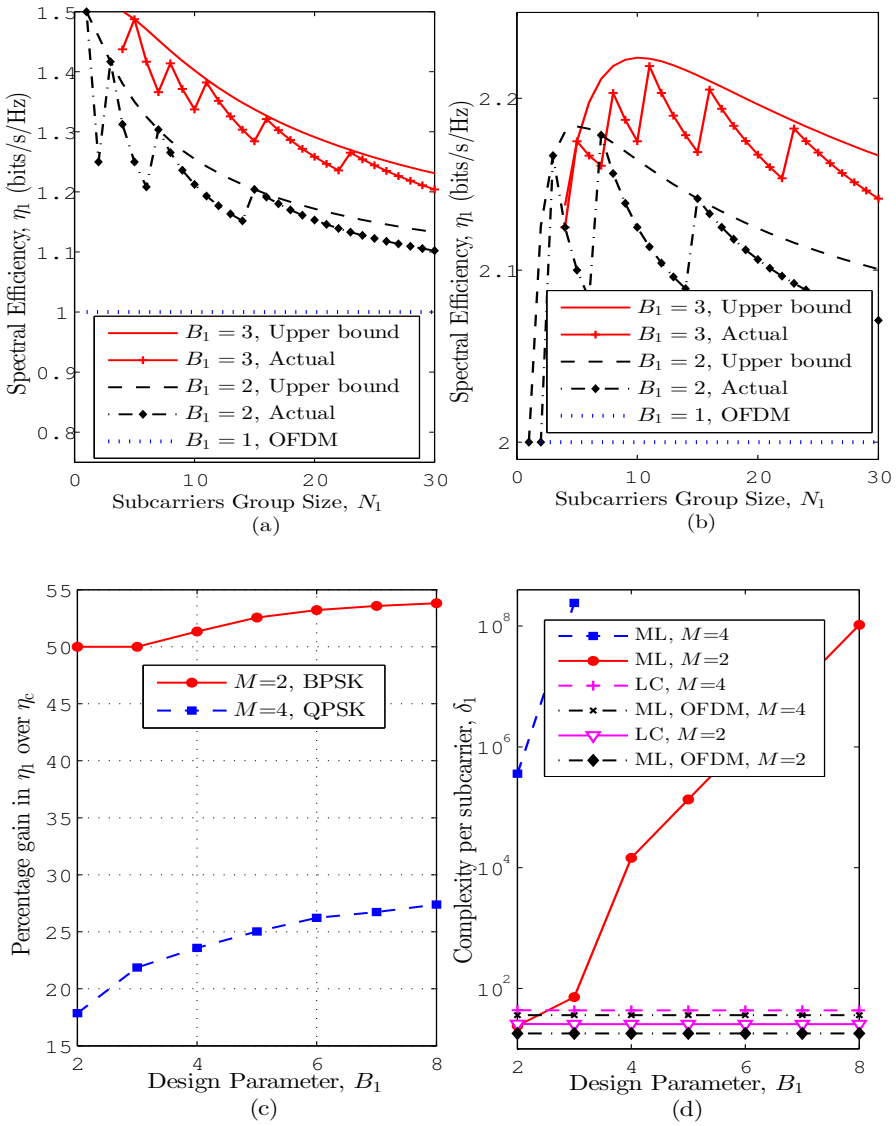

Figure A.1: OFDM-GIM$_1$: data-rate vs. the subcarriers' group size N_1 under $B_1 = 2, 3$ for (a) $M = 2$, (b) $M = 4$; and effect of design parameter B_1 on (c) percentage gain in data-rate, and (d) detection complexity (optimal ML vs. low-complexity (LC) detection).

A.3 OFDM-GIM$_2$: Design Tailored for High Energy Efficiency

A.3.1 Energy Efficiency

The energy efficiency under PSP is $\text{EE}_2^{\text{PSP}} = \frac{N_2}{K_2}\frac{\eta_2}{P_t}$ bits/J, which depends on the ratio $\frac{N_2}{K_2}$, as η_2 is smaller. A target data-rate η_{target} can be achieved with several settings of the design elements (N_2, B_2, M). The EE_2 maximization problem, which is equivalent to maximizing $\frac{N_2}{K_2}$ such that $\eta_2 \geq \eta_{\text{target}}$ and $N_2 \in \mathbb{Z}^+$, is a pure integer model and, hence, difficult to solve.

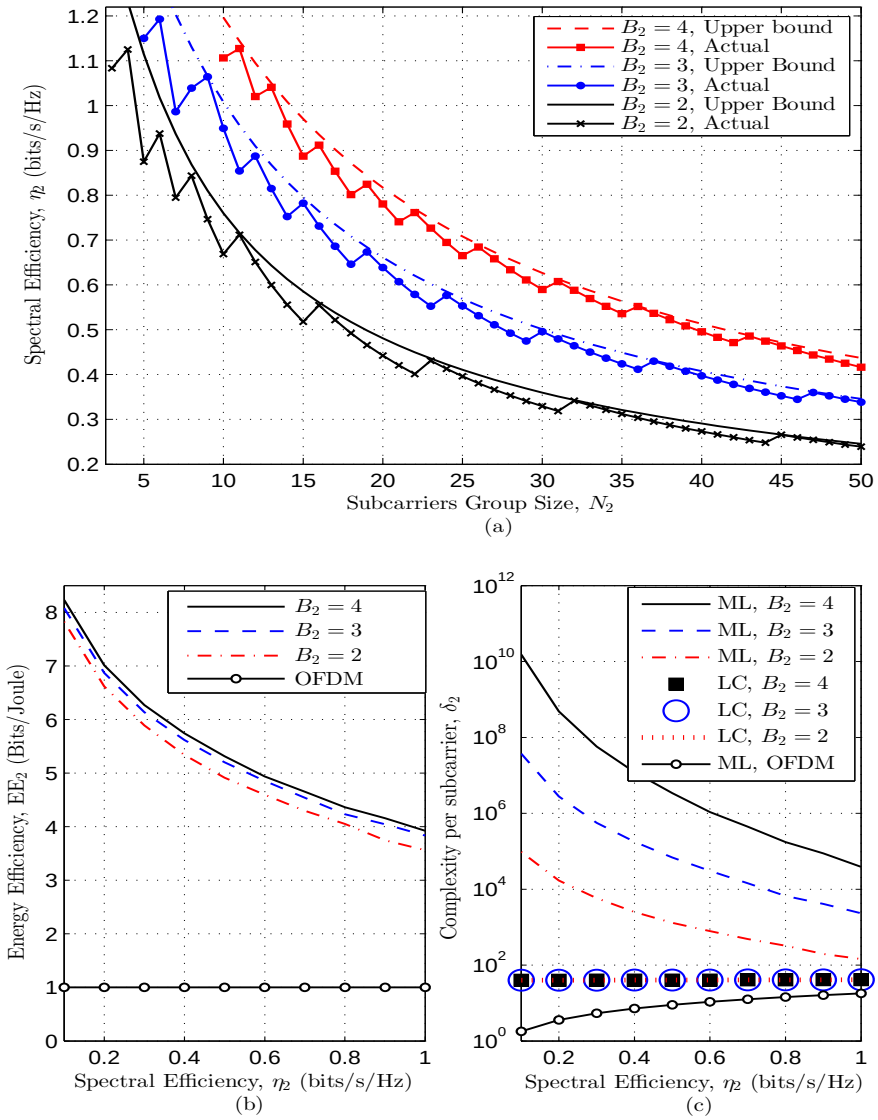

Figure A.2: OFDM-GIM$_2$: (a) Effect of the subcarriers' group size N_2 on data-rate, for $B_2 = 2, 3, 4$ and $M = 2$; (b) energy efficiency vs. data-rate; (c) Complexity vs. data-rate.

In order to determine the optimal group size N_2^*, we first choose the design parameters B_2 and M, and define η_{target}. It is further assumed that $N_2 \notin \mathbb{Z}^+$, but $N_2 \in \mathbb{R}^+$, and the optimal N_2 in terms of EE_2^{PSP} is denoted by N_2'. Equating the upper bound of (2.13) to η_{target} and solving for N_2 results in N_2'. For instance, the upper bound of (2.13) for the case of $B_2 = M = 2$ is $\eta_2^{\text{up}} = \frac{2\,N_2}{N_2^2 - N_2 + 2} + \frac{\ln\left(N_2^2 - N_2 + 2\right)}{N_2 \ln 2} - \frac{1}{N_2}$, which, for $\eta_{\text{target}} = 0.5$, results in $N_2' = 19.07$. Since (2.13) is a decreasing function of N_2, the digitized or actual optimal group size always satisfies $N_2^* \leq N_2'$.

Finally, the ratio of average number of active subcarriers to group size, in OFDM-GIM and OFDM-IIM, is such that $\frac{N_2}{K_2} > \frac{N_1}{K_1} \geq \frac{N}{K} > 1$. Therefore, $\text{EE}_2 > \text{EE}_1 \geq \text{EE} > \text{EE}_{\text{c}}$, where EE_{c} is the energy efficiency pertaining to classical OFDM. Figure A.2(a) illustrates the effect of varying N_2 on η_2, for different values of B_2. Consider a data-rate requirement $\eta_{\text{target}} = 1$ bits/s/Hz, and

$B_2 = 2, 3, 4$. The figure shows that all the group sizes, i.e., $N_2 = 10, 11, 12$ and 13, can satisfy the requirement, but that the optimal group size is $N_2^* = 13$.

Figure A.2(b) compares the energy efficiency of OFDM-GIM$_2$ versus classical OFDM, for varying η_{target}. OFDM with some η_{target} of 0.1 or 0.2 bits/s/Hz needs to transmit 1 bit every tenth or fifth subcarrier, and can only achieve an EE$_\text{c}$ of 1 bit/J. In OFDM-GIM$_2$, the optimal group size N_2^* decreases as the target on η_2 increases. This reduces the total power savings per group, i.e., $(N_2^* - K_2)P_\text{t}$ W, thereby reducing EE$_2$, which is justified by the EE$_2$ versus η_{target} performance in Fig. A.2(b). A small gain in EE$_2$ can be attained by increasing B_2, but at the cost of additional receiver complexity (cf. Fig. A.2(c)) as will be thoroughly discussed in Section A.4.

In essence, OFDM-GIM$_2$ can achieve superior EE$_2$ at low values of η_{target}, compared to classical OFDM, OFDM-IM, OFDM-IIM, and OFDM-GIM$_1$, thereby making it well suited for state-of-the-art wireless sensor networks and machine-type communications. Its use can indeed reduce the energy consumption and enhance the network lifetime.

A.4 Detection and Complexity Analysis

In support of the detection complexity discussions presented so far in Sections 2.1.3 and 2.2.3 for OFDM-IIM, in Section A.2.1 (cf. Fig. A.1(d)) for OFDM-GIM$_1$, and in Section 2.3.2 (cf. Fig. A.2(c)) for OFDM-GIM$_2$, this section quantifies the overall detection complexity in terms of their resource elements (N, K, M), (N_1, K_1, M), and (N_2, K_2, M).

In OFDM-IIM and OFDM-GIM, the received signal vector for a group of N_λ subcarriers at l^{th} group is $\mathbf{y}_\lambda^{(l)} = \mathbf{h}_\lambda^{(l)}\mathbf{s}_\lambda^{(l)} + \mathbf{u}_\lambda^{(l)}$. At the receiver, the group size N_λ and the modulation level M are known. Also, K in case of OFDM-IIM, B_1 in case of OFDM-GIM$_1$, and B_2 in case of OFDM-GIM$_2$ are known to the receiver, but the number of active subcarriers, the active/idle state of each N_λ subcarrier, and the symbol vector $\mathbf{s}_\lambda^{(l)}$ at a given transmission instant, are not known.

A.4.1 Maximum Likelihood Detection

Detection

The ML detection on l^{th} group of subcarriers, in OFDM-IIM or OFDM-GIM, is similar to (4.4), where $\mathbf{s}_\lambda^{(l)} \in \mathbf{S}_\lambda$, $\mathbf{S}_\lambda \in \mathbb{C}^{N_\lambda \times R_\lambda}$. The value of R_λ depends on the modulation order M, the total number of patterns m_λ, and the total number of active subcarriers K_λ. The values of R_1 for OFDM-GIM$_1$ and R_2 for OFDM-GIM$_2$ are formulated as follows:

$$R_1 = \sum_{i=N_1-B_1+2}^{N_1} \binom{N_1}{i} M^i + \kappa_1 M^{N_1-B_1+1} \tag{A.18a}$$

$$R_2 = \sum_{j=1}^{B_2-1} \binom{N_2}{j} M^j + \kappa_2 M^{B_2}. \tag{A.18b}$$

Complexity, $\delta_\lambda^{\mathrm{ML}}$

The overall detection complexity of OFDM-IIM and OFDM-GIM is denoted by $\delta_\lambda^{\mathrm{ML}} = f(\mathrm{ML}) + f(M)$, and given by

$$\delta_\lambda^{\mathrm{ML}} = 8R_\lambda + \frac{K_\lambda}{N_\lambda} M. \tag{A.19}$$

Prior work on detection complexity reduction in IM-based systems consist in methods to minimize the number of complex operations for each entry of the code-book $\mathbf{S}_\lambda$ (cf. [31] and references therein). On the other hand, the proposed OFDM-IIM and OFDM-GIM$_1$ achieve the least possible detection complexity under a given detector, by using the smallest code-book $\mathbf{S}_\lambda$. While the aforementioned low-complexity methods can be adopted to further reduce the detection complexity of OFDM-IIM and OFDM-GIM, their investigation is beyond the scope of the paper.

A.4.2 Low-Complexity Detection

Detection

Unlike ML detector, the low-complexity (LC) detector considers the fact that each subcarrier can take one realization out of the total of $M+1$, and inspired by [67–69], performs detection on a per subcarrier basis. This reduces the code-book size $N_\lambda R_\lambda$ of ML detector to $M+1$. As such, the complexity remains independent of N_λ and K_λ, and only depends on the total number of symbol realizations per subcarrier, i.e., $M+1$. The state (active/idle) of the k^{th} subcarrier in the l^{th} group, i.e., $\iota_\lambda^{(k,l)}$, and the possible transmit symbol $s_\lambda^{(k,l)}$ are determined as follows. First, through minimization to find the estimate as per

$$\widehat{s}_\lambda^{(k,l)} = \arg\min_{s_\lambda^{(k,l)}} (|y_\lambda^{(k,l)} - h_\lambda^{(k,l)} \chi|^2), \tag{A.20}$$

where $\chi \in \mathbb{C}^{M+1}$, $k = 1, \cdots, N_\lambda$, and $l = 1, \cdots, L$. Then, the state (active/idle) is determined by the following rule:

$$\begin{cases} \widehat{\iota}_\lambda^{(k,l)} = \text{Active}, & \text{if } \widehat{s}_\lambda^{(k,l)} \neq 0 \\ \widehat{\iota}_\lambda^{(k,l)} = \text{Idle}, & \text{if } \widehat{s}_\lambda^{(k,l)} = 0. \end{cases} \tag{A.21}$$

Eq. (A.20) estimates one of the $M+1$ complex realizations on each subcarrier. As per (A.21), if the estimated symbol is not zero, the subcarrier is classified as active, otherwise the subcarrier is idle. This kind of detection mechanism can estimate or return patterns that may not be part of the mapping-table (cf. Eq. (2.8) and κ_2), and may contribute to error propagation. In OFDM-GIM$_1$, the problem is naturally avoided when $B_1 = N_1 + 1$, which results in a total of $m_1 = 2^{N_1}$ patterns. In such a case, all the patterns are available in the look-up table so that to avoid the problem of choosing a pattern out of the table. This changes the sub-optimal nature of the proposed LC detector to near-optimal with a considerably smaller complexity. When $B_1 \neq N_1 + 1$, error propagation can be avoided by using the bit-padding method as proposed in [70], or by spreading a symbol on each subcarrier over multiple symbol periods as detailed in [42]. The method of [42] can also minimize the $2^{\log_2 \binom{N}{K}} - 2^{\log_2 \lfloor \binom{N}{K} \rfloor}$ number of unused patterns in OFDM-IIM, the $m_1 - 2^{b_1}$ unused patterns in

OFDM-GIM$_1$, and the $m_2 - 2^{b_2}$ unused patterns in OFDM-GIM$_2$, which can further enhance the data-rate of these techniques.

Complexity, $\delta_\lambda^{\mathrm{LC}}$

The overall detection and de-modulation complexity of the LC detector per subcarrier is

$$\delta_\lambda^{\mathrm{LC}} = 8(M+1) + \frac{K_\lambda}{N_\lambda} M. \tag{A.22}$$

The ML detector in classical OFDM system achieves an overall detection complexity of $\delta_{\mathrm{c}}^{\mathrm{ML}} = 9M$ [28]. By comparing $\delta_\lambda^{\mathrm{LC}}$ and $\delta_{\mathrm{c}}^{\mathrm{ML}}$, it is easily confirmed that the proposed LC detector has the potential to achieve less complexity than $\delta_{\mathrm{c}}^{\mathrm{ML}}$ when $\frac{K_\lambda}{N_\lambda} < \frac{M-8}{M}$.

A.5 Performance Analysis

The bit error rate, achievable data rate, and the number of successfully transmitted bits per joule, are considered as performance metrics.

A.5.1 Bit Error Rate

We recall that the reception is an estimation problem of two processes: 1) classifying each subcarrier of a group as active or idle, and 2) estimating the transmitted symbols on the active subcarriers. The active subcarriers are used for symbol transmission and, thus, a wrong estimation of a subcarrier activity can lead to an error in the symbol detection. Hereinafter, for the sake of performance analysis, we assume a detector where the symbol estimation depends on the subcarrier index estimation, e.g., an energy/power based detector, where first the subcarrier index is estimated based on an energy/power threshold and then a symbol is estimated on the subcarrier if its energy/power is above a threshold.

Considering Nakagami-n fading channel, we denote the incorrect subcarrier state estimation probability by P_{a}. The incorrect symbol detection probability is represented by P_{b} when $P_{\mathrm{a}} = 0$, and by P_{c} when $P_{\mathrm{a}} \neq 0$. The symbol detection process depends on the subcarrier estimation process. Detection is deemed correct when both, the subcarrier activity estimation ($\widehat{\mathbf{i}}_\lambda^{(l)}$) and the symbol estimation ($\widehat{\mathbf{s}}_\lambda^{(l)}$) are correct. The incorrect symbol detection probability under $P_{\mathrm{a}} \neq 0$ is

$$P_{\mathrm{c}} = 1 - (1 - P_{\mathrm{a}})(1 - P_{\mathrm{b}}) = P_{\mathrm{a}} + P_{\mathrm{b}} - P_{\mathrm{a}} P_{\mathrm{b}}. \tag{A.23}$$

When $B_1 = 1$, only one pattern having $i = N_1$ active subcarriers exists in OFDM-GIM$_1$. This is the special case of a classical OFDM system, where the receiver already knows the state of all the subcarriers as active and, thus, $P_{\mathrm{a}} = 0$. The overall error probability becomes $P_{\mathrm{c}} = P_{\mathrm{b}}$, which is similar to the OFDM system.

The use of IM increases the overall error probability by a factor of $P_{\rm a} - P_{\rm a}P_{\rm b} \geq 0$. This effect is minor compared to the data-rate and energy efficiency gains of OFDM-IIM and OFDM-GIM. Also, the use of the PRP policy can help in reducing the $P_{\rm a} - P_{\rm a}P_{\rm b}$ increment in error probability. The symbol and subcarrier activity estimations contribute to the overall error probability $P_{{\rm e}_\lambda}$, where dropping λ in the variables involved corresponds to OFDM-IIM, while $\lambda = 1, 2$ denote OFDM-GIM$_1$ and OFDM-GIM$_2$, respectively. According to the law of total probability, $P_{{\rm e}_\lambda}$ is given by

$$P_{{\rm e}_\lambda} = P_{\rm a}P({\rm a}) + P_{\rm c}P({\rm c}) = \frac{b_\lambda}{N_\lambda \eta_\lambda} P_{\rm a} + \frac{K_\lambda \log_2 M}{N_\lambda \eta_\lambda} P_{\rm c}, \tag{A.24}$$

where $P({\rm a})$ and $P({\rm c})$ are the frequency of occurrence of the *index bits* of length b_λ and of the *mod bits* of length d_λ, respectively. Next, we determine $P_{\rm a}$ and $P_{\rm b}$.

Error Probability of Subcarrier's Activity, $P_{\rm a}$

A given subcarrier can either transmit one of M possible symbols of the M-APM constellation, or remain idle. Assume that symbol s_λ is transmitted on a subcarrier, and results in the received signal $y_\lambda = s_\lambda + u_\lambda$ in an AWGN channel. Then, the probability of error $P_{\rm a}(\gamma)$ in the AWGN channel is given by

$$\begin{aligned} P_{\rm a}(\gamma) &= \frac{N_\lambda - K_\lambda}{N_\lambda} \int_{\sqrt{\frac{P_{\rm t}}{2}}}^{\infty} p(y_\lambda \mid 0){\rm d}y + \frac{K_\lambda}{N_\lambda} \int_{-\infty}^{\sqrt{\frac{P_{\rm t}}{2}}} p(y_\lambda \mid s_\lambda){\rm d}y \\ &= \frac{1}{\sqrt{2\pi}} \int_{\sqrt{P_{\rm t}/N_0}}^{\infty} \exp\left(\frac{-x^2}{2}\right){\rm d}x = Q\left(\sqrt{\frac{P_{\rm t}}{N_0}}\right) = Q\left(\sqrt{\gamma}\right), \end{aligned} \tag{A.25}$$

where $\gamma = P_{\rm t}/N_{\rm o}$ is the average SNR per symbol, and $Q(x) = \frac{1}{2\pi}\int_x^\infty e^{\frac{-t^2}{2}}{\rm d}t$ is the Q-function. Using the Craig's definite integral form of the Q-function [71], i.e., $Q(x) = \frac{1}{\pi}\int_0^{\pi/2} \exp\left(\frac{-x^2}{2\sin^2\phi}\right){\rm d}\phi$, the error probability in (A.25) can be expressed as

$$P_{\rm a}(\gamma) = \frac{1}{\pi}\int_0^{\pi/2} \exp\left(\frac{-\gamma}{2\sin^2\phi}\right){\rm d}\phi. \tag{A.26}$$

The average SNR in a time-varying channel is $\overline{\gamma} = \gamma E(h^2)$, where h is the fading amplitude of some random variable with distribution function $p(\gamma;\overline{\gamma})$. The BER over the fading channel is obtained by averaging $P_{\rm a}(\gamma)$ over $p(\gamma;\overline{\gamma})$, that is $P_{\rm a} = \int_0^\infty P_a(\gamma)p(\gamma;\overline{\gamma}){\rm d}\gamma$. Substituting (A.26) into $P_{\rm a}$ for multiple receiving antennas ($L_{\rm r}$) and i.i.d. fading parameters yields [72]:

$$P_{\rm a} = \frac{1}{\pi}\int_0^{\pi/2} \left(\mathcal{M}\left(\frac{-g}{\sin^2\phi};\overline{\gamma}\right)\right)^{L_r}{\rm d}\phi, \tag{A.27}$$

where $g = 1/2$ for the case of $P_{\rm a}$. The moment-generating function (MGF) in the case of Nakagami-n fading is given by [72]

$$\mathcal{M}\left(\frac{-g}{\sin^2\phi};\overline{\gamma}\right) = \frac{(1+n^2)\sin^2\phi}{(1+n^2)\sin^2\phi + g\overline{\gamma}} \exp\left(\frac{-n^2 g\overline{\gamma}}{(1+n^2)\sin^2\phi + g\overline{\gamma}}\right), \tag{A.28}$$

where $n = 0$ for the Rayleigh fading case, and $n = \infty$ for AWGN channel.

Error Probability of Transmit Symbols, P_{b}

The error probability P_{b} for $M = 2$ and multiple receive antennas L_{r} in a Nakagami-n fading channel is obtained by replacing $g = 1$ in (A.27). For $M > 2$, the average symbol error rate (SER) of a square Quadrature amplitude modulation (QAM) scheme over generalized fading channel is [72]

$$\begin{aligned} P_{\mathrm{b}}^{\mathrm{SER}} = \frac{4}{\pi}\left(1-\frac{1}{\sqrt{M}}\right)\int_0^{\pi/2}\prod_{l_r=1}^{L_{\mathrm{r}}}\mathcal{M}\left(\frac{-g}{\sin^2\phi};\overline{\gamma}\right)\mathrm{d}\phi \\ -\frac{4}{\pi}\left(1-\frac{1}{\sqrt{M}}\right)^2\int_0^{\pi/4}\prod_{l_r=1}^{L_{\mathrm{r}}}\mathcal{M}\left(\frac{-g}{\sin^2\phi};\overline{\gamma}\right)\mathrm{d}\phi, \end{aligned} \tag{A.29}$$

where $g = 3/2(M-1)$ for the case of square M-QAM and the MGF is given by (A.28). An accurate approximation of the BER from the SER is $P_{\mathrm{b}} = P_{\mathrm{b}}^{\mathrm{SER}}/\log_2 M$. The BER expression holds true only in the unrealistic case of $P_{\mathrm{a}} = 0$. For the realistic case of $P_{\mathrm{a}} \neq 0$, the BER is obtained by substituting P_{b} and (A.27) into (A.23). The resultant expression is obtained as

$$P_{\mathrm{c}} = \frac{F\left(\ln 2^{-\pi}(1-M) + \pi\ln 4 - M\pi\ln(4M) - 2F\right) - \pi}{2M\pi^2\ln M}, \tag{A.30}$$

where F is given by

$$F = \left[\frac{(\cosh(\mathrm{j}_1) - \sinh(\mathrm{j}_2))\,\left(n^2+1\right)\,\left(\frac{\cos(2\,\phi)}{2}-\frac{1}{2}\right)}{g\,\overline{\gamma} - \left(n^2+1\right)\,\left(\frac{\cos(2\,\phi)}{2}-\frac{1}{2}\right)}\right]^{\mathrm{L_r}}, \tag{A.31}$$

and where $\mathrm{j}_1 = \frac{2\,g\,n^2\,\overline{\gamma}}{2\,g\,\overline{\gamma}-\cos(2\,\phi)-n^2\,\cos(2\,\phi)+n^2+1}$ and $\mathrm{j}_2 = \frac{g\,n^2\,\overline{\gamma}}{-n^2\cos(\phi)^2+n^2-\cos(\phi)^2+g\,\overline{\gamma}+1}$.

Overall Bit Error Probability, P_{e_λ}

The overall BER is obtained by substituting (A.30) and (A.27) into (A.24), yielding

$$\begin{aligned} P_{\mathrm{e}_\lambda} = \frac{1}{2N_\lambda\eta_\lambda\pi\ln 2}\Big[\pi - F\Big(\frac{2K_\lambda\ln 2\,(M-1)}{M} \\ + b_\lambda\ln 2 + K_\lambda\ln M\Big) + F\left(\frac{M\pi-\pi-M}{M\pi}\right)\Big]. \end{aligned} \tag{A.32}$$

Next, a comparison of the BER, achievable rate, and energy efficiency performance of OFDM-IIM and OFDM-GIM against classical OFDM is presented. Then, potential applications of OFDM-IIM and OFDM-GIM in various IEEE 802.11 standards are highlighted.

Appendix B

Multiple Active Spatial Modulation: A Possibility of More than Spatial Modulation

B.0.1 Data-rate Enhancement

The Data-rate of MASM is compared to that of SMx according to the inequality rule $\eta \lessgtr N_{\mathrm{t}} \log_2 M$. The latter, after some algebraic manipulation, can be written as

$$\left|\left|\left\lfloor \binom{N_{\mathrm{t}}}{N_{\mathrm{a}}} \right\rfloor\right|\right| - M^{N_{\mathrm{t}}-N_{\mathrm{a}}} \lessgtr 0, \tag{B.1}$$

where $||\lfloor . \rfloor||$ is the approximation to the greatest lower integer power of two. The Data-rate of MASM is less, equal, or higher than that of SMx if the left-hand-side (LHS) of (B.1) is less, equal, or higher than 0.

Firstly, a parameter $0 \leq \theta < 1$ is introduced such that $b_1 = \log_2 \binom{N_{\mathrm{t}}}{N_{\mathrm{a}}} - \theta$. Then, the objective function (3.1a), rewritten in terms of the Gamma function and Sterling's formula, i.e. $\Gamma(Z+1) = Z! \approx \sqrt{2\pi} \exp(-Z) Z^{Z+\frac{1}{2}}$, is given by

$$\begin{aligned} \eta \approx \frac{1}{\ln 2} \Bigg(& N_{\mathrm{a}} \ln M - \ln \sqrt{2\pi} + \ln N_{\mathrm{t}} \left(N_{\mathrm{t}} + \frac{1}{2} \right) - \theta \ln 2 \\ & - \ln N_{\mathrm{a}} \left(N_{\mathrm{a}} + \frac{1}{2} \right) - \left(N_{\mathrm{t}} - N_{\mathrm{a}} + \frac{1}{2} \right) \ln (N_{\mathrm{t}} - N_{\mathrm{a}}) \Bigg), \end{aligned} \tag{B.2}$$

where $\theta = 0$ results in an upper bound on (3.1a) and (B.2), meaning $b_1 = \log_2 \binom{N_{\mathrm{t}}}{N_{\mathrm{a}}}$. The second-order derivative of (B.2) w.r.t. N_{a} yields

$$\eta''(N_{\mathrm{a}}) \leq \frac{1}{\ln 2} \left[\frac{1}{2(N_{\mathrm{t}} - N_{\mathrm{a}})^2} + \frac{1}{2N_{\mathrm{a}}^2} - \frac{1}{N_{\mathrm{t}} - N_{\mathrm{a}}} - \frac{1}{N_{\mathrm{a}}} \right], \tag{B.3}$$

where $\frac{1}{2(N_{\mathrm{t}}-N_{\mathrm{a}})^2} < \frac{1}{N_{\mathrm{t}}-N_{\mathrm{a}}}$ and $\frac{1}{2N_{\mathrm{a}}^2} < \frac{1}{N_{\mathrm{a}}}$, given that $N_{\mathrm{t}} - N_{\mathrm{a}} \geq 1$. Therefore, $\eta''(N_{\mathrm{a}}) \leq 0$. This shows that $\eta'(N_{\mathrm{a}})$ is a decreasing function of N_{a}. Next, $\eta'_{\min}(N_{\mathrm{a}}) = \eta'(N_{\mathrm{t}} - 1)$ and $\eta'_{\max}(N_{\mathrm{a}}) = \eta'(1)$

are respectively given by

$$\eta'_{\min}(N_{\rm a}) = \frac{1}{\ln 2}\left[\ln M - \ln(N_{\rm t}-1) + \frac{1}{2}\left(1 - \frac{1}{N_{\rm t}-1}\right)\right], \tag{B.4}$$

$$\eta'_{\max}(N_{\rm a}) = \frac{1}{\ln 2}\left[\ln M + \ln(N_{\rm t}-1) - \frac{1}{2}\left(1 - \frac{1}{N_{\rm t}-1}\right)\right]. \tag{B.5}$$

In (B.5), $\ln(N_{\rm t}-1) - \frac{1}{2}(1-\frac{1}{N_{\rm t}-1}) \geq 0$ and, thus, $\eta'_{\max}(N_{\rm a})$ is an increasing function. The modulation order M can be represented in terms of $N_{\rm t}$ to understand the varying nature of $\eta'_{\min}(N_{\rm a})$. The following two cases are distinguished.

Case-1: $N_{\rm t} \leq 2M-1$. Substituting $M \geq \frac{N_{\rm t}+1}{2}$ into (B.4), it can be easily shown that $\eta''^{(1)}_{\min}(N_{\rm a}) \geq 0$, meaning (B.4) is an increasing function of $N_{\rm a}$ when $N_{\rm t} \leq 2M-1$. Then, $\eta'^{(1)}_{\min}(N_{\rm a}) \leq \eta'^{(1)}(N_{\rm a}) \leq \eta'^{(1)}_{\max}(N_{\rm a})$, implies that (B.2) is an increasing function of $N_{\rm a}$ in *Case*-1. Hence, the optimal $N_{\rm a}$ in terms of Data-rate is $N_{\rm a} = N_{\rm t} - 1$.

Case-2: $N_{\rm t} \geq 2M$. Substituting $M \leq \frac{N_{\rm t}}{2}$ into (B.4), it can be shown that $\eta''^{(2)}_{\min}(N_{\rm a}) \leq 0$, meaning (B.4) is a decreasing function of $N_{\rm a}$ when $N_{\rm t} \geq 2M$. According to $\eta'^{(2)}_{\min}(N_{\rm a}) \leq \eta'^{(2)}(N_{\rm a}) \leq \eta'^{(2)}_{\max}(N_{\rm a})$, it can be concluded that (B.2) is a first increasing and then decreasing function of $N_{\rm a}$. For $N_{\rm t} \geq 2M$, maximum Data-rate can be attained when $N_{\rm a}$ is solution to $\eta'(N_{\rm a}) = 0$. The resultant expression is transcendental in nature and, therefore, it is hard to obtain a closed-form solution.

The following theorems compare the Data-rate of MASM to SMx under similar settings for $N_{\rm t}$ and M.

Theorem 4. *For $N_t < M$, we have*

$$\underset{\forall N_t}{max}(\eta) \quad < N_t \log_2 M. \tag{B.6}$$

Proof. As η is an increasing function of $N_{\rm t}$ and $N_{\rm a}$, then for $N_{\rm t} < M$, $\max(\eta)$ occurs at $N_{\rm t} = M-1$ and $N_{\rm a} = N_{\rm t} - 1 = M-2$. Substituting these values into the LHS of (B.1) results in $||\lfloor M-1 \rfloor| - M$, where $||\lfloor M-1 \rfloor|| < M$. Therefore, the maximum Data-rate of MASM is less than SMx for $N_{\rm t} < M$. □

Theorem 5. *For $M \leq N_{\rm t} < 2M$, we have*

$$\underset{\forall N_t}{max}(\eta) \quad = N_t \log_2 M. \tag{B.7}$$

Proof. Substituting $(N_{\rm t} = M, N_{\rm a} = M-1)$ and $(N_{\rm t} = 2M-1, N_{\rm a} = 2M-2)$ into (B.1) results in $||\lfloor M \rfloor| - M = 0$ for the first case and in $||\lfloor 2M-1 \rfloor| - M = 0$ for the latter. Hence, the maximum η remains similar to the case of SMx. □

Theorem 6. *For $N_{\rm t} \geq 2M$, we have*

$$\underset{\forall N_t}{max}(\eta) \quad > N_t \log_2 M. \tag{B.8}$$

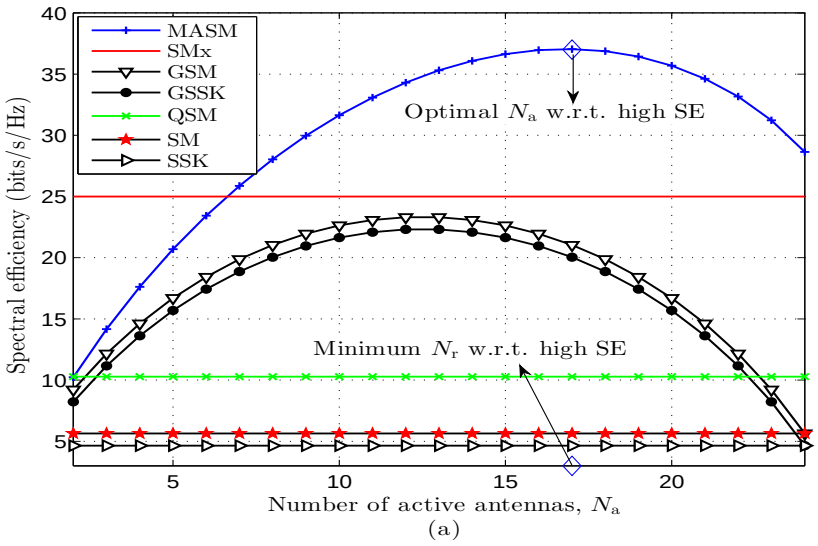

Figure B.1: Effect of N_a on data-rate of different space modulation techniques (SMTs)

Proof. The minimum condition, i.e. the boundary values ($N_t = 2M, N_a = 2M - 1$) are substituted in (B.1), which results in $||\lfloor 2M \rfloor| - M = M$. Thus, MASM with $N_t \geq 2M$ can achieve superior Data-rate and energy efficiency with reduced detection complexity as compared to SMx. □

Selection of the optimal N_a for $N_t < 2M$ is known, i.e. $N_a = N_t - 1$. The optimal N_a for $N_t > 2M$ is not clear due to the lack of closed-form solution for $\eta'(N_a) = 0$. We resort to a brute-force search method. An example is shown in Fig. B.1 when $N_t = 25$ and $M = 2$. Figure B.1 confirms the conclusion drawn above, namely, that the Data-rate of MASM first increases and then decreases for varying N_a when $N_t \geq 2M$ (cf. *Case*-2). It also shows that careful selection of N_t and N_a in MASM can make it surpass SMx and other prominent SMTs in terms of Data-rate and energy efficiency.

B.0.2 Bit Error Rate

The BER performance of SMTs with $N_a > 1$, i.e. MASM, E-MASM, GSM and SMx, is evaluated using the tight union bounding technique [9], as

$$P_e \leq \frac{1}{\lambda 2^{\lambda}} \sum_{\hat{\mathbf{i}},\hat{\mathbf{x}}} \sum_{\mathbf{i},\mathbf{x}} E(P_e(\mathbf{x} \to \hat{\mathbf{x}}))e(\mathbf{x}, \hat{\mathbf{x}}), \tag{B.9}$$

where $\lambda = \eta,\ \hat{\eta},\ \log_2 M + \log_2 \binom{N_t}{N_a}$, $\log_2 \binom{N_t}{N_a}$ and $N_t \log_2 M$, for MASM, E-MASM, GSM, GSSK and SMx, respectively, and where $e(\mathbf{x}, \hat{\mathbf{x}})$ denotes the number of bits in error, and $P_e(\mathbf{x} \to \hat{\mathbf{x}})$ is the pairwise error probability (PEP). The PEP per the ML criterion [35] is $Q\left(\sqrt{\rho N_a^{-1} \parallel \mathbf{H}(\mathbf{x} - \hat{\mathbf{x}}) \parallel_F^2}\right)$, which according to the Craig's representation of the Q-function is given by

$$P_e(\mathbf{x} \to \hat{\mathbf{x}}) = \frac{1}{\pi} \int_0^{\pi/2} \exp\left(\frac{-\rho \parallel \mathbf{H}\Psi \parallel_F^2}{2N_a \sin^2\phi}\right) d\phi, \tag{B.10}$$

where $\Psi = \mathbf{x} - \widehat{\mathbf{x}}$, and $E(P_{\mathrm{e}}(\mathbf{x} \to \widehat{\mathbf{x}}))$ is achieved by modifying Eq. 4.53 in [9], yielding (B.11) wherein $\mathbf{I}_{N_{\mathrm{r}}}$ denotes the $N_{\mathrm{r}} \times N_{\mathrm{r}}$ identity matrix, and $\otimes$ is the Kronecker product.

$$E(P_{\mathrm{e}}(\mathbf{x} \to \widehat{\mathbf{x}})) \leq 1 \Big/ 2 \Big| \mathbf{I}_{N_{\mathrm{r}}} + \frac{\rho}{2\sqrt{2}N_{\mathrm{a}}} \mathbf{I}_{N_{\mathrm{r}}} \otimes \Psi \Psi^{H} \Big|. \tag{B.11}$$

Appendix C

Space-time Equiprobable Antenna Activation in Spatial Modulation

C.1 Bit Error Rate

The transmitted codeword $\mathbf{X} = [\mathbf{x}_1, \cdots, \mathbf{x}_L]$ is estimated at the receiver according to the ML principle (4.4) as $\widehat{\mathbf{X}} = [\widehat{\mathbf{x}}_1, \cdots, \widehat{\mathbf{x}}_L]$. Let the number of bits in difference between $\mathbf{X}$ and $\widehat{\mathbf{X}}$ be $\mathrm{e}(\mathbf{X}, \widehat{\mathbf{X}})$. An upper-bound on the error probability of SM technique is given by

$$P_{\mathrm{e}} \leq \frac{1}{\overline{\eta} 2^{\overline{\eta}}} \sum_{\mathbf{n},\mathbf{s}} \sum_{\widehat{\mathbf{n}},\widehat{\mathbf{s}}} E\left[P(\mathbf{X} \to \widehat{\mathbf{X}})\right] \mathrm{e}\left(\mathbf{X}, \widehat{\mathbf{X}}\right), \tag{C.1}$$

where $E[P(\mathbf{X} \to \widehat{\mathbf{X}})] \leq E\left[Q\left(\sqrt{\left\|(\mathbf{X} - \widehat{\mathbf{X}})\tilde{\mathbf{H}}\right\|_{\mathrm{F}}^2 / 2N_{\mathrm{o}}}\right)\right]$, $Q(.)$ is the Q-function and the SNR is defined as $\frac{1}{2N_{\mathrm{o}}}$. The average pairwise error probability $E[P(\mathbf{X} \to \widehat{\mathbf{X}})]$ can be approximated for high SNR with the Chernoff bound [50, Eq. 25], as

$$E\left[P(\mathbf{X} \to \widehat{\mathbf{X}})\right] \leq \left(\frac{1}{4N_0}\right)^{-N_{\mathrm{r}}\tau} \left(\prod_{t=1}^{\tau} \lambda_t\right)^{-N_{\mathrm{r}}}, \tag{C.2}$$

where $\tau = \mathrm{rank}(\psi)$, and λ_t is the t^{th} eigenvalue of matrix $\psi = (\mathbf{X} - \widehat{\mathbf{X}})(\mathbf{X} - \widehat{\mathbf{X}})^{\mathrm{H}}$.

C.2 Coding Gain

Let $\mathbf{Z} \in \mathbb{C}^{\vartheta \times \vartheta}$ denote a diagonal matrix with entries being the $\vartheta = \mathrm{e}(\mathbf{X}, \widehat{\mathbf{X}})$ non-zero elements of $\mathbf{X} - \widehat{\mathbf{X}}$, and denote the channel coefficients across the wrongly decoded codeword $\widehat{\mathbf{X}}$ by $\mathbf{Q} \in \mathbb{C}^{\vartheta \times N_{\mathrm{r}}}$. Similarly, for the conventional mapping case, organize the non-zero elements of $\mathbf{x} - \widehat{\mathbf{x}}$ in the diagonal matrix $\tilde{\mathbf{Z}} \in \mathbb{C}^{\tilde{\vartheta} \times \tilde{\vartheta}}$, where codeword $\mathbf{x} \in \mathbb{C}^{N_{\mathrm{t}} \times 1}$ and $\tilde{\vartheta} = \mathrm{e}(\mathbf{x}, \widehat{\mathbf{x}})$, and denote the channel matrix pertaining to the entries of $\tilde{\mathbf{Z}}$ by $\tilde{\mathbf{Q}} \in \mathbb{C}^{\tilde{\vartheta} \times N_{\mathrm{r}}}$. The coding gain with the *space-time* mapping over

the conventional approach can be expressed in decibels as

$$\mathcal{G} = 10\log_{10}\left(\prod_{t'=1}^{\tau'}\left(\frac{1}{\lambda_{t'}}\right)^{N_{\mathrm{r}}} \Bigg/ \left\|4\mathbf{I}N_{\mathrm{o}} + \frac{1}{\sqrt{2}}\mathbf{I}\otimes\tilde{\mathbf{Z}}\tilde{\mathbf{Z}}^{\mathrm{H}}\tilde{\mathbf{Q}}\right\|_{\mathrm{F}}^{\frac{1}{\Lambda}}\right), \tag{C.3}$$

where the numerator is obtained from (C.2), and denotes the coding gain when using the *space-time* mapping in SM techniques. The denominator in (C.3) is the coding gain when conventional mapping is used, and satisfies [9, Eq. 4.53] according to the BER definition, i.e., $P_{\mathrm{e}} \approx \frac{1}{2N_{\mathrm{o}}}||4\mathbf{I}N_{\mathrm{o}} + \frac{1}{\sqrt{2}}\mathbf{I}\otimes\tilde{\mathbf{Z}}\tilde{\mathbf{Z}}^{\mathrm{H}}\tilde{\mathbf{Q}}||_{\mathrm{F}}^{-1}$. Further, $\tau' = \mathrm{rank}\{\mathbf{Z}\mathbf{Z}^{\mathrm{H}}\mathbf{Q}\}$, the λ's are the eigenvalues of $\mathbf{Z}\mathbf{Z}^{\mathrm{H}}\mathbf{Q}$, and $\Lambda = \min(\mathrm{rank}(\tilde{\mathbf{Z}}\tilde{\mathbf{Z}}^{\mathrm{H}}\tilde{\mathbf{Q}}))$. The coding gain in (C.3) arises from the selection of codeword $\mathbf{X}$, which determines a transmit antenna activation probability, the eigenvalues (λ's), and the total number of errors $\mathrm{e}(\mathbf{X}, \widehat{\mathbf{X}})$.

Appendix D

Information-Guided Antenna Selection and Activation for Spatial Modulation MIMO Systems

D.1 Average Achievable Rate

The event probability $P(\mathcal{E} \to [r]|g_a)$ can be expressed as $P(\mathcal{E} \to [r]|g_a) = P(\mathcal{E} \to [q]|g_{a'}) \sum_{i=1}^{q-1} \frac{1}{A}\frac{1}{A^{i-1}}$, where $\sum_{i=1}^{q-1} \frac{1}{A}\frac{1}{A^{i-1}} = \frac{1}{A}(1+\frac{1}{A}) + \cdots \frac{1}{A^{q-2}}$. Using the method of differences, it can be shown that $\frac{1}{A} + \frac{1}{A^2} + \cdots + \frac{1}{A^{q-2}} = 1 - \frac{1}{A^{q-1}}$. Therefore, $P(E \to [r]|g_a) = P(\mathcal{E} \to [q]|g_{a'})(1 - \frac{1}{A^{q-1}})$. Similarly, we have $P(\mathcal{E} \to [r]|g_a) - (1 - \frac{1}{A^{r-1}})P(\mathcal{E} \to [q]|g_{a'}) = \frac{1}{A^{r-1}}$. Solving the two equations for $P(\mathcal{E} \to [r]|g_a)$ and $P(\mathcal{E} \to [q]|g_{a'})$, we get

$$P(\mathcal{E} \to [r]|g_a) = \frac{A^{1-r}}{(A^{1-r}-1)(A^{1-q}-1)-1}, \tag{D.1a}$$

$$P(\mathcal{E} \to [q]|g_{a'}) = 1 + \frac{1}{A^{-r}(A-A^q)-1}. \tag{D.1b}$$

Then, substituting (D.1a) and (D.1b) into $P(\mathcal{E} \to [r,q]) = \frac{1}{A}P(\mathcal{E} \to [r]|g_a) + \frac{1}{A}P(\mathcal{E} \to [q]|g_{a'})$, we attain (5.3).

D.1.1 Constellation Rearrangement

Let θ be the phase-shift to be applied to a M-APM symbol s_m to distinguish the r number of consecutive 0's or consecutive 1's at the receiver based on the estimated $\hat{m}$ and $\hat{n}$. The design challenge is to find θ that maximizes the minimum Euclidean distance between the constellation points s_m, which can be expressed as

$$\delta_{\min} = (s_m e^{j}\theta - s_{m'} e^{j}\theta)^2. \tag{D.2}$$

Optimal θ, denoted by $\tilde{\theta}$, is obtained by solving $\tilde{\theta} = \arg\max_{\theta}(\delta_{\min})$. Since the event $\mathcal{E} \rightarrow [1]$ denotes a zero number of consecutive equal bits, the $\tilde{\theta} = 0$ when $r = 1$. For events $\mathcal{E} \rightarrow [1], \cdots, \mathcal{E} \rightarrow [N_{\mathrm{t}}]$, the optimal $\tilde{\theta}$ for different modulations can be obtained as per the approach in [73]. That is,

$$\tilde{\theta} = \begin{cases} \frac{\pi}{2}, & \text{when } M = 2 \text{ (BPSK)} \\ \frac{\pi}{4}, & \text{when } M = 4 \text{ (QPSK)} \\ \frac{\pi}{7}, & \text{when } M = 16 \text{ } (16-\text{QAM}) \\ \frac{\pi}{16}, & \text{when } M = 64 \text{ } (64-\text{QAM}). \end{cases} \tag{D.3}$$

D.2 Performance Analysis

A closed-form upper-bound on the average BER of SM technique implementing I-AA with/without the proposed AS methods considering transmissions over Rayleigh fading channels and single- or multiple-antenna reception is derived in this section.

D.2.1 Average SNR without Antenna Selection

The average received SNRs achieved by the conventional SM, the proposed I-SM, and the optimal O-MIMO (cf. Subsection D.2.2) without AS and employing one receive antenna are now derived.

SM with Uniform Antenna Activation

During a symbol period, each column of the channel matrix $\mathbf{H}$ in SM technique implementing U-AA is chosen at a uniform rate of $\frac{1}{N_{\mathrm{t}}}$. Therefore, the average received SNR can be expressed as

$$\rho^{\mathrm{u}} = \begin{cases} \frac{1}{\sigma^2}\left(|s_m - s_{m'}|^2\right) & \text{if } n = n', \\ \frac{1}{\sigma^2}\left(|s_m|^2 + |s_{m'}|^2\right) & \text{if } n \neq n'. \end{cases} \tag{D.4}$$

SM with Irregular Antenna Activation

Let $x_1, \cdots, x_{N_{\mathrm{t}}}$ be i.i.d. random variables (RVs), each with probability density function (PDF) $f_n(x)$, and cumulative distribution function (CDF) $F_n(x)$. The PDF of the r^{th} order statistics is given by

$$f_r(x) = N_{\mathrm{t}} \binom{N_{\mathrm{t}} - 1}{r - 1} F(x)^{r-1} (1 - F(x))^{N_{\mathrm{t}} - r} f(x). \tag{D.5}$$

For exponential RVs, substituting $F(x) = 1 - \mathrm{e}^{-x}$ and $f(x) = \mathrm{e}^{-x}$ into (D.5) yields

$$f_r(x) = N_{\mathrm{t}} \binom{N_{\mathrm{t}} - 1}{r - 1} (1 - \mathrm{e}^{-x})^{r-1} \mathrm{e}^{-x(N_{\mathrm{t}} - r + 1)}. \tag{D.6}$$

Using (D.6), the mean value of the r^{th} order statistics, i.e., $\mathrm{E}_r[x,r] = \int_0^\infty x f_r(x)dx$, can be obtained in a closed-form as

$$\mathrm{E}_r[x,r] = \frac{1}{\Gamma(N_\mathrm{t}+1)}\left[N_\mathrm{t}\binom{N_\mathrm{t}-1}{r-1}\Gamma(r)\Gamma(N_\mathrm{t}-r+1)\big(\mathrm{Har}(N_\mathrm{t})-\mathrm{Har}(N_\mathrm{t}-r)\big)\right], \tag{D.7}$$

where $\Gamma(.)$ is the Gamma function, and $\mathrm{Har}(n) = \sum_i^n \frac{1}{i}$ is the n^{th} harmonic number. Eq. (D.7) can be numerically verified by executing "Mean[OrderDistribution[{ExponentialDistribution[λ], N_t}, r]]" in *Mathematica*. Based on (D.7), the average SNR of I-SM technique is evaluated as

$$\begin{aligned}\widehat{\rho} &= \sum_{r=1}^{N_\mathrm{t}} P(\mathcal{E}\to[r])\mathrm{E}_r[x,r] \\ &= \frac{2^{-N_\mathrm{t}}\left(-2N_\mathrm{t}\mathrm{Har}(N_\mathrm{t}-1)\Gamma(N_\mathrm{t})+\mathrm{Har}(N_\mathrm{t})\Lambda_4+\Lambda_5\right)}{\Gamma(N_\mathrm{t}+1)},\end{aligned} \tag{D.8}$$

where $\Lambda_4 = -2(N_\mathrm{t}-1)N_\mathrm{t}\Gamma(N_\mathrm{t}-1)+2N_\mathrm{t}\Gamma(N_\mathrm{t})+2^{N_\mathrm{t}}\Gamma(N_\mathrm{t}+1)$, $\psi^{(0)}(n) \sim \log n - \frac{1}{2n}$ is the first of the Polygamma functions, and $\Phi(n_1,n_2,n_3) = \sum_{n=0}^\infty \frac{n_1^n}{(n+n_3)^{n_2}}$ is the Lerch transcendent function. Finally, the average receive SNR of I-SM technique can be obtained as follows:

$$\rho^\mathrm{I} = \begin{cases}\rho^\mathrm{u}\widehat{\rho}\left(|s_m - s_{m'}|^2\right) & \text{if } n=n' \text{ and } \omega=1\\ \rho^\mathrm{u}\widehat{\rho}\left(|s_m e^{j\tilde{\theta}} - s_{m'}e^{j\tilde{\theta}}|^2\right) & \text{if } n=n' \text{ and } \omega=0\\ \rho^\mathrm{u}\widehat{\rho}\left(|s_m|^2+|s_{m'}|^2\right) & \text{if } n\neq n' \text{ and } \omega=1\\ \rho^\mathrm{u}\widehat{\rho}\left(|s_m e^{j\tilde{\theta}}|^2+|s_{m'}e^{j\tilde{\theta}}|^2\right) & \text{if } n\neq n' \text{ and } \omega=0,\end{cases} \tag{D.9}$$

where $\omega=0$ and $\omega=1$ indicate that events $\mathcal{E}\to[r]$ correspond to r consecutive 1's or r consecutive 0's, respectively.

MIMO with Optimal Antenna Activation

First, the optimal antenna activation (O-AA) terminology is explained. For a fair comparison with SM technique, only one transmit antenna is allowed to be activated in a MIMO setting implementing O-AA. Such technique will be denoted by O-MIMO throughout this paper.

Clearly, in a given symbol period, the index of the active transmit antenna when implementing O-AA is $\arg\max_n \|\mathbf{h}_n\|^2$. Unlike U-AA and I-AA, where the index of an active antenna is chosen by a block of information bits in U-AA and by r consecutive equal bits in I-AA, the antenna index in O-AA is chosen based on the maximum channel gain. Therefore, O-MIMO can only yield a rate of $\log_2 M$ bits/s/Hz, which is less than the one of SM and I-SM (cf. (5.1) and (5.6)). The O-MIMO is adopted here as a benchmark.

According to (D.7), $\max(\mathrm{E}_r[x,r])$ is achieved at the N_t^{th} order statistics. Thus, O-AA results in the average received SNR

$$\begin{aligned}\rho^\mathrm{o} &= \rho^\mathrm{u}\mathrm{E}_r[x,N_\mathrm{t}] \\ &= \frac{\rho^\mathrm{u}N_\mathrm{t}\ \Gamma(N_\mathrm{t})\ \mathrm{Har}(N_\mathrm{t})}{\Gamma(N_\mathrm{t}+1)}.\end{aligned} \tag{D.10}$$

The correctness of (D.4), (D.9), and (D.10) will be verified shortly.

D.2.2 Average BER without Antenna Selection

The average BER of SM, I-SM, and O-MIMO can be computed by the pairwise error probability (PEP). Assume that s_m is transmitted using the n^{th} antenna. Considering ML detection at the receiver, assume that the index of the active antenna and the transmitted M-APM symbol are estimated as $\widehat{n}$ and $\widehat{m}$, respectively. The PEP is $P_{\text{e}} = Q(\sqrt{\xi})$, where $Q(.)$ is the Q-function and $\xi = \frac{1}{2\sigma^2}|h_n s_m - h_{n'} s_{m'}|^2$ is an exponential RV with PDF given by (D.11a). For multiple receive antennas N_{r}, $\Psi = \sum_{i=1}^{N_{\text{r}}} \xi_i$ is a Chi-squared RV with PDF given by (D.11b).

$$f(\xi) = \frac{1}{\nu} \text{e}^{\frac{-\xi}{\nu}}. \tag{D.11a}$$

$$f(\Psi) = \frac{1}{\Gamma(N_{\text{r}})\nu^{N_{\text{r}}}} \Psi^{N_{\text{r}}-1} \text{e}^{\frac{-\Psi}{\nu}}. \tag{D.11b}$$

In (D.11a) and (D.11b), ν depends on the choice of the AA strategy. Specifically, $\nu = \rho^{\text{u}}$ for U-AA (cf. (D.4)), $\nu = \rho^{\text{I}}$ for I-AA (cf. (D.9)), and $\nu = \rho^{\text{o}}$ for O-AA (cf. (D.10)). Finally, the average PEP can be computed as

$$\text{E}[Q(\sqrt{\xi})] = P_{\text{e}} = \int_0^\infty \frac{1}{\nu} \text{e}^{\frac{-\xi}{\nu}} Q(\sqrt{\xi}) d\xi. \tag{D.12a}$$

$$\text{E}[Q(\sqrt{\Psi})] = \mathfrak{p}_{\text{e}} = \int_0^\infty \frac{1}{\Gamma(N_{\text{r}})\nu^{N_{\text{r}}}} \Psi^{N_{\text{r}}-1} \text{e}^{\frac{-\Psi}{\nu}} Q(\sqrt{\Psi}) d\Psi. \tag{D.12b}$$

Based on (D.12), the average PEP of SM technique implementing U-AA, I-AA, or O-AA strategies is obtained as follows.

SM with Uniform Antenna Activation

When $N_{\text{r}} = 1$, substituting (D.4) into (D.12a) yields the average PEP shown in (D.13a). For $N_{\text{r}} > 1$, following (D.12b), the average PEP is calculated as per (D.13b).

$$P_{\text{e}}^{\text{u}} = \frac{1}{2} - \frac{1}{2\sqrt{\frac{2+\rho^{\text{u}}}{\rho^{\text{u}}}}}. \tag{D.13a}$$

$$\mathfrak{p}_{\text{e}}^{\text{u}} = (P_{\text{e}}^{\text{u}})^{N_{\text{r}}} \sum_{i=0}^{N_{\text{r}}-1} \binom{N_{\text{r}}-1+i}{i} \left[1 - P_{\text{e}}^{\text{u}}\right]^i. \tag{D.13b}$$

SM with Irregular Antenna Activation

For $N_{\text{r}} = 1$, substituting (D.9) into (D.12a) yields the average PEP under I-AA as

$$P_{\text{e}}^{\text{I}} = \frac{0.5\Gamma(N_{\text{t}}+1)\left(\Phi\left(\frac{1}{2}, 1, N_{\text{t}}\right) + 2^{N_{\text{t}}}(\psi^{(0)}(N_{\text{t}}+1) - \log(2) + \gamma)\right)\Lambda_1}{(-2N_{\text{t}}\Gamma(N_{\text{t}})\text{Har}(N_{\text{t}}-1) + \Lambda_6 \text{Har}(N_{\text{t}}) + N_{\text{t}}\Gamma(N_{\text{t}})\Lambda_3)\,\Lambda_2}, \tag{D.14}$$

where $\Lambda_1 = \sqrt{1 + \frac{2^{N_\mathrm{t}+1}}{\sigma^2\left(\Phi\left(\frac{1}{2},1,N_\mathrm{t}\right)+2^{N_\mathrm{t}}(\psi^{(0)}(N_\mathrm{t}+1)-\log 2+0.577216)\right)}} - 1$, $\Lambda_2 = \Lambda_1 + 1$, $\Lambda_3 = \Phi\left(\frac{1}{2},1,N_\mathrm{t}\right) + 2\psi^{(0)}(N_\mathrm{t}) - 2^{N_\mathrm{t}}\log 2 + 1.15443$, and $\Lambda_6 = -2(N_\mathrm{t}-1)N_\mathrm{t}\Gamma(N_\mathrm{t}-1) + 2N_\mathrm{t}\Gamma(N_\mathrm{t}) + 2^{N_\mathrm{t}}\Gamma(N_\mathrm{t}+1)$.

The average PEP under I-AA for $N_\mathrm{r} > 1$ can be evaluated by substituting (D.14) into (D.12b), yielding

$$\mathfrak{p}_\mathrm{e}^\mathrm{I} = (P_\mathrm{e}^\mathrm{I})^{N_\mathrm{r}} \sum_{i=0}^{N_\mathrm{r}-1} \binom{N_\mathrm{r}-1+i}{i} \left[1 - P_\mathrm{e}^\mathrm{I}\right]^i. \tag{D.15}$$

MIMO with Optimal Antenna Activation

The average PEP of a MIMO system implementing O-AA when $N_\mathrm{r} = 1$ can be computed by substituting (D.10) into (D.12a), which yields

$$P_\mathrm{e}^\mathrm{o} = \frac{0.5\rho^\mathrm{u}\Gamma(N_\mathrm{t}+1)\left(\sigma^2\ \mathrm{Har}(N_\mathrm{t}) - \Lambda_4\right)}{N_\mathrm{t}\mathrm{H}(N_\mathrm{t})\Gamma(N_\mathrm{t})} \tag{D.16}$$

where $\Lambda_4 = \frac{\left(\sigma^2\mathrm{Har}(N_\mathrm{t})\right)^2\sqrt{\frac{2}{\sigma^2\mathrm{Har}(N_\mathrm{t})}+1}}{\sigma^2\mathrm{Har}(N_\mathrm{t})+2}$. For $N_\mathrm{r} > 1$, substituting (D.16) into (D.12b) gives

$$\mathfrak{p}_\mathrm{e}^\mathrm{o} = (P_\mathrm{e}^\mathrm{o})^{N_\mathrm{r}} \sum_{i=0}^{N_\mathrm{r}-1} \binom{N_\mathrm{r}-1+i}{i} \left[1 - P_\mathrm{e}^\mathrm{o}\right]^i. \tag{D.17}$$

D.2.3 Average SNR with Antenna Selection

Now, the average received SNR in SM, I-SM, and O-MIMO systems employing AS is derived. When using REAS and/or RLAS, N_t out of N_T transmit antennas are chosen. Let us denote the index set of the chosen antennas by $\hat{I}$. With $N_\mathrm{r} = 1$ receive antenna, assume that $\hat{I} = [1, \cdots, N_\mathrm{t}]$. The channel vector $\tilde{\mathbf{H}}(\hat{I}) = [h_1, \cdots, h_{N_\mathrm{t}}] \in \mathbb{C}^{1\times N_\mathrm{t}}$, where h_1 and h_{N_t} are the $(N_\mathrm{t}+1)^{\mathrm{th}}$ and $N_\mathrm{T}^{\mathrm{th}}$ order statistics of $\tilde{\mathbf{H}}$. The SM, I-SM, and O-MIMO systems utilize each of the $(N_\mathrm{t}+1)^{\mathrm{th}}, \cdots, N_\mathrm{T}^{\mathrm{th}}$ order statistics of $\tilde{\mathbf{H}}$ with different probabilities, achieving different SNRs, as detailed next.

SM with Uniform Antenna Activation

When using SM, each of the N_t order statistics of $\tilde{\mathbf{H}}$ is chosen at the uniform rate of $\frac{1}{N_\mathrm{t}}$. Therefore, the average received SNR of SM system employing AS can be evaluated as

$$\gamma^\mathrm{u} = \begin{cases} \frac{\rho^\mathrm{u}\tau^\mathrm{u}}{N_\mathrm{t}}\left(|s_m - s'_m|^2\right) & \text{if } n = n' \\ \frac{\rho^\mathrm{u}\tau^\mathrm{u}}{N_\mathrm{t}}\left(|s_n|^2 + |s_n|^2\right) & \text{if } n \neq n', \end{cases} \tag{D.18}$$

where $\tau^\mathrm{u} = \sum_{r=N_\mathrm{T}-N_\mathrm{t}+1}^{N_\mathrm{T}} \mathrm{E}_r[x,r]$. $\mathrm{E}_r[x,r]$ is shown in (D.7).

SM with Irregular Antenna Activation

In I-SM, each of the $(N_{\mathrm{t}}+1)^{\mathrm{th}}, \cdots, N_{\mathrm{T}}^{\mathrm{th}}$ order statistics of $\tilde{\mathbf{H}}$ is chosen with a different probability. Particularly, the N_{t} order statistics are chosen with probabilities as defined in (5.5). Explicitly, the $(N_{\mathrm{t}}+1)^{\mathrm{th}}$ order statistics is chosen with probability $\frac{2}{2^{N_{\mathrm{t}}}}$ (cf. (5.5)), whereas the $N_{\mathrm{t}}+2, \cdots, N_{\mathrm{T}}$ order statistics are respectively chosen at a rate of $\frac{1}{2^k}$, where $k = N_{\mathrm{t}}-1, \cdots, 1$. Hence, the average received SNR of I-SM technique implementing AS, i.e., REAS or RLAS, can be evaluated as

$$\gamma^{\mathrm{I}} = \begin{cases} \rho^{\mathrm{u}}\tau^{\mathrm{I}}\left(|s_m - s_{m'}|^2\right) & \text{if } n = n' \text{ and } \omega = 1 \\ \rho^{\mathrm{u}}\tau^{\mathrm{I}}\left(|s_m e^{j\tilde{\theta}} - s_{m'}e^{j\tilde{\theta}}|^2\right) & \text{if } n = n' \text{ and } \omega = 0 \\ \rho^{\mathrm{u}}\tau^{\mathrm{I}}\left(|s_m|^2 + |s_{m'}|^2\right) & \text{if } n \neq n' \text{ and } \omega = 1 \\ \rho^{\mathrm{u}}\tau^{\mathrm{I}}\left(|s_m e^{j\tilde{\theta}}|^2 + |s_{m'}e^{j\tilde{\theta}}|^2\right) & \text{if } n \neq n' \text{ and } \omega = 0, \end{cases} \tag{D.19}$$

where τ^{I} is given by

$$\tau^{\mathrm{I}} = \sum_{r=N_{\mathrm{T}}-N_{\mathrm{t}}+1}^{N_{\mathrm{T}}} P(\mathcal{E} \to [r])\mathrm{E}_r[x,r] = \frac{1}{\Gamma(N_{\mathrm{T}}+1)}\left[\Lambda_7 + 2^{1-N_{\mathrm{t}}}N_{\mathrm{T}}\,\Gamma(N_{\mathrm{t}})\binom{N_{\mathrm{T}}-1}{N_{\mathrm{T}}-N_{\mathrm{t}}}\Lambda_8\right], \tag{D.20}$$

and where $\Lambda_7 = \sum_{k=N_{\mathrm{T}}-N_{\mathrm{t}}+2}^{N_{\mathrm{T}}} N_{\mathrm{T}}2^{k-N_{\mathrm{T}}-1}\Gamma(k)\binom{N_{\mathrm{T}}-1}{k-1}(\mathrm{Har}(N_{\mathrm{T}}) - \mathrm{Har}(N_{\mathrm{T}}-k))\Gamma(-k+N_{\mathrm{T}}+1)$ and $\Lambda_8 = \mathrm{Har}(N_{\mathrm{T}}) - \mathrm{Har}(N_{\mathrm{t}}-1)\Gamma(-N_{\mathrm{t}}+N_{\mathrm{T}}+1)$.

MIMO with Optimal Antenna Activation

O-MIMO without AS chooses the $N_{\mathrm{t}}^{\mathrm{th}}$ order statistic of $\mathbf{H}$ (cf. (D.10)). Also, O-MIMO with AS chooses the $N_{\mathrm{T}}^{\mathrm{th}}$ order statistic of $\tilde{\mathbf{H}}$. Therefore, the received SNR expression in (D.10) for O-MIMO without AS is equally valid for O-MIMO with AS when the number of transmit antennas N_{t} is replaced by N_{T}.

D.2.4 Average PEP with Antenna Selection

Now, the average PEPs of SM, I-SM, and O-MIMO with AS are computed.

SM with Uniform Antenna Activation

For $N_{\mathrm{r}} = 1$, substituting (D.18) in (D.12a) yields the average PEP of SM technique implementing AS (cf. (D.21a)). For $N_{\mathrm{r}} > 1$, following (D.12b), the average PEP is calculated as shown in (D.21b).

$$A_{\mathrm{e}}^{\mathrm{u}} = \frac{1}{2} - \frac{1}{2\sqrt{\frac{2+\gamma^{\mathrm{u}}}{\gamma^{\mathrm{u}}}}}. \tag{D.21a}$$

$$\mathfrak{g}_{\mathrm{e}}^{\mathrm{u}} = (A_{\mathrm{e}}^{\mathrm{u}})^{N_{\mathrm{r}}}\sum_{i=0}^{N_{\mathrm{r}}-1}\binom{N_{\mathrm{r}}-1+i}{i}(1-A_{\mathrm{e}}^{\mathrm{u}})^i. \tag{D.21b}$$

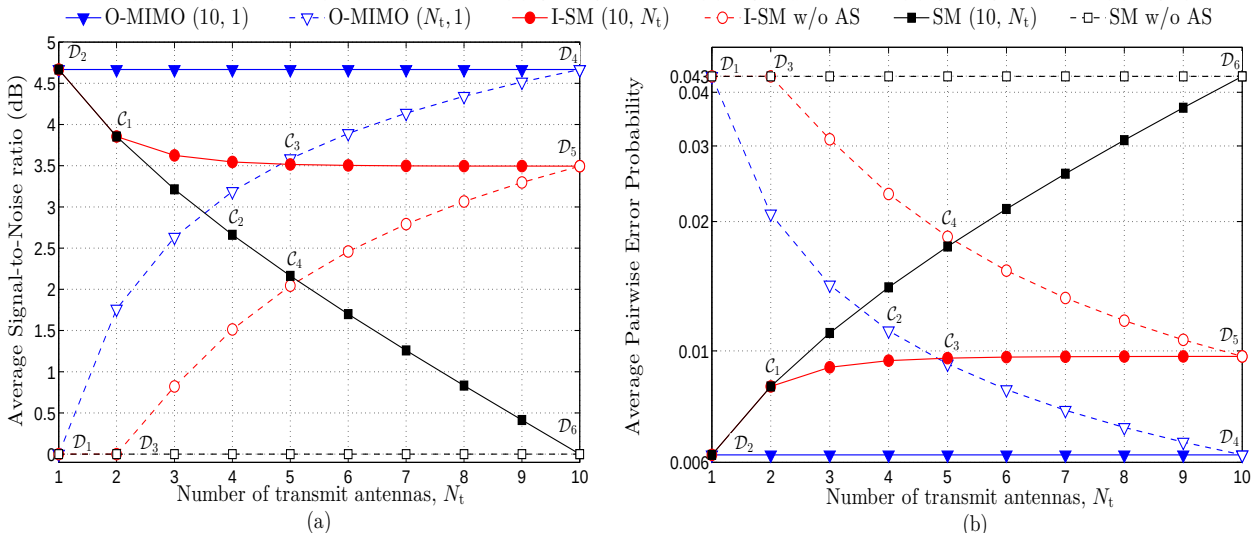

Figure D.1: Performance comparison of SM, I-SM, and O-MIMO techniques in terms of (a) average SNR, and (b) average PEP.

SM with Irregular Antenna Activation

For $N_r = 1$, substituting (D.19) in (D.12a) gives the average PEP of I-SM with AS (cf. (D.22a)). For $N_r > 1$, the average PEP is provided in (D.22b), and can be evaluated by substituting (D.22a) in (D.12b).

$$A_e^I = \frac{1}{2} - \frac{1}{2\sqrt{\frac{2+\gamma^I}{\gamma^I}}}. \tag{D.22a}$$

$$\mathfrak{g}_e^I = (A_e^I)^{N_r} \sum_{i=0}^{N_r-1} \binom{N_r - 1 + i}{i} (1 - A_e^I)^i. \tag{D.22b}$$

MIMO with Optimal Antenna Activation

The average PEP of O-MIMO with AS when $N_r = 1$ is the same as (D.16). When $N_r > 1$, the average PEP is as shown in (D.17).

D.2.5 Correctness of the Derived Expressions

In this part, the correctness of the PEP expressions of SM, I-SM, and O-MIMO, with and without AS, is verified.

SM with Uniform Antenna Activation

The average PEP performance of SM without AS shown in (D.13a) for the case with $N_{\mathrm{r}} = 1$ can be verified against [9, (4.6)]. For $N_{\mathrm{r}} > 1$, (D.13b) can be verified against [9, (4.12)]. Next, the expressions of the average PEP of SM with AS given in (D.21a) for $N_{\mathrm{r}} = 1$ and in (D.21b) for $N_{\mathrm{r}} > 1$ are verified. Setting $N_{\mathrm{t}} = N_{\mathrm{T}}$, it can be seen that $\frac{\tau^{\mathrm{u}}}{N_{\mathrm{t}}}$ in (D.18) converges to 1, i.e., γ^{u} (cf. (D.18)) becomes equal to ρ^{u} (cf. (D.4)). Using the same analogy, it can easily be proven that (D.21b) converges to (D.13b) when $N_{\mathrm{t}} = N_{\mathrm{T}}$.

SM with Irregular Antenna Activation

Let us assume $N_{\mathrm{t}} = 2$ and $N_{\mathrm{r}} = 1$, and the channel vector $\mathbf{H} = [h_1, h_2]$ such that $h_1 > h_2$. When using I-SM, h_1 and h_2 are chosen at the uniform rate of $\frac{1}{2}$, resulting in the average received SNR shown in (D.4), and the average PEP given in (D.13a). Observe from (5.5) that each element of $\mathbf{H}$ will be chosen at the rate of $\frac{1}{2}$ and, hence, the working principle of I-SM becomes identical to that of SM. Explicitly, substituting $N_{\mathrm{t}} = 2$ into (D.8) yields $\widehat{\rho} = 1$, and (D.14) converges to (D.13a), which proves the correctness of (D.14). Similarly, it can easily be shown that (D.15) converges to (D.13b) when $N_{\mathrm{t}} = 2$.

Replacing N_{T} with N_{t} in the average PEP of I-SM with AS when $N_{\mathrm{r}} = 1$ (cf. (D.22a)), it can easily be shown that the expression converges to (D.14). Substituting $N_{\mathrm{T}} = N_{\mathrm{t}} = 2$ into (D.22a) leads to the convergence of the expression to (D.13a). Similarly, it can be shown that (D.22b) converges to (D.13b) when $N_{\mathrm{T}} = N_{\mathrm{t}}$, and to (D.13a) when $N_{\mathrm{T}} = N_{\mathrm{t}} = 2$.

MIMO with Optimal Antenna Activation

O-MIMO always activate a transmit antenna pertaining to the $N_{\mathrm{t}}^{\mathrm{th}}$ order statistics of $\mathbf{H}$. Therefore, the working principle of O-MIMO is the same as SM when $N_{\mathrm{t}} = 1$. Substituting $N_{\mathrm{t}} = 1$ in (D.16) and (D.17) converges to (D.13a) and (D.13b), respectively.